A New Photoremovable Protecting Group – Synthesis and Reaction Mechanism

INAUGURALDISSERTATION

zur

Erlangung der Würde eines

Doktors der Philosophie

vorgelegt der
Philosophisch-Naturwissenschaftlichen Fakultät
der Universität Basel

von

Yavor Kamdzhilov

aus Sofia, Bulgarien

Basel, 2005

Genehmigt von der Philosophisch-Naturwissenschaftlichen Fakultät der Universität Basel auf Antrag der Herren

Prof. Dr. Hans-Jakob Wirz

Prof. Dr. Bernd Giese

Basel, den 17. Juli 2005

Prof. Dr. Hans-Jakob Wirz
(Dekan)

Dedicated to my family and to Katja

Acknowledgments

I wish to express my sincere thanks to Prof. Jakob Wirz (“Joggi”) for his continuous support during my PhD studies and for the numerous stimulating discussions.

I thank Prof. Bernd Giese for agreeing to act as a co-referee.

Special thanks to all my former and present colleagues in the research group of Prof J. Wirz: Hassen Boudebous, Dragana Zivkovic, Jürgen Wintner, Pavel Müller, Gaby Persy, Bruno Hellrung, Bogdan Tokarczyk, Martin Gaplovsky, Markus Ramseier, Anna-Paolla Ingebrand, Christian Ley, and to Uwe Pischel, Daniela Hristova, Tsvetanka Stanoeva, Cesar Marquez, Roxana Stoenescu, Petre Birza, Stanislav Ivan, Ivan Shnitko for always being open and ready to help.

I wish to thank my family for their everlasting affection and encouragement.

“Nature guards her secrets jealously; it is necessary to lay violent siege to her for a long time to discover a single one of them, however small it be”.

Richet, Charles, The Savant XIII (p.149)

Table of Contents

1. Introduction

1.1 Photoremovable Protecting Groups

Photoremovable protecting groups (ppg's) have been known to the chemical community for a long time. They differ conceptually from the classical protecting groups used in organic synthesis because they do not require addition of a cleaving reagent. This is a major advantage, allowing chemists to perform reactions with high selectivity at very mild reaction conditions. The possibility of breaking bonds only by illumination seems to be very appealing not only to classical organic synthesis but also to the solid-phase organic synthesis. A number of excellent reviews and books, dedicated to synthetic[1-5] and mechanistic aspects[1, 6] of the topic, have appeared in the recent years.

Ppg's were introduced to the "World of life sciences" more than two decades ago. Since the pioneering work by Kaplan and co-workers[7], possible applications of the ppg's in biochemistry, physiology and medicine have sparked a considerable interest in designing new systems. Excellent reviews, covering a wide range of applications in biology and related fields, are available.[6, 8-11]

Several synonymous words can be found in the literature, as the scientists exploring and/or exploiting the chemistry of ppg's differ substantially in their background. Ppg's have been referred to as "phototriggers", "caged compounds" and as "photolabile groups". The term "caged compounds" is a pictorial way of describing a molecule that has been prevented from exerting its usual action. In nearly all successful caged compounds a covalent bond between the protecting group and a substrate of interest is formed. It masks some features that are important for the biorecognition, thus rendering the caged substrate bio-inactive. Photochemical cleavage of this bond releases the active species. Caged compounds are useful molecules as irradiation with light can be very easily controlled in time, space and intensity.

Several criteria for designing new ppg's have to be considered, with the following being the most important ones:

- General prerequisite is a clean and uniform photoreaction, having relatively high quantum efficiency and providing fast rate of release.
- The reactive chromophore has to posses an absorption spectrum that extends beyond 320 nm in order to avoid irradiation of the cellular content.
- The photolysis products should not absorb light at the wavelength of irradiation of the ppg's, thus not competing for the incident light. Moreover, they should be biologically compatible.
- The protected compound should be soluble in the medium that is required by a specific application; in most cases this is water or buffered aqueous solutions.
- The ppg's should not generate any stereogenic centres upon photolysis.
- The ppg's have to be easy to install and should not require laborious synthetic protocols.

Clearly, not a single ppg could satisfy all these conditions and the number of requirements that ppg's have to fulfil is constantly growing. At the same time, the pool of available groups is still very small.

A summary of the major families of ppg's with some of their advantages and drawbacks is given in the first part of the introduction. The chapter continues with an arbitrary selection of applications.

1.1.1 Major Groups. Mechanism of Deprotection. Properties

1.1.1.1 The 2-Nitrobenzyl Group

2-Nitrobenzyl cages (2NB) were employed in over 80% of the published applications of ppg's. Despite this fact, the 2NB has a good number of drawbacks when compared with other ppg's. Its rate of release varies depending on many factors, and in water solution it is slowest around physiological pH values, which is undesirable when fast release rates in biological applications are required; the final product is quite reactive due to its nitroso group and is toxic for living cells; the spectrum of the final product is bathochromically shifted and competes for the incident light, leading to inefficient photolysis; the absorption spectrum of non-substituted 2NB's hardly extends beyond 350 nm and so, harmful UV radiation cannot be avoided; a complex cascade of often slow reactions precedes the release, thereby allowing trapping agents to intercept intermediates and retard the release. It seems that its widespread use in biology and related fields has more historical than rational reasons, simply because it was the first to be applied[7].

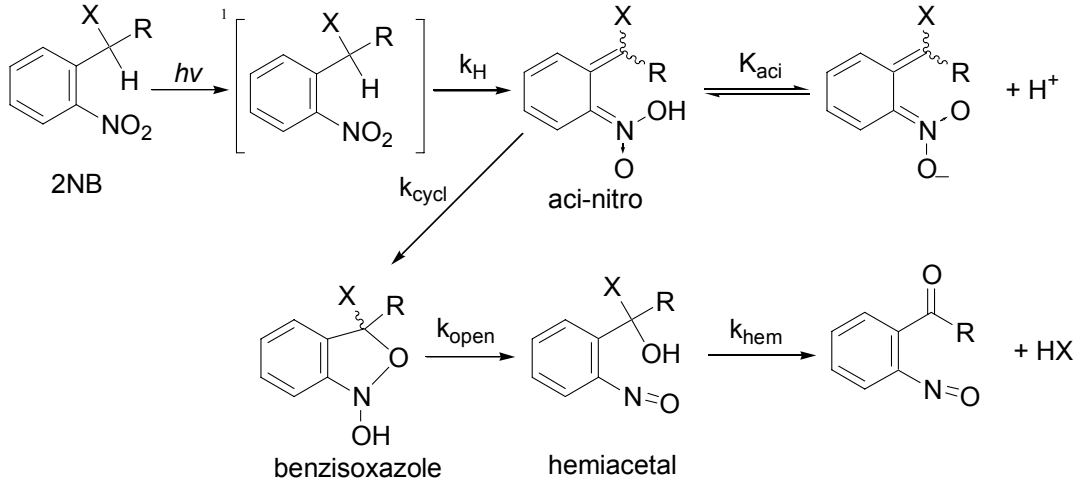

Scheme 1. Reaction mechanism of 2-nitrobenzyl group

The sequence of events that is taking place between the light absorption and the release of the substrate **X** (Scheme 1) is complex and depends on many factors such as nucleofugacity of **X**, nature of substituent **R**, pH and solvent. After a photon

has been absorbed, the 2NB is promoted to its singlet excited state where it can either cross over to a triplet excited state or undergo a hydrogen abstraction (k_H). The multiplicity of the reactive state has not been established for all members of the NB family. It is generally accepted that the hydrogen abstraction is fast enough to compete with the intersystem crossing. This shift of a proton to the oxygen leads to formation of an aci-nitro intermediate. The aci-nitro is a short-lived species, which can be detected by laser-flash photolysis and was often taken as an indicator for the rate of release. Wirz and colleagues have shown that the *E,E*-aci nitro isomer cyclizes directly to benzisoxazole, which is a UV-VIS silent intermediate and its presence was established mainly by time-resolved IR spectroscopy. The decay of benzisoxasole gives rise to new signals in the IR spectrum, which were assigned to a hemiacetal. Its IR spectrum exhibits a strong nitroso absorption band but no signal for a carbonyl group. Finally, the carbonyl group stretching vibration appearance of the nitrozobenzaldehyde signals the release rate of the substrate **X**. This seems to be the only reliable measure for the release rates of the members of the 2NB family.

1.1.1.2 The Benzoin Group

The benzoin (Desyl**,** Bnz) protecting group has several advantages. Its synthesis is straightforward and usually accomplished in high yield; its absorption in the near UV allows more efficient irradiation; the photoreaction is relatively clean and uniform and leads to a biologically inert by-product. The overall photoreaction is shown in scheme 2.

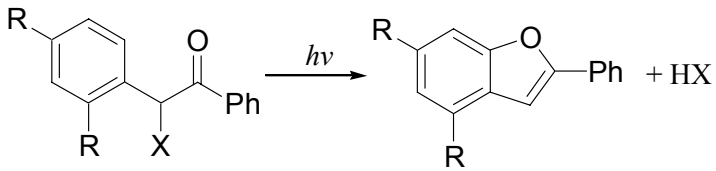

R = H, OMe

Scheme 2. Photoreaction of the benzoin group.

At first sight, the reaction seems to be simple but when scrutinized, the complexities of the desyl groups become apparent. Several different mechanisms of release have

been proposed. Wirz and Givens[12] provided sufficient information on the mechanism of the non-substituted benzoin group (R=H, X = $OPO(OEt)_2$). They have reported that two different pathways are necessary to account for their results (Scheme 3).

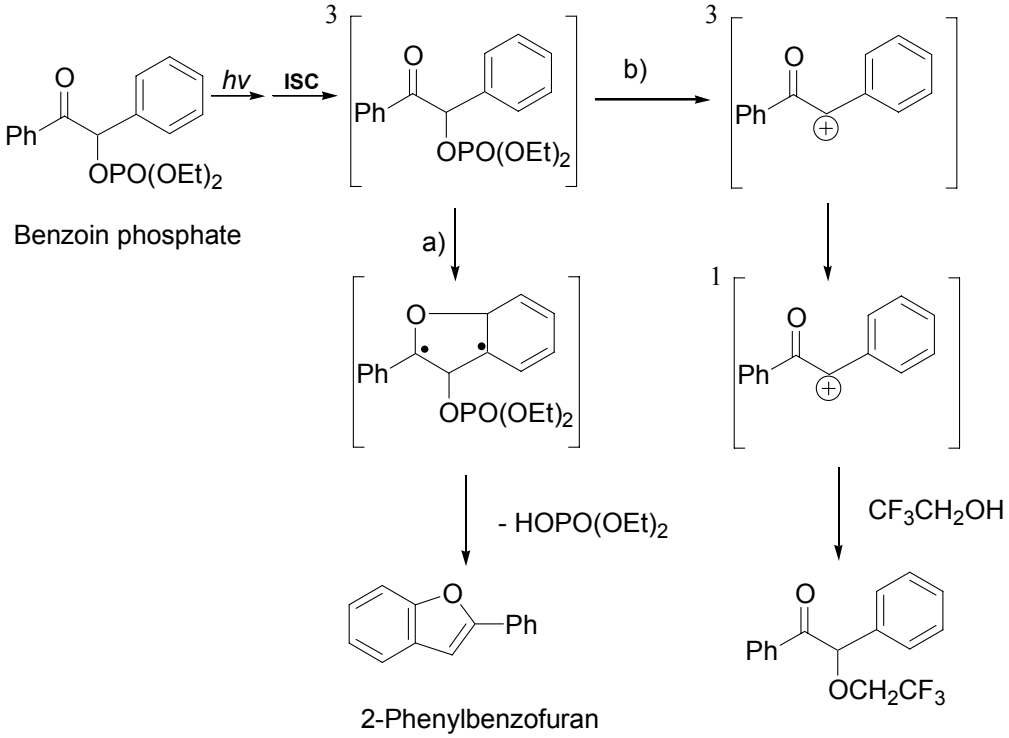

Scheme 3. Mechanism of deprotection of the non-substituted benzoin group.

In their study, the lowest excited state was established to be the triplet excited state of the benzoin. It is formed within a few picoseconds through intersystem crossing of the singlet. Two competing reaction pathways (a, b) originate from the triplet and are solvent dependent. In all solvents, but water and fluorinated alcohols, 2-phenylbenzofuran is formed within 20 ns. This remarkably fast transformation is accomplished via a biradical intermediate, which, however, has not been observed. It is assumed that it reacts faster than it is formed. The second reaction leads to products of nucleophilic substitution and decreased chemical yield of 2-phenylbenzofuran. A transient, observed in nanosecond-laser flash photolysis experiments (λ_{max} = 570 nm, τ = 660 ns), was assigned to the triplet cation formed after loss of the leaving group. Its presence was additionally confirmed by DFT calculations and quenching studies. As the addition of nucleophiles to a triplet cation is a spin forbidden process, intersystem crossing was invoked as the next step in order to explain the slow addition of solvent. The authors explained the partitioning of the

photoreaction with the coexistence of two interconvertible conformers (rotation around α and β carbons) of the benzoin phosphate in the ground state. The “anti” isomer is favoured by solvents forming strong hydrogen bonds to the carbonyl group and thereby allowing a heterolytic fission and funnelling the reaction towards nucleophilic addition.

In contrast to the relatively well understood mechanism of unsubstituted derivatives of Bnz, the 3’,5’-dimethoxy benzoins have more complex behaviour. For instance, the reactive state of benzoin caged acetic acid could not be quenched, suggesting that this derivative reacts either via a singlet excited state or a very short-lived triplet state. An intramolecular exciplex, Paterno-Büchi reaction of the singlet excited state or a formation of an ion pair and subsequent closure and elimination are among the proposed mechanisms[13-15].

Bnz offers quite a few advantages as a ppg and indeed has been applied in several research areas. Nevertheless, it is worth mentioning that it also possesses several drawbacks, such as its intrinsic chirality. This could be a problem when optically active substrates are protected. Another problem for biological applications is the fact that it lowers the solubility of the protected substrate and the main by-product is fairly insoluble in aqueous media.

1.1.1.3 The p-Hydroxyphenacyl Group

The p-hydroxyphenacyl group (pHP) is an excellent alternative to the 2-nitrobenzyl and the benzoin groups. In fact, it seems to be one of the most promising ppg’s for investigating biological events. It has a number of remarkable properties: (1) fast release rates on the order of 1 ns, depending on the substrate released; (2) high solubility in aqueous media; (3) the main by-product is transparent at the irradiation wavelength due to its blue-shifted absorption and thus allows quantitative chemical conversion; (4) pHP has high quantum yields of release; (5) it is easily accessible through simple synthetic protocols; (6) its by-products are biologically benign. However, since it was introduced relatively recently, there have not been many studies that employ pHP. Nevertheless, the cases where it has been used are very informative and show its unique potential[16-19].

All details of the mechanism of release from pHP still remain to be clarified. Nevertheless, a working hypothesis based on a number of photochemical studies exists. (Scheme 4)

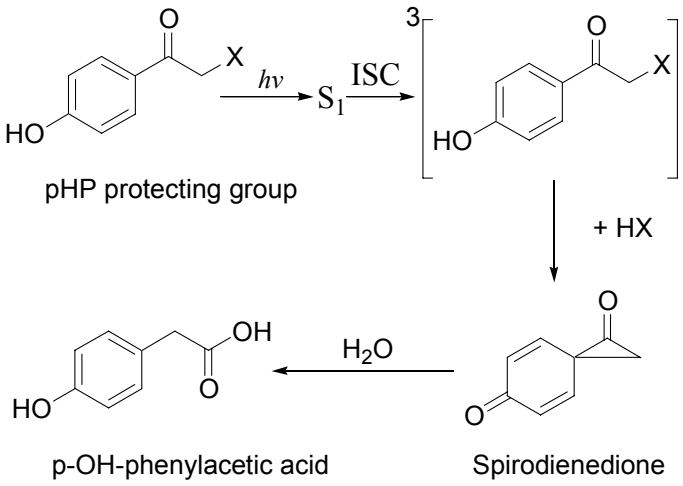

Scheme 4. Mechanism of release of pHP protecting group.

Givens and colleagues reported that the reaction is quenched by naphthalene-2-sulfonate and potassium sorbate, indicating a triplet reactive state of release with a life-time of 0.5 ns[17]. Later, Wirz[20] and co-workers investigated pHP diethyl phosphate and observed the triplet excited state by pump-probe spectroscopy (λ_{max}=380 nm, τ = 0.4 ns in acetonitrile/water = 1:1), quenchable by oxygen and piperylene. The agreement between the results from the two groups has led the researchers to the conclusion that the pHP expels the caged substrate from its triplet excited state although the actual release rate was not measured. The deprotection occurs either simultaneously or follows deprotonation of the *para*-hydroxyl group in the triplet excited state. The triplet pKa of this group was measured to be 3.6 versus 7.9 in the ground state. The acidity of the triplet should be considered, when new derivatives are designed. This is evident from the work of Conrad and Givens[21]. The authors attempted to tackle one of the main drawbacks of pHP, namely its weak extinction in the visible part of the spectrum. They managed to shift the absorption maximum from ca. 325 nm to 380 nm by synthesizing 3,5-dimethoxy derivative of pHP, but the quantum efficiencies of release dropped significantly, very likely due to decreased acidity of the triplet.

Since the first report[22] on the photochemistry of pHP, the presence of a spirodienedione intermediate (**2**, Scheme 5) has been inferred. The main argument supporting this hypothesis is the change in the bond connectivity in going from pHP **1** to p-OH-phenylacetic acid **3**. So far **2** has escaped detection. In an attempt to detect this intermediate, Kamdzhilov and Wirz[23] performed a number of time resolved IR experiments in different solvent mixtures (water/acetonitrile). At low water concentrations (5-10%) they observed a long-lived species, which they assigned to *p*-quinonemethide **4** on the basis of its IR spectrum. Moreover, they detected 4-hydroxymethylphenol **5** in the photolysis mixture, which is very likely to be derived from a water addition to *p*-quinonemethide. DFT calculations suggested that two competitive reaction manifolds exist (water addition to the spirodienedione and thermal decomposition with a loss of CO of the latter), thereby indirectly proving the presence of the putative spirodienedione intermediate. In order to slow down the decomposition of the spirodienedione and unequivocally establish its existence, additional time-resolved IR experiments at low temperature are required.

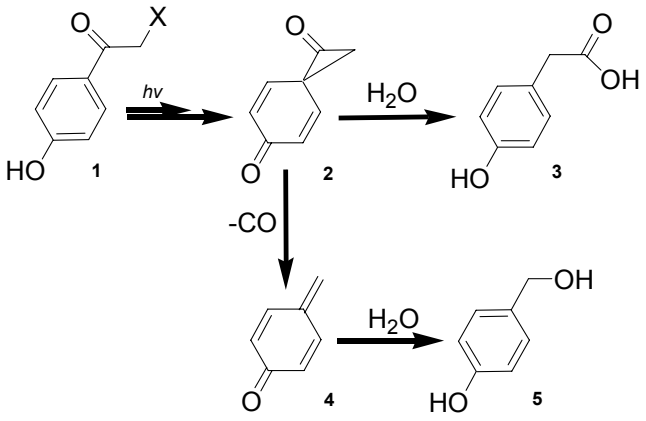

Scheme 5. The fate of the spirodienedione intermediate

1.1.1.4 The Coumarinyl Group

Coumarinyl derivatives generated a considerable interest in the last ten years. The coumarinyl group (Cou) has been applied in a number of biological studies, including the photorelease of phosphates, cyclic nucleotides (*vide infra*) and carboxylic acids. Very recently, Geissler and co-workers demonstrated the use of six coumarinyl derivatives in producing ultrafast pH jumps[24]. Schade *et. al*[25] proposed a mechanistic scheme (photo S_N1 mechanism) that outlines the photoreaction of the coumarinyl ppg (Scheme 6).

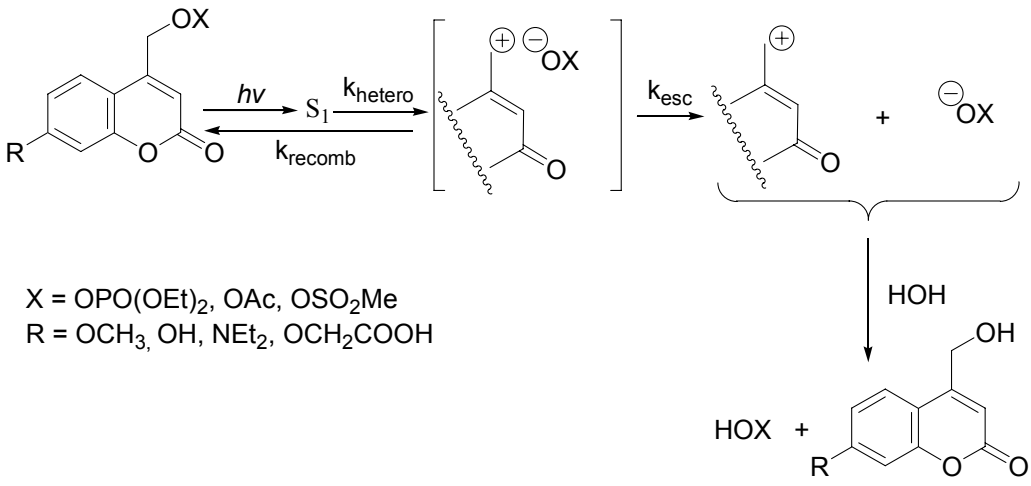

Scheme 6. Mechanism of release of the Coumarinyl protecting group.

After initial excitation, the coumarinyl chromophore is promoted to its singlet excited state. Almost all derivatives from that series have very week fluorescence, which suggests an efficient photoreaction. At the same time, the product of photolysis is a strongly emitting compound. This fact has been proposed as a mean to monitor the process of release. Heterolytic cleavage (k_{hetero}) of the CO bond follows the excitation and is the rate-determining step of release (~10^9 s^{-1}). Not much evidence is available about this step of the mechanism and it is often speculated on the nature of the bond cleavage (hetero- vs. homolytic)[25, 26]. In a series of experiments, Schade has shown that dependence between the polarity of the solvent and the quantum efficiencies exists. More polar solvents solvate better the ion pair and increase the

quantum yield. The trapping of the solvated ions by water is thought to be close to diffusion control.

This system has only few drawbacks. Some of the derivatives are not stable for long time in neutral aqueous media and most of them exhibit low to moderate quantum yields (a few new derivatives have Φ ~ 0.7)[24]. Nevertheless, the high extinction coefficients in the visible range of the spectrum (λ = 380 nm, ε = 1-2 x 10^4 $M^{-1}cm^{-1}$), the fast rate of release and the high photochemical stability of the photoproduct make the coumarinyl a very promising photoremovable protecting group.

1.1.1.5 Other Groups

7-Nitroindolines have been used for more than two decades as ppg's but only recently have they gained considerable attention. Photocleavage involves the triplet excited state and proceeds in the submicrosecond range. The photoreaction is clean and depends strongly on the nature of the solvent[8]. Their photoreactions are summarised in Scheme 7.

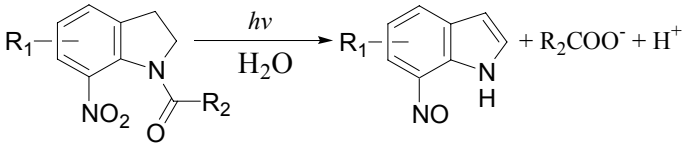

Scheme 7. Photolysis of the 7-nitroindoline protecting group.

The dimethoxy benzyl group is employed in the release of amino acids[8]. The photoreaction originates from a short-lived excited state and fragmentation occurs with rate constants in the order of 10^8 s^{-1}. The actual release rate, however, is three orders of magnitude slower, because decarboxilation the carbamate ester is slow. This protecting group has the restriction of relatively low quantum yields.

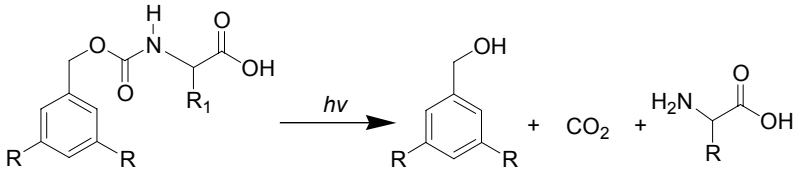

R = H, OCH_3
R_1 = H, CH_2SH, Ph, CH_2OH

Scheme 8. Photolysis of the benzyl protecting group.

1.1.2 Applications

1.1.2.1 Photorelease of Neurotransmitters

Photorelease of neurotransmitters is the area where ppg's have been most extensively applied. A number of monographs and reviews cover this broad area of applications and the present summary does not have the intention of being comprehensive on the subject. A brief introduction to the topic as well as several intriguing examples, illustrating the significance of the ppg's, are discussed.

Many clinically important compounds (for example tranquilizers, antidepressants, anti-convulsants) and abused drugs (for example cocaine) affect the receptor functions of membrane bound proteins. Other receptor proteins regulate the transmission of signals between the cells of the mammalian central nervous system and between nerve and muscle cells. They are fundamental to the ability of the nervous system to receive, store and process information. Beyond any doubt, an understanding of their function and structure would deliver invaluable knowledge to us. In essence, a neurotransmitter binds to a specific surface cell receptor, which in turn causes a transient (usually in the μs or ms time domain) rearrangement of the latter and a formation of channels (ligand-gated ion channels), through which small inorganic ions can cross membranes of neural or muscle cells, thus giving rise to a transient voltage across it. Measuring this voltage has proven to be very informative about the function of a particular receptor. There are several electrophysiological methods used in observing such processes. Among them is pulsed laser photolysis, which employs photolabile precursors of the neurotransmitters. Ppg's are used to block a particular functional group within the neurotransmitter and so convert it into a biologically inert molecule. Mixing of the protected substance and the cells does not produce any physiological change in the receptor. Later, the cell is irradiated with a short pulse of light, the active substance is released and the physiological response of interest can be measured with a time resolution restricted only by the rate of deprotection of the ppg. This technique has verified that the time needed for the current to reach its maximum is much shorter than the time found in other experiments, using older methods like the cell flow technique. Many photoactivatable precursors of neurotransmitters (glutamates, γ-aminobutyric acid, caged glycine, *etc*.)

have been synthesised. Glutamate is the major excitatory neurotransmitter in the vertebrate central nervous system. It has been used for mapping neuronal connectivity, probing neuronal integration and synaptic plasticity. A few examples of glutamate, protected with different ppg's, are shown below.

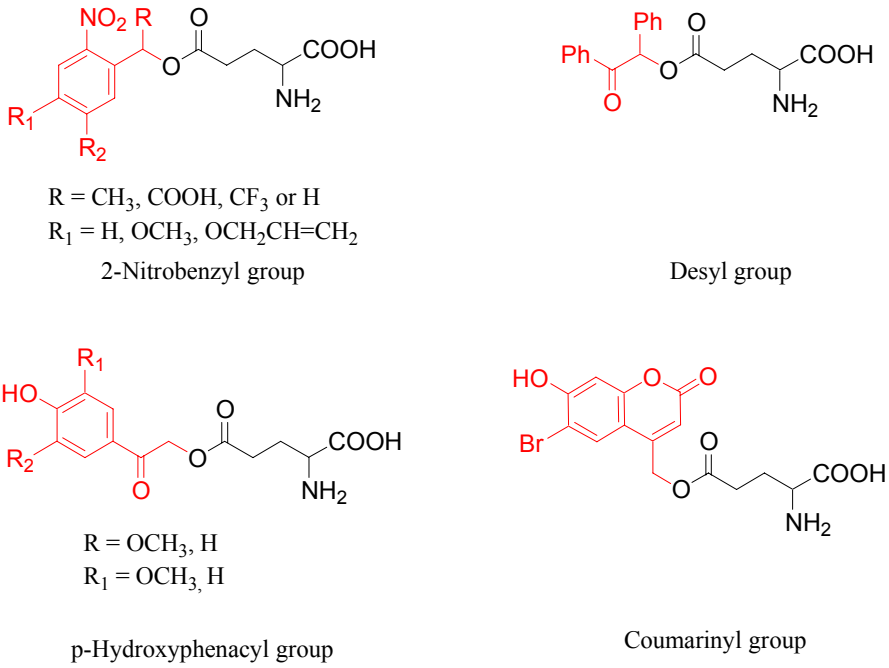

Figure 1. Diverse ppg's used for protection of glutamate

About 24 different derivatives of caged glutamate have been synthesized and employed in biological studies[8], emphasizing the interest and the need of finding an ideal probe for glutamate. The glutamate molecule offers three different functional groups that can be protected. These are the α and γ – carboxylic functions as well as the amino group. All of the applied ppg's have advantages and drawbacks. In the nitobenzyl series, for example, relatively slow rates of release are seen, with the fastest derivative (R=COOH, R_1=H). In contrast, the p-hydroxyphenacyl ppg releases the caged substrate with rate constants of ca. 10^8 s^{-1} and satisfactory quantum yields of glutamate release, but suffers from low extinction coefficient at wavelengths above 350 nm. Very often the rate constants in the literature do not correctly refer to the rate of release of glutamate and caution should be taken. The desyl series performs very poorly. Only the γ-derivative does the desired fragmentation but with a very low photolytic efficiency at higher wavelength of irradiation.

An interesting example is the use of p-hydroxyphenacyl caged glutamate in mapping synaptic plasticity (SP) of brain cells. SP is one of the many nervous system phenomena that has been receiving a great deal of attention in the recent years. SP is the variability of the strength of a signal transmitted through a synapse and is a part of the Hebbian theory about the neurochemical foundations of memory and learning. The memory storage processes in the brain as well as the ability of the neural system to adapt to novel situations are thought to be closely related to SP. Using caged glutamate Kandler *et al.*[18] succeeded in inducing LTD (long-term depression) in the postsynaptic part of the synapses and thus clarifying that LTD, but not LTP (long-term potentiation), is induced by stimulated neurotransmitter release and is purely postsynaptic.

Hess *et al.*[27] have investigated the function of nicotinic acetylcholine receptors (AChR). A variety of therapeutically important drugs and abused ones, such as cocaine, inhibit the function of namely these receptors. The Hess group used pulsed laser photolysis, employing αCNB-caged (nitrobenzyl series) carbamoylcholine. They studied the whole-cell current, induced after opening and closing of the ion-gated channel, as a result of the action of the neurotransmitter. The time-resolution achieved in this experiment was in the microsecond time domain. Their work led to two important conclusions: (1) Ligands that bind with higher activity to the open-channel form shift the equilibrium towards the closed form, thereby inhibiting the receptor. (2) Ligands that bind to a regulatory site with an affinity to the open conformation higher or equal to their affinity to the closed form are expected not to inhibit the receptor and to displace inhibitors. In other words, it was discovered that small ligands like aptamer II-3 can recover the activity of AChR (inhibited by cocaine) by about 50 % without inhibiting the receptor.

1.1.2.2 Photorelease of Second Messengers

The cyclic nucleoside monophosphates, adenine- and guanidine-3',5'-cyclic monophosphates (cAMP, cGMP), control a large variety of cellular processes. Cyclic AMP is a second messenger used for intracellular signal transduction, such as transferring the effects of hormones like glucagon and adrenaline, which cannot pass through the cell membrane. Its main purpose is the activation of protein kinases and it

is also used to regulate the passage of Ca^{2+} through ion channels. Cyclic GMP acts much like cAMP, most notably by activating intracellular protein kinases in response to the binding of membrane-impermeable peptide hormones to the external cell surface. Caged cAMP and cGMP are very useful in studying signaling pathways in cells, where spatial and time-dependent resolution is required. The cyclic nucleotides are rendered inactive by esterification of the free phosphate moiety by several photoremovable protecting groups, with 2-nitrobenzyl and the coumarinyl derivatives being the most used ones (scheme 9 and 10).

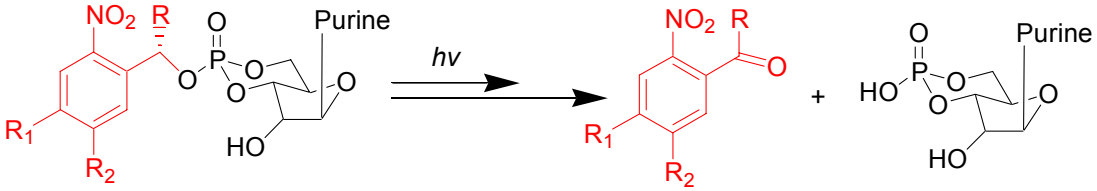

DMNB-caged cAMPs R = H, $R_1 = R_2 = OCH_3$, Purine = adenin-9-yl
DMNB-caged cGMPs R = H, $R_1 = R_2 = OCH_3$, Purine = guanin-9-yl
BCMCNB-caged cAMPs R = R_2 = H, $R_1 = CON(CH_2COOH)_2$, Purine = adenin-9-yl

Scheme 9. Photolysis of nitrobenzyl-caged cNMPs

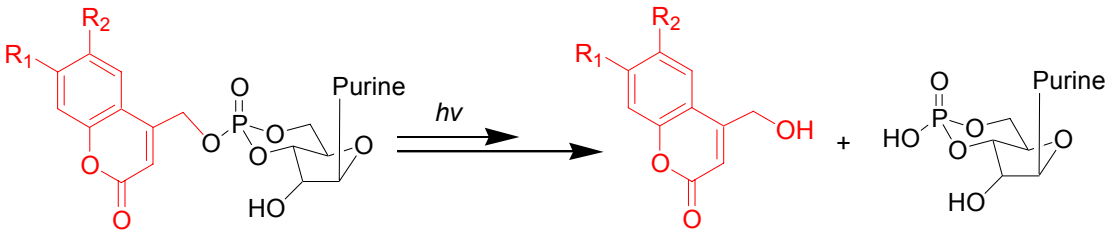

DMCM-caged cAMPs $R_1 = R_2 = OCH_3$, Purine = adenin-9-yl
BCMCM-caged cGMPs $R_1 = R_2 = OCH_2COOH$, Purine = guanin-9-yl
BECMCM-caged cAMPs $R_1 = R_2 = OCH_2COOEt$, Purine = adenin-9-yl

Scheme 10. Photolysis of coumarinylmethyl-caged cNMPs

Cyclic AMP and GMP have as principal targets cyclic nucleotide-gated channels, cGMP- and cAMP dependant kinases, and regulated phosphodiesterases, guanisine-nucleotide exchange factors and bacterial transcription factors. An interesting example of the use of BECMCM caged cAMP and cGMP is the work of Kaupp and co-workers[28]. They investigated the Ca^{2+} influx in sperm. The egg and the sperm meet through a process called chemotaxis. The sperm utilizes chemical gradients of a specific chemo-attractant in order to locate the egg. The egg releases a chemical

compound that binds to the outer shell of the sperm, causing a Ca^{2+} influx into the cell. This, in turn, changes the beating patterns of the tail of the sperm and thereby introduces correction in its trajectory of movement. In his work, Kaupp demonstrated that the Ca^{2+}-channels are opened through the action of cGMP, thus demonstrating that cGMP is the primary messenger. This discovery introduces significant corrections in the model underlying the process of chemotaxis and was made possible by the use of ppg's.

As discussed before, Ca^{2+} is a very important second messenger. Many physiological processes are triggered by influx of Ca^{2+} through the cellular membrane. Photolabile Ca^{2+}-chelators are used to define its role by rapid concentration jumps following a short laser pulse. It can not be caged by derivatization as in most other caged molecules. Instead, a simple strategy of changing binding abilities by photolysis of chelators is used. Ca-chelators have a many-fold decreased affinity to Ca^{2+} after photolysis, whereas Ca^{2+} scavengers bind strongly after being irradiated. In Figure 2 two examples of commercially available Ca^{2+} chelators are shown.

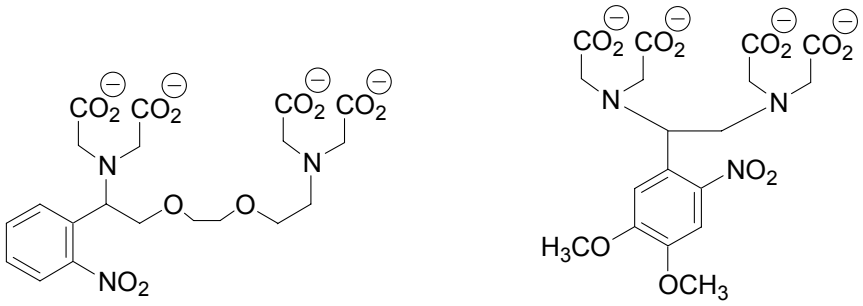

NP-EGTA DMNP-EDTA

Figure 2. Commercially available Ca^{2+} chelators

1.1.2.3 Photorelease of Nitric Oxide

Recent research has shown that nitric oxide, previously considered an environmental pollutant, is involved in many important bioregulatory processes. It is thought to participate in blood clotting, blood pressure regulation and to be a retrograde messenger and so playing an important role in neurotransmission. Moreover, it is considered a potential active agent in the treatment of cancer by photo-dynamic therapy. It is known[29] that high concentrations of NO are killing tumour cells, but its mode of action is still under investigation. The use of caged NO will open new possibilities for treating cancer.

A number of caged compounds, able to release NO, has been synthetically developed, others are found in living organisms. A brief summary includes: (I) Endogenous photosensitive precursors of NO. These are “NO-stores” within the living cells and their role in the cells is under active investigation. They are thought to be S-nitrosothiols or N-nitrosoamines formed by the action of a nitric oxide synthase (NOS). (II) Inorganic photosensitive precursors. This group includes several inorganic salts, oxide-metalloprotein adducts and a number of organometallic complexes able to bind NO. For example, $K_2RuCl_5(NO)$ has been used in eliciting smooth muscle relaxation and studies of long-term potentiation (LTP) of synaptic transmission and interneuronal activity in molluscs. Another interesting example is the dinitrosyl Mo complex, which was recently studied by Yonemura[30]. The complex is thermally stable and releases NO upon illumination with visible light (Scheme 11).

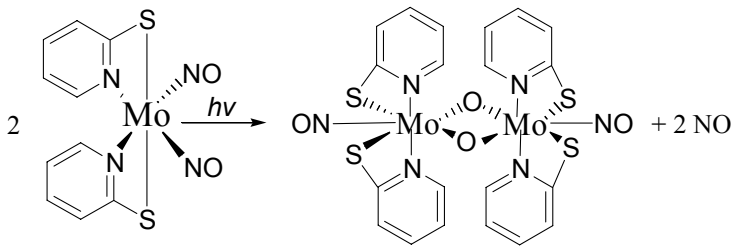

Scheme 11

(III) Organic photosensitive precursors. The class of Bis-*N*-nitroso-*p*-phenylenediamine derivatives developed by Namiki[31] holds a great promise. These

derivatives are thermally stable and release up to 2 equivalents of NO with high quantum yield (Φ_{NO} = 2). They posses very large extinction coefficients at 300 nm (13500 $M^{-1}cm^{-1}$) and their absorption tails to 425 nm (Scheme 12).

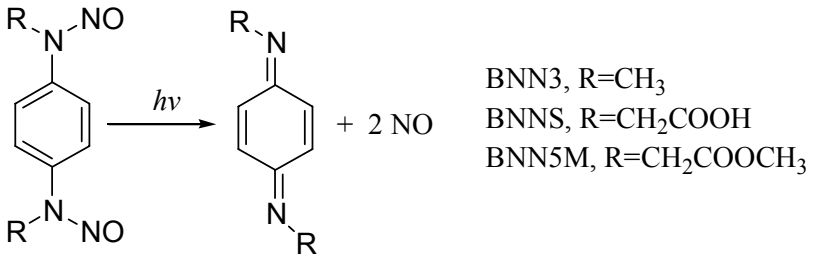

Scheme 12

Another noticeable advantage of this series is the fact that by changing the substituents R, different, tailor-made properties are achieved. For instance, BNN3 is readily incorporated in vascular smooth muscle cells and easily localised in lipids. On the contrary, BNN5M is membrane impermeable and once hydrolysed by cytosolyc esterases in the cell to BNN5Na, it remains inside.

1.1.2.4 Studying Protein Folding

Protein folding and especially the early events of it are poorly understood and very difficult to study. Most of the applied methods, namely stopped-flow mixing, hydrogen-deuterium exchange and site-directed mutagenesis have a time resolution of 0.1 ms. An interesting approach to study the complexity of protein folding processes was undertaken by Hansen and co-workers[32]. They studied the time-dependent changes of α-helix formation of the protein villin employing the benzoin ppg. The phototrigger was attached to the N-terminus of the peptide and the cysteine residue, thus forming a stable unfolded conformation. A short laser pulse cleaved the ppg and the refolding processes were followed by time-resolved photoacoustic calorimetry. The great promise that this approach holds is in the fact that no denaturant is used and the protein folding can be observed in natural environment.

1.1.2.5 Two Photon Excitation

Another approach in the photolysis of caged compounds is the two-photon excitation (2PE). This newly emerging technology is promising as it provides highly improved spatial control over the investigated processes on one hand and utilizes IR radiation as excitation source on the other hand, which has greater penetration depth and much lowered damaging effect on the biological tissues. In essence, this technique uses short laser pulses of IR radiation in the region between 700 nm and 1100 nm. Two photons are simultaneously absorbed by the chromophore, promoting the molecule to its excited state. In principal, every chromophore can be excited by this method, which essentially means that any of the available ppg's can be successfully photolysed. The dark photochemistry or the reaction sequence that follows the excitation is, in most cases, the same as if the molecule was excited with UV radiation. The probability of two-photon excitation is proportional to the square of the power of the laser pulse. Hence, photolysis occurs only in the focal point of the laser beam, thus allowing for a greater spatial control. The excitation volume can be as small as a femtoliter at a precisely controlled x,y,z-positioning. The development of ultra short tunable lasers and confocal microscopes greatly accelerates the implementation of this method in many research areas. However, a note of caution is necessary here. Many of the available ppg's suffer poor efficiency, when photolysed in this manner. A quantitative measure for their efficiency is the two-photon absorption cross-section δ_μ, given in GM (Göppert-Mayer = 10^{-50} cm^4 s $photon^{-1}$). A drawback of the 2PE is the fact that the laser power used in biological experiments should not exceed a certain limit (5-10 mW), above which a photodamage due to multiphoton absorption sets in. Multiphoton phototriggers with improved δ_μ will be needed and will play an increasing role in the exploration of cell physiology and other bio-relevant areas[8].

1.1.2.6 Solid-Phase Synthesis, Caged Peptides, DNA Microarray Fabrication and Photocleavable DNA Building Blocks

Solid-phase synthesis (SPS) is a widely recognized method used in organic synthesis. In particular, peptide synthesis is the area that makes the most use of it. In essence, a building block (often an amino acid) is attached to a polymer matrix and a second block is added. After coupling, the product is easily separated from the reaction mixture by simple procedures like washing and filtration. When repeated, this process leads to elongation of the peptide sequence from C- to the N-terminus. Peptides are moieties with a rich functionality and naturally, in order to achieve chemoselectivity during synthesis, protecting groups need to be used. Apart from the classical Fmoc and Boc methods, ppg's have been identified as being one of the best protecting strategies. They offer the advantage of being essentially orthogonal to all other protecting groups, as their deprotection does not require any chemical reagents. The 2-nitrobenzyl group and the p-hydroxyphenacyl group are commonly used ppg's in orthogonal protection of peptide synthesis. They have been used in protecting amino-, hydroxyl- and carboxyl groups (reviewed in [7]). An interesting concept concerning the orthogonality issue was proposed by Bochet and colleagues[33]. They showed that 2-nitrobenzyl alcohol derivatives react at different rates according to the irradiation wavelength. This approach is in its infancy but the ultimate goal would be a set of ppg's that are selectively removed by irradiation at different wavelengths.

Ppg's are used not only in the synthetic methodologies in SPS but also in preparing caged peptides. There have been many reports in the literature on peptides with elucidated structure-reactivity relationships. If the amino acids responsible for the biological activity of a peptide are known, a photocleavable group can be attached and decrease or fully block its activity. A short pulse of intense light removes the protection and renders the peptide active. An illustrative example was described by Tatsu and co-workers[34]. The authors prepared a caged derivative of Fmoc-Tyr using the 2-nitrobenzyl cage and successfully incorporated it in the amino acid sequence of neuropeptide Y (NPY). It is a 36 amino acid polypeptide found in both peripheral and central nervous systems. NPY is thought to play an important role in the processes of

blood pressure regulation, anxiety and feeding behaviour. The researchers showed that the binding affinity of caged NPY for the Y1 receptor was one or two orders of magnitude lower than that of intact NPY but increased to the value of the intact peptide within 7 μs upon irradiation with UV light. The structure of the caged tyrosine residue is shown in Figure 3.

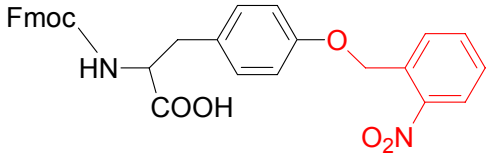

Figure 3. Caged tyrosine residue

A combination of SPS and photolithography, both relatively well developed methodologies, is called a microarray fabrication. In this technique protected building blocks are attached to a solid support and irradiated through a mask, thereby leaving some of the molecules unchanged and deprotecting others. The free functional groups are then made to react with other building blocks. Repetition of the irradiation through masks with different patterns and coupling steps leads to the desired set of products. Microarrays prepared by *in situ* synthesis are thus examples of spatially addressable combinatorial libraries. Quite a few ppg's are suitable for this type of light directed combinatorial synthesis, among which are the nitrobenzyl protecting group, dimethoxybenzoin group and nitrophenylpropyloxycarbonyl group. A good example is the 5-phenoxyphenyl-NPPpoc group. It exhibits a half time of deprotection of 16 s and a chemical yield of 98% that is superior to many other groups. Its structure is shown in Figure 4. The literature in the microarray methodology is copious and a good general review with many references is included in a recently published book[8].

Recently Dussy and colleagues[35] developed a new photocleavable DNA building block, comprising of a nucleic acid derived structure and the 2-nitrobenzyl cage. The photochemistry of a single-stranded DNA, modified with the photocleavable building block, showed that site specific breaks can be easily induced by irradiation with light above 360 nm. Their results are potentially applicable in several important research areas, such as studies of DNA strand break/repair processes and DNA topology. The authors incorporated the building block into oligonucleotides, which

were able to build stable DNA duplexes. The structure of the modified strand is shown in Figure 4.

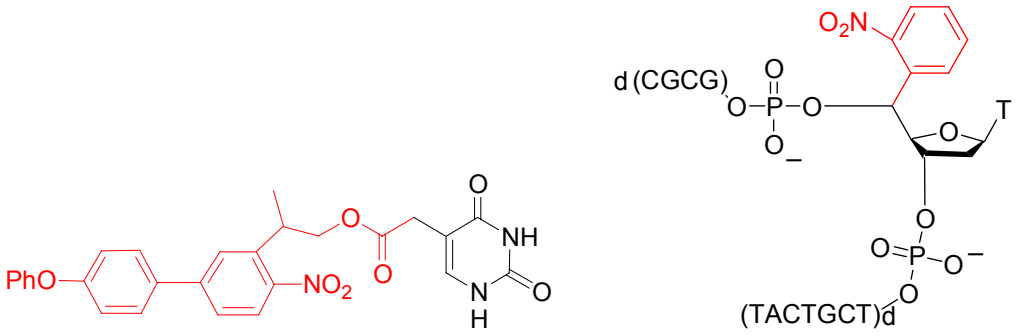

Figure 4. Left: 5-phenoxyphenyl-NPPpoc group;
right: Modified single-stranded DNA

The above selection of applications is arbitrary and does not cover all available applications. There are a number of smaller but not less important areas of research, where the ppg's are being extensively used. Some of them address drug delivery strategies, where a pharmacologically active substance is caged and delivered with spatial and temporal control to specific regions of the human body. These are some of the future challenges, in which photoremovable protecting groups will be playing crucial role.

1.2 Photochemistry of 5-methyl-1,4-naphthoquinone (MeNQ)

5-Methyl-1,4-naphthoquinone (**1**, Scheme 13) was synthesised more than 50 years ago by Diels-Alder addition of piperylene and *p*-benzoquinone [36]. In two later studies, Wirz and Kresge have investigated its photochemistry[37,38]. Excited 1,4-naphthoquinones are known for their reactivity towards many organic substrates. They abstract hydrogen atoms to form radicals, participate in 2+2 cycloaddition reactions and transport electrons[39, 40]. In water, 1,4-naphthoquinone forms water adducts via heterolytic reaction in the triplet excited state[41]. Interestingly, this photochemistry is fully suppressed in the case of **1**, because the 5-methyl group provides a very efficient deactivation channel via intramolecular hydrogen atom shift (**1**→**2**). The predominant process, operating with close to unit quantum efficiency, is intramolecular H-abstraction. The resultant photoenol **2** is formed within 2 ps after excitation, directly from the singlet excited state of **1** and no triplet population is observed. The rate of intersystem crossing in 1,4-naphthoquinone amounts to $1.1 \times 10^{11} s^{-1}$, whereas the photoenolization is at least 5-fold faster. In their study, Wirz and colleagues concluded that the enol formation is an adiabatic process, proceeding by a passage through a conical intersection of the lowest S_1 and S_0 hypersurfaces.

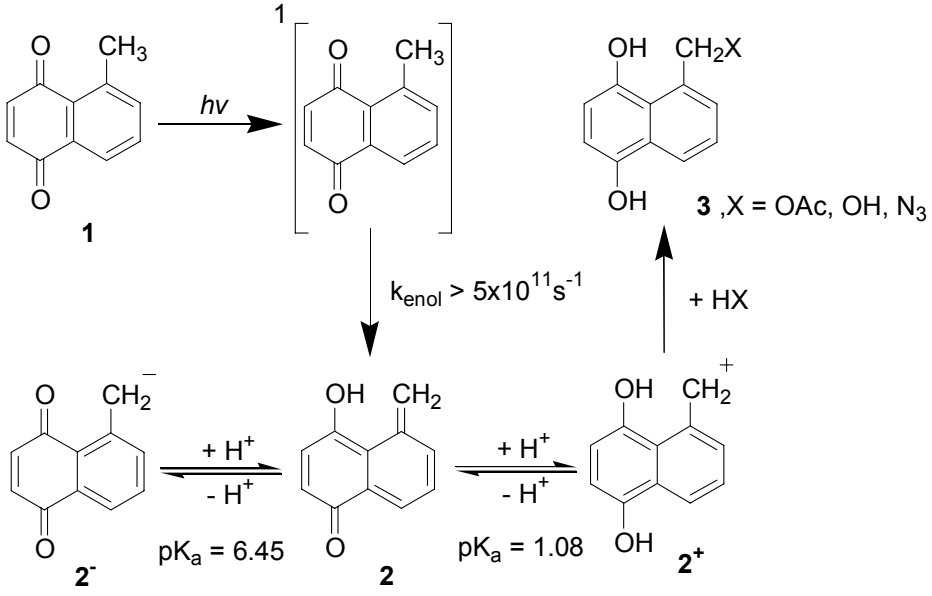

Scheme 13. Photochemistry of 5-methyl-1,4-naphthoquinone

4-Hydroxy-5-methylidene-1(5H)-naphthalenone **2** is persistent in rigid glasses at 77K and its absorption spectrum is shown in Figure 5 [37]. The authors discovered a solvent dependence of the back ketonization process (**2**→**1**). The reaction is retarded by more than three orders of magnitude upon going from cyclohexane to dimethylsulfoxide, suggesting that hydrogen bonding of the enolic proton by the solvent increases significantly the lifetime of **2**. In the present work, additional evidence on its structure, from time resolved FTIR experiments with similar systems, is presented (*vide infra*). **2** is an amphoteric intermediate (pK_a(**2**) = 6.45, pK_a(**2**$^+$) =1.08). In water protonation gives **2**$^+$ (detected by pump-probe experiments, 320 nm and 420 nm, $\tau = 10^{-8}$ s^{-1} in 1M $HClO_4$), which is later trapped by a nucleophile, giving 5-substituted-1,4-naphthalendiols **3**. Deprotonation yields the anionic species **2**$^-$, which in turn reacts with the starting material **1** and/or other species susceptible to a nucleophilic attack.

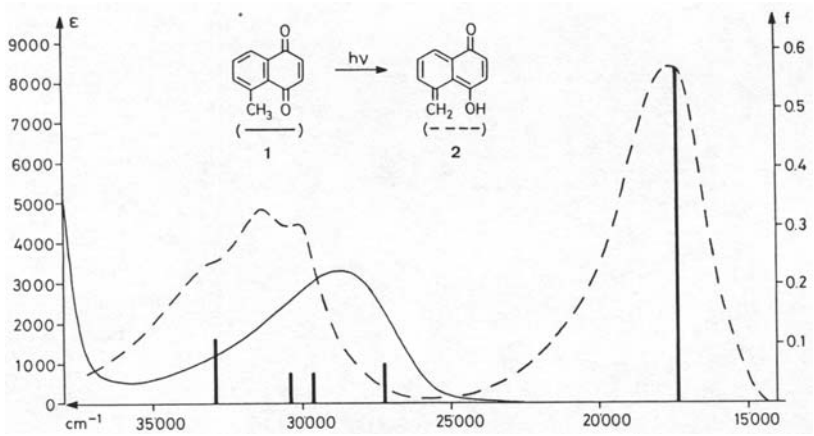

Figure 5. Absorption spectra of **1** (full line) and **2** (dashed line) at 77K.
Vertical bars indicate the oscillator strength predicted by PPP SCF CI calculations

It is rational to think that **2** and **2**$^+$ can be protonated on the benzylic carbon and not on the oxygen. It was shown that despite the huge thermodynamic bias in favour of carbon protonation (ca.100 kJ mol^{-1}), the process is kinetically driven and occurs predominantly at the oxygen atom. A number of facts have been put forward in favour of rate determining nucleophilic attack on the protonated species **2**$^+$. The fast protonation-deprotonation processes **2** + **H**$^+$ ↔ **2**$^+$ and **2** ↔ **2**$^-$ + **H**$^+$ can be considered as pre-equilibria and the rate constant of protonation amounts to (1.6 ± 0.5) x $10^{11}$$s^{-1}$.

2. Problem Statement

The main goal of the present work is to synthesise and study a novel photoremovable protecting group for acids and phosphates. Our idea is based on the photochemistry of 5-methyl-1,4-naphthoquinone (MeNQ), which is fairly well established and described in the introductory chapter of the present work. MeNQ undergoes a very efficient and fast photoenolization. We presumed that the same would occur if we extend the methyl substituent to ethyl, bearing a leaving group **X** at its terminus (Figure 6).

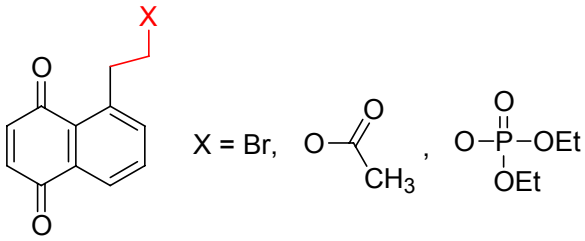

Figure 6. A new photoremovable protecting group for acids and phosphates.

We hoped to achieve a fast and efficient liberation of **X** due to a strong re-aromatization driving force of the photoenol **2** (Scheme 14). In the course of our work we discovered that the same idea was proposed by Banerjeee and co-workers[42]. The presence of a well characterized intermediate, exhibiting long-wavelength absorption, would allow for a direct observation of the actual release rates. Relatively high extinction coefficients of 1,4-naphthoquinones at 350 nm and absorption extending to the visible range of the spectrum would allow minimizing the harmful effect of UV radiation in possible biological applications. The 1,4-naphthoquinones are moderately soluble in aqueous media and we expected the same for our new derivatives.

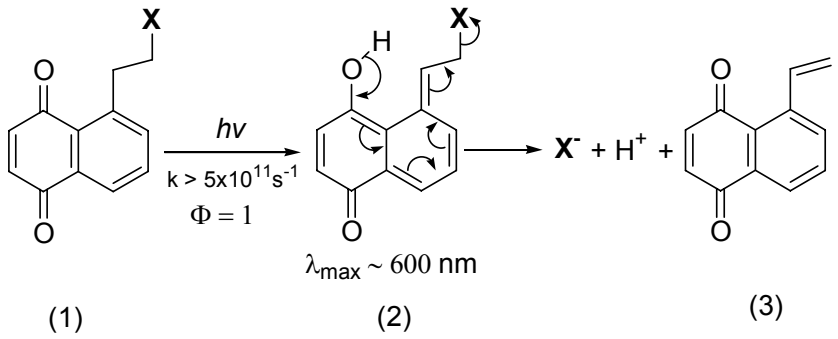

Scheme 14. Expected mechanism of liberation of the protected substrate HX

1. Synthesis of 5-substituted 1,4-naphthoquinones

Retrosynthetic analysis of the 5-substituted naphthoquinone moiety suggested that a convenient synthetic route to 5-(2-bromoethyl)-1,4-naphthoquinone (**BrNQ**), acetic acid 2-(5,8-dioxo-5,8-dihydronaphthalen-1-yl)-ethyl ester (**AcNQ**) and phosphoric acid 2-(5,8-dioxo-5,8-dihydro-naphthalen-1-yl)-ethyl ester diethyl ester (**PsNQ**) would include a Diels-Alder cycloaddition of an appropriately designed diene and p-benzoquinone, and a subsequent oxidative aromatization to yield the desired product (Scheme 15).

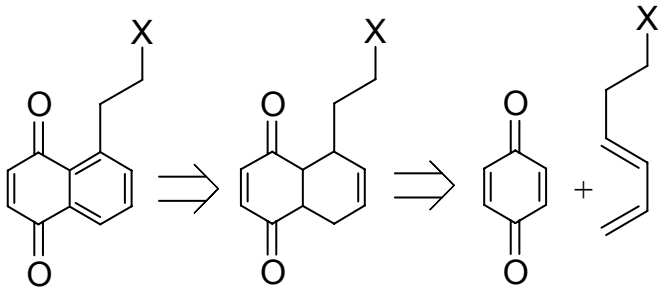

Scheme 15. Retrosynthetic analysis of the 5-substituted-1,4-naphthoquinone derivatives

The dienes, needed for the cyclization, were synthesized by using literature procedures with minor modifications. All reactions proceeded smoothly with satisfactory chemical yields. The next step ([4+2] cycloaddition) is a common reaction for constructing six-membered rings and usually proceeds with high yields. The last step required was an oxidation of the hydroquinone adduct. There are a number ways to carry out this reaction, some of which include oxidation with Br_2, air, DDQ or chloranil and with active MnO_2. The latter is rather simple from an experimental point of view [43]. Being an inorganic compound, not soluble in organic solvents, the oxidizing agent is conveniently removed from the reaction mixture and essentially no purification is needed. Finally, the expected photoproduct, namely 5-vinyl-1,4-naphthoquinone, was also synthesized using the same sequence but starting from commercially available 1,3,5-hexatriene. The following general schemes describe the synthetic pathways that were utilized in the present work (Scheme 16, 17, 18).

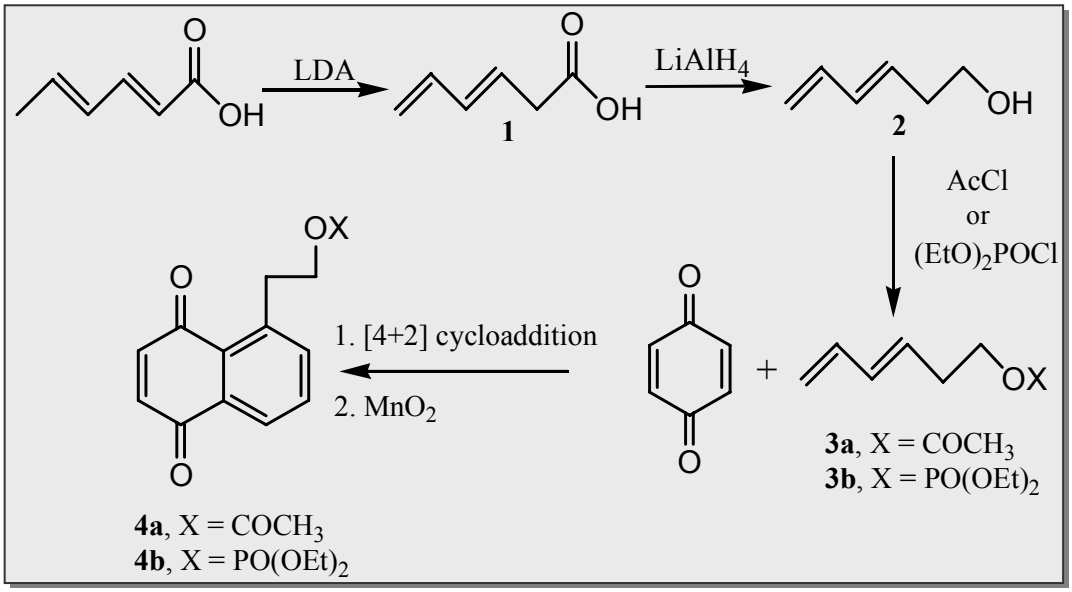

Scheme 16. Synthetic route to AcNQ (**4a**) and PsNQ (**4b**)

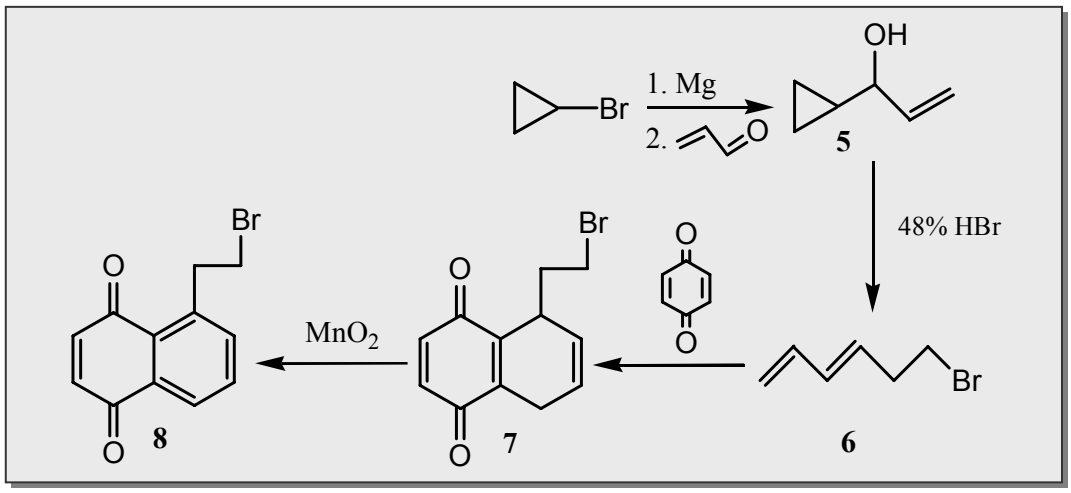

Scheme 17. Synthetic route to BrNQ (**8**)

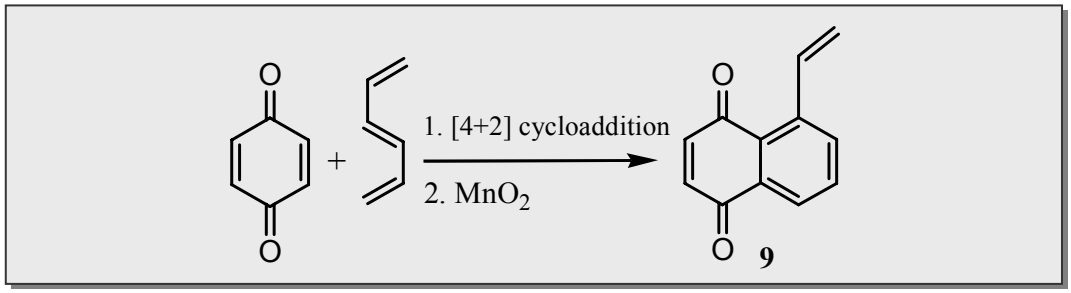

Scheme 18. Synthetic route to VinNQ (**9**)

1. Synthesis of hexa-3,5-dienoic acid (1)

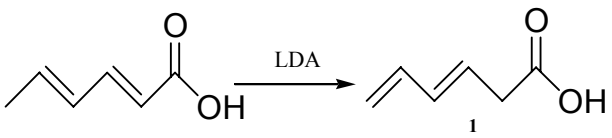

1

Compound **1** was synthesized according to the method of Stevens[44] with some minor changes. A solution of lithium diisopropylamid was prepared from solid LDA (4.25 g, 39.7 mmol) and abs. THF (60 ml) in a glove box under a nitrogen atmosphere. The solution was cooled to – 10^0 C and a suspension of sorbic acid (2 g, 17.9 mmol) in 10 ml abs. THF was added dropwise for one hour. The solution was stirred for an additional two hours at room temperature. The reaction was quenched with 60 ml of 3N HCl and extracted with 3 x 50 ml diethyl ether. The combined extracts were washed with water and saturated water solution of NaCl, and dried over $MgCO_3$. Evaporation of the solvent gave yellow oil.

Mol. formula / Mol. weight: $C_6H_8O_2$ / 112.13 g/mol
Yield: 1.8 g (90%).

^{1}H-NMR (400 MHz, $CDCl_3$, δ/ppm): 9.30 (*bs*., 1H, OH), 6.34 (*m,* 1H, H-5), 6.17 (*m*, 1H, H-4), 5.77 (*m*, 1H, H-3), 5.19 (*d*, *J*= 16.8, 1H, H-6a), 5.09 (*d*, *J*= 10.1, 1H, H-6b) 3.18 (*d*, *J* = 7.2, 2H, H-2).

^{13}C-NMR (100 MHz, $CDCl_3$, δ/ppm): 178.1(C-1), 136.6(C-5), 135.3(C-4), 125.1(C-3), 117.7(C-6), 38.0(C-2).

2. Synthesis of hexa-3,5-dien-1-ol (2)

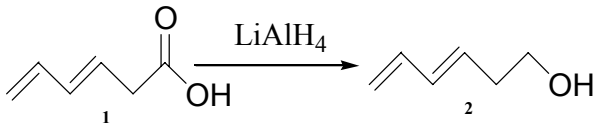

A solution of hexa-3,5-dienoic acid **1** (1 g, 9 mmol) in anhydrous diethyl ether (5 ml) was added dropwise to a suspension of lithium aluminum hydride (0.44 g, 12 mmol) in 10 ml dry diethyl ether. After the addition was completed, the reaction mixture was heated at reflux for 16 hours. The reaction was quenched by adding water in small portions and cooling the reaction mixture with ice. 2N sulfuric acid was added to the suspension until it dissolved. The two layers were separated and the aqueous one was extracted with 3 x 20 ml diethyl ether. The combined extracts were washed with water, $NaHCO_3$, saturated water solution of NaCl and dried over $MgCO_3$. Evaporation of the solvent gave 0.9 g crude brownish material, which was purified by high vacuum distillation (10^{-3} Torr).

Mol. formula / Mol. weight: $C_6H_{10}O$ / 98.14 g/mol
Yield: 0.8 g (91.4%).

^{1}H-NMR (400 MHz, $CDCl_3$, δ/ppm): 6.33 (*dt*, *J*= 10.2, *J*= 16.9, 1H, H-5), 6.15 (*dd*, *J*= 10.5, *J*= 15.2, 1H, H-4), 5.68 (*dt*, *J*= 7.2, *J*= 15.2, 1H, H-3), 5.14 (*d*, *J*= 16.8, 1H, H-6a), 5.01 (*d*, *J*= 10.5, 1H, H-6b), 3.69 (*t*, *J*=6.3, 2H, H-1), 2.36 (*q*, *J*= 12.8, *J*= 6.4, 2H, H-2), 1.6 (*bs*, 1H, OH).

^{13}C-NMR (100 MHz, $CDCl_3$, δ/ppm): 136.8(C-5), 133.8(C-3), 130.5(C-4), 116(C-6), 62(C-1), 36.3 (C-2).

IR (CD_3CN, $\tilde{\nu}$ /cm^{-1}): 3610, 2950, 2900, 1600.

3. Synthesis of acetic acid hexa-3,5-dienyl ester (3a)

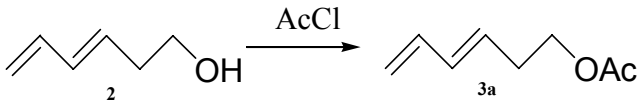

A solution of **2** (0.3 g 3.06 mmol) and (0.5 g, 5 mmol) Na_2CO_3 in 5 ml dry benzene was heated to 50 ^{0}C and acetyl chloride (0.39 g, 5mmol) was added dropwise at a sufficient rate to maintain a gentle reflux. After the addition was completed the temperature was increased to 70 ^{0}C for one hour. The reaction was quenched with 10 ml of water and the organic layer was separated and washed with water, $NaHCO_3$ and saturated water solution of NaCl. After being dried over night over $MgCO_3$, the solvent was evaporated, yielding 0.3 g of crude **3a**.

Mol. formula / Mol. weight: $C_8H_{12}O_2$ / 140.18 g/mol
Yield: 0.3 g (71%).

^{1}H-NMR (400 MHz, $CDCl_3$, δ/ppm): 6.31 (*m*, 1H, H-5), 6.15 (*q*, 1H, H-4), 5.68 (*m*, 1H, H-3), 5.10 (*d*, *J*=16.5, 1H, H-6a), 5.01 (*d*, *J*= 9.6, 1H, H-6b), 4.15 (*t*, *J*= 6.4, 2H, H-1), 2.36 (*q*, *J*=19.9, *J*= 2.4, 2H, H-2), 2.02 (*s*, 3H, CH_3).

^{13}C-NMR (100 MHz, $CDCl_3$, δ/ppm): 171.6(CO), 138.7(C-5), 133.8(C-3), 130.1(C-4), 116.4(C-6), 64(C-1), 32.3(C-2), 21.3(CH_3)

4. Synthesis of phosphoric acid diethyl ester hexa-3,5-dienyl ester (3b)

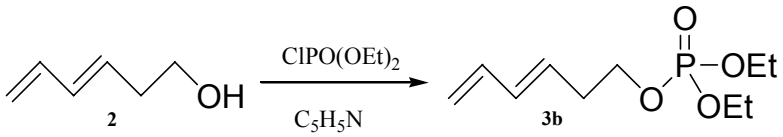

Diene **2** (0.5 g 5.1 mmol) and pyridine (0.79 g, 10.0 mmol) were mixed in 5 ml dry THF and cooled down to 0 ^{0}C. Diethylchlorphosphate (1.20 g, 7.0 mmol) was added dropwise for 10 min. After the addition was completed, the reaction mixture was stirred for an additional hour at room temperature. A white precipitate of pyridinium hydrochloride was formed. In order to remove it from the reaction mixture, cold diethylether (3 x 10 ml) was added, filtered and the mother liquors were concentrated under vacuum. The product was a dense yellowish oil. Its purity was sufficient and no additional purification was needed.

Mol. formula / Mol. weight: $C_{10}H_{19}O_4P$ / 234.23 g/mol
Yield: 1.2 g (87%)
TLC: $R_f = 0.3$ (Si-gel, Et_2O/n-C_6H_{14} 1:1)

^{1}H-NMR (400 MHz, $CDCl_3$, δ/ppm): 6.29 (*m*, 1H, H-5), 6.13 (*q*, 1H, H-4), 5.65 (*m*, 1H, H-3), 5.12 (*d*, *J*=16.8, 1H, H-6a), 5.01 (*d*, *J*= 10, 1H, H-6b), 4.09 (m, 6H, H-1 and $\underline{CH_2}CH_3$), 2.46 (*q*, *J*=6.8, 2H, H-2), 1.32 (*t*, *J*=7.1, 6H, CH_3).

^{13}C-NMR (100 MHz, $CDCl_3$, δ/ppm): 136.63(C-5), 133.76(C-3), 129.0(C-4), 116.18(C-6), 66.56(*d,* $\underline{CH_2}CH_3$), 63.70(*d,* C-1), 33.45(*d,* C-2), 16.10(*d,* CH_3)

^{31}P-NMR (162 MHz, $CDCl_3$, δ/ppm) - 4.01

MS(FAB,m/z): $M^{+\cdot}$ 235(52), 155(74), 127(20), 99(29), 81(100), 55(11).

5. Synthesis of acetic acid 2-(5,8-dioxo-5,8-dihydronaphthalen-1-yl)-ethyl ester (4a)

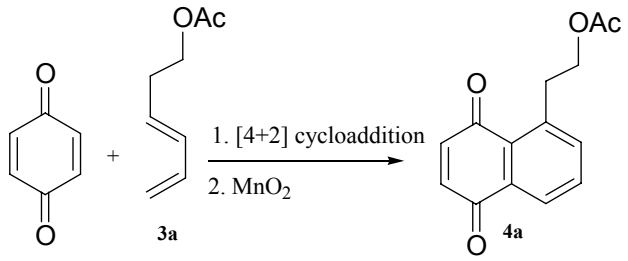

A suspension of p-benzoquinone (0.8 g, 7.4 mmol), acetic acid hexa-3,5-dienyl ester **3a** (1.2 g, 8.6 mmol) and 5 ml benzene was stirred for 40 hours in the dark at ambient temperature. After a period of *ca.* 24 hours, the p-benzoquinone fully dissolved. The Diels-Alder adduct was not isolated. After 40 hours stirring, a 10-fold excess of active MnO_2 was added and the reaction mixture was stirred for an additional 1.5 hours at room temperature. Filtration under vacuum and evaporation of the solvent furnished aromatized crude product **4a**, which was purified by flash chromatography.

Mol. formula / Mol. weight: $C_{14}H_{12}O_4$ / 220.12 g/mol

Yield: 1.49 g (75.5%)

TLC: $R_f = 0.12$ (Si-gel, n-C_6H_{14}/Et_2O = 2:1)

^{1}H-NMR (500 MHz, $CDCl_3$, δ/ppm): 7.93 (*dd*, 1H, *J*=7.6, J=1.4, H-8), 7.66 (*t*, 1H, *J* = 7.6, H-7), 7.59 (*dd*, 1H, *J*=7.7, *J*=1.4, H-6), 6.90 (*d*, 1H, *J* = 10.4, H-2), 6.88 (*dd*, 1H, *J* = 10.4, H-3), 4.24 (*t*, 2H, *J*=6.6, $\underline{C}H_2OAc$), 3.37 (*t*, 2H, *J*=6.6, $\underline{C}H_2CH_2OAc$), 1.91 (*s*, 3H, CH_3).

^{13}C-NMR (125 MHz, $CDCl_3$, δ/ppm): 188.6(C-4), 187.0(C-1), 173.17($\underline{C}$OMe), 141.6(C-3), 141.5(C-5), 139.4(C-6), 138.0(C-2), 134.5(C-7), 134.4(C-9), 130.4 (C-10), 126.8(C-8), 64.94($\underline{C}H_2OAc$), 34.37($\underline{C}H_2CH_2OAc$), 21.15(CH_3).

Elemental analysis:	**Calculated:**	**Found:**
	C = 68.85 %	67.97 %
	H = 4.95 %	5.87 %
	O = 26.20 %	25.50 %

6. Synthesis of phosphoric acid 2-(5,8-dioxo-5,8-dihydronaphthalen-1-yl)-ethyl ester diethyl ester (4b)

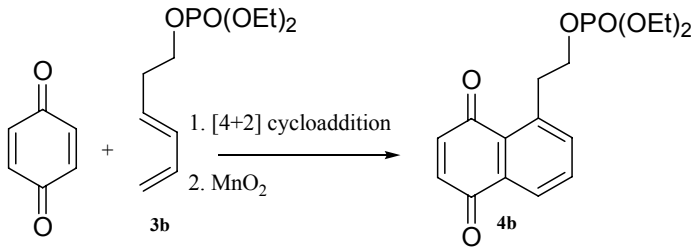

A suspension of p-benzoquinone (0.4 g, 3.7 mmol) and phosphoric acid diethyl ester hexa-3,5-dienyl ester (1.1 g, 4.1 mmol) in 4 ml of benzene was stirred in the dark at ambient temperature. The p-benzoquinone fully dissolved after approximately 24 hours. The reaction mixture was stirred continuously for 40 hours until most of the p-benzoquinone was consumed (by TLC). The apparent instability of the Diels-Alder adduct rendered us to conduct the oxidative step without isolating. A 10-fold excess of activated MnO_2 (3.22 g, 37 mmol) suspended in 10 ml dry benzene was added and the reaction mixture was stirred for additional 1.5 hours at room temperature. The suspension was then filtered under reduced pressure and the precipitate was washed with chloroform. Evaporation of the solvent furnished aromatized crude product **4b**, which was purified by column chromatography.

Mol. formula / Mol. weight: $C_{16}H_{19}O_6P$ / 338.29 g/mol

Yield: 0.690 g (55%)

TLC: $R_f = 0.43$ (Si-gel, CH_2Cl_2/MeOH 20:1)

^{1}H-NMR (500 MHz, $CDCl_3$, δ/ppm): 8.05 (*dd*, 1H, *J*=6.8, *J*=1.7, H-8), 7.64 (*t*, 1H, *J* = 7.5, H-7), 7.60 (*dd*, 1H, *J*=7.8, *J*=1.7, H-6), 6.92 (*d*, 1H, *J* = 10.4, H-2), 6.88 (*dd*, 1H, *J* = 10.4, H-3), 4.28 (*t*, 2H, *J*=6.5, $\underline{CH_2}OPO(OEt)_2$), 4.02 (*t*, 2H, *J*=6.5, $\underline{CH_2}CH_3$), 3.52 (*t*, 2H, *J*=6.3, $Ar\underline{CH_2}CH_2$), 1.27 (*t*, 3H, *J*=6.6, CH_3).

^{13}C-NMR (125 MHz, $CDCl_3$, δ/ppm): 187.0(C-4), 185.1(C-1), 140.4(C-3), 140.1(C-5), 138.6(C-6), 137.1(C-2), 133.6(C-9), 133.2(C-7), 129.4(C-10), 126.4(C-8), 66.9(*d*, $\underline{CH_2}OP$), 63.7 (*d*, $\underline{CH_2}CH_3$), 35.7($Ar\underline{CH_2}CH_2$), 16.1(*d,* CH_3).

^{31}P-NMR (162 MHz, $CDCl_3$, δ/ppm) - 4.1

MS (FAB, m/z (rel. intensity)): $M^{+\cdot}$ 339(15), 237(42), 185(100), 155(51), 55(53).

7. Synthesis of 1-cyclopropyl-prop-2-en-1-ol (5)[45]

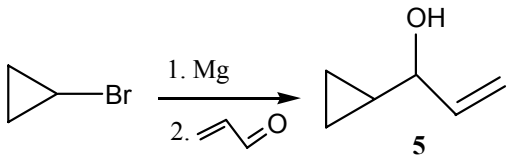

5

Cyclopropyl bromide (15 g, 0.125 mol) in 35 ml of dry THF was added dropwise to magnesium (4.23 g, 0.5 mol) in 100 ml dry THF under argon at a rate sufficient to maintain a gentle reflux. The mixture was stirred for one hour after the completion of the addition. The solution of the formed Grignard reagent was then cooled to 0 ^{o}C and acrolein (6.9 ml, 0.106 mol) in 35 ml dry THF was added dropwise. The mixture was stirred over night at ambient temperature and quenched with H_2O and 10% aq. $NaHSO_3$. The crude cyclopropylvinyl carbinol was extracted with 3 x 60 ml diethyl ether. The combined extracts were washed with 25 ml distilled water, saturated water solution of NaCl, and dried over Na_2SO_4. Evaporation of the solvent under reduced pressure gave colorless liquid.

Mol. formula / Mol. weight: $C_6H_{10}O$ / 98.06 g/mol
Yield: 3.1g (25%).

^{1}H-NMR (400 MHz, $CDCl_3$, δ/ppm): 5.91 (*m*, 1H, H-1), 5.22 (*td*, *J*=18.7, *J*=1.7, 1H, H-3b), 5.07 (*td*, *J*=11.3, *J*=1.7 1H, H-3a), 3.45 (*t*, 1H, H-1), 1.83 (*bs,* 1H, OH), 0.97 (*m,* 1H, H-1'), 0.51 (*m*, 2H, H-2a'), 0.28 (*m*, 2H, H-2b').

^{13}C-NMR (100 MHz, $CDCl_3$, δ/ppm): 140.1(C-2), 115.0(C-3), 77.1(C-1), 17.7(C-1'), 3.4(C-2'), 2.3(C-3').

MS (70eV, m/z): $M^{+\cdot}$ 98 (2), 70 (100).

8. Synthesis of 1-bromo-3,5-hexadien (6)[45]

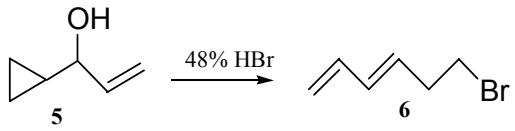

1.5 g (15.3 mmol) of alcohol **5** were cooled in an ice bath and 48% aq. hydrobromic acid (15 ml, 27 mmol) was added dropwise with stirring for 3 minutes. The mixture was stirred for an additional 5 minutes and then was diluted with water. The crude bromide was extracted with 3 x 45 ml diethyl ether and the combined extracts were washed with water, aq. solution of $NaHCO_3$, saturated NaCl and dried over $MgSO_4$. Evaporation of the solvent gave 1.87 g of **6**.

Mol. formula / Mol. weight: C_6H_9Br / 161.05 g/mol
Yield: 1.87g (74.8%)

^{1}H-NMR (400 MHz, $CDCl_3$, δ/ppm): 6.31 (m, 1H, H-5), 6.13 (q, 1H, H-4), 5.68 (m, 1H, H-3), 5.17(*d*, *J*= 16.5, 1H, H-6a), 5.05 (*d*, *J*= 9.6, 1H, H-6b), 3.39 (*t*, 2H, H-1), 2.66 (*q*, *J*= 19.9, *J*= 2.4, 2H, H-2).

^{13}C-NMR (100 MHz, $CDCl_3$, δ/ppm): 136.95 (C-5), 134.01 (C-3), 131.12 (C-4), 117.02 (C-6), 36.22 (C-2), 32.39 (C-1).

MS (70eV, m/z): 162 (20), 81 (100), 67 (30), 53 (30), 41 (50).

UV/VIS: λ_{max} **(cyclopentane):** 226 nm.

9. Synthesis of 5-(2-bromoethyl)-4a,5,8,8a-tetrahydro-1,4-naphtho-quinone (7)

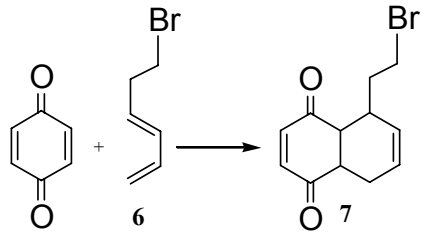

A mixture of p-benzoquinone (0.8 g, 7.4 mmol) and 6-bromo-1,3-hexadien **6** (1.2 g, 8.6 mmol) in 5 ml of benzene was stirred for 40 hours in the dark at ambient temperature. After this period the solvent was removed at reduced pressure and the resultant dark yellow oil was recrystallized from diethyl ether at low temperature. The pure adduct **7** was isolated by vacuum filtration as white amorphous crystals and stored at – 24 ^{o}C.

Mol. formula / Mol. weight: $C_{12}H_{13}O_2Br$ / 269.15 g/mol
Yield: 0.79 g (39.5%)
TLC: R_f = 0.55 (Si-gel, n-C_6H_{14}/C_2H_5OH 16:1)

^{1}H-NMR (400 MHz, $CDCl_3$, δ/ppm): 6.64 (*q*, *J*= 3.0, 2H, H-2, H-3), 5.68 (*m*, 2H, H-6, H-7), 3.45 (*t*, J = 3.3, 2H, CH_2Br), 3.42 (*m*, 1H, H-9), 3.24 (*m*, 1H, H-10), 2.68 (*m*, 1H, H-5), 2.25 (*m*, 4H, $C\underline{H_2}CH_2Br$, H-8).

^{13}C-NMR (100 MHz, $CDCl_3$, δ/ppm): 200.7, 199.9, 141.3, 138.7, 128.7, 124.8, 49.3, 48.4, 35.5, 35.1, 32.2, 25.8.

MS (70 eV, m/z): M^+ 268.1(10.2), 270.0(10.1), (M^+-Br) 188.1(27.2), 171.1 (5.69) 161.1(100), 131.1(12.1), 115.1(15.2), 77(9.5), 51(4.8).

mp.: decomposed before melting

The cycloadduct **7** is unstable at room temperature. It undergoes a slow isomerization to **7a** (Scheme 19). Addition of traces of a strong acid to a solution of **7** in acetonitrile gives rise to an absorption band in the UV-spectrum, with a maximum at 295 nm, identical with the absorption of 2,3-dimethyl-p-hydroquinone.

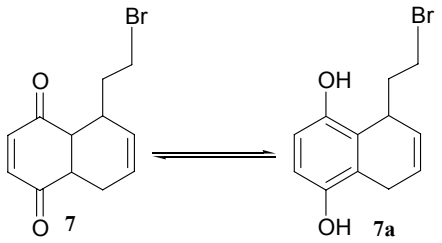

Scheme 19

Mol. formula / Mol. weight: $C_{12}H_{13}O_2Br$ / 269.15 g/mol

^{1}H-NMR (400 MHz, $CDCl_3$, δ/ppm): 6.60-6.68 (2H, q), 5.92-6.08 (2H, m), 4.43 (1H, s), 4.33 (1H, s), 3.80 (1H, m), 3.20-3.50 (3H, m), 3.02-3.12 (1H, m), 2.20 (2H, t).

^{13}C-NMR (100 MHz, $CDCl_3$, δ/ppm): 150.1, 142.3, 128.1, 125.4, 113.5, 113.2, 39.4, 33.9, 31.5, 24.9.

UV/VIS: λ_{max} **(acetonitrile):** 295 nm

mp.: decomposed before melting

10. Synthesis of 5-(2-bromoethyl)-1,4-naphthoquinone (8)

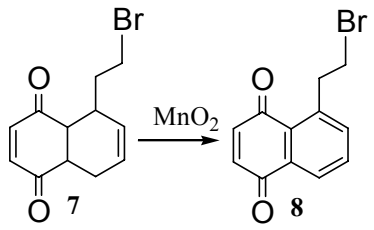

The oxidative dehydrogenation of cycloadduct **7** was successfully carried out using active MnO_2 by the method of Mashraqui and Keehn [43]. Mashraqui and coworkers have carried out this reaction in refluxing benzene and azeotropically removing of water. In our hands these conditions were not appropriate because a substantial amount of dehydrobrominated product was formed. Thus, adduct **7** (0.1 g, 0.37 mmol) and a 10-fold excess of active MnO_2 were stirred in 3ml dry benzene for 1.5 hours, at room temperature. The reaction mixture was filtered and the precipitate washed with 15-20 ml hot benzene and chloroform. Evaporation of the solvent furnished aromatized crude product **7,** which was purified by flash chromatography.

Mol. formula / Mol. weight: $C_{12}H_9O_2Br$ / 265.92 g/mol
Yield: 71.1 mg (71.1%).
TLC: R_f = 0.61 (Si-gel,n-C_6H_{14}/C_2H_5OH 5:1).

^{1}H-NMR (500 MHz, $CDCl_3$, δ/ppm): 8.04 (*dd*, *J*=7.7, *J*=1.3, 1H, H-8), 7.62 (*t*, *J* = 7.7, 1H, H-7), 7.53 (*dd*, *J*=7.7, *J*=1.2, 1H, H-6), 6.88 (*d*, *J* = 10.3, 1H, H-2), 6.84 (*d*, *J* = 10.3, 1H, H-3), 3.61 (*m*, 4H, $C\underline{H_2}C\underline{H_2}Br$).

^{13}C-NMR (125 MHz, $CDCl_3$, δ/ppm): 186.9(C-4), 185.0(C-1), 141.0(C-5), 140.3(C-2), 138.5(C-6), 137.2(C-3), 133.7(C-9), 133.3(C-7), 129.3(C-10), 126.7(C-8), 38.1($\underline{C}H_2CH_2Br$), 32.4($\underline{C}H_2Br$).

MS (70eV, m/z): $(M^+-Br)^{\cdot}$ 185(100), 171(27), 128(18), 102(10).
MS(C.I. , m/z): M^+ 267(25), 265(24), (M^+-Br)185(71), 136(48),73(52), 57(100).
mp: decomposed before melting

11. Synthesis of 5-vinyl-1,4-naphthoquinone (9)

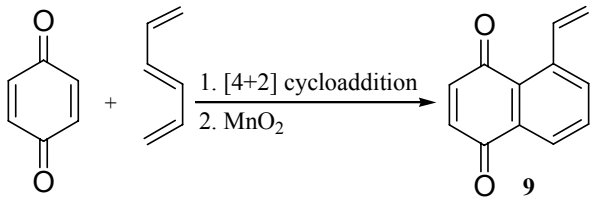

p-Benzoquinone (0.108 g, 1 mmol, 1,3,5-hexatriene (0.25 g, 3.12 mmol) and 4 ml benzene were stirred for 3 hours at 60 ^{0}C. The mixture was allowed to cool down to room temperature and 10-fold excess of active MnO_2 (0.87 g, 10 mmol) was added. The reaction mixture was stirred for additionally 1.5 hours at room temperature and filtered under reduced pressure. The MnO_2 was washed with hot chloroform. Evaporation of the solvent furnished aromatized crude product **9**, which was purified by flash chromatography

Mol. formula / Mol. weight: $C_{12}H_8O_2$ / 184.92 g/mol
TLC: R_f = 0.55 (Si-gel, C_6H_{14}:Et_2O=5:1).
Yield: 70 mg (71.4%)

^{1}H-NMR (500 MHz, $CDCl_3$, δ/ppm): 8.09 (*dd*, *J*=7.7, *J*=1.4, 1H, H-8), 7.82 (*dd*, *J*=7.7, *J*=1.4, 1H, H-6), 7.69 (*t*, *J*=7.7, 1H, H-8), 7.73 (*dd*, *J*=17.5, *J*=11, 1H, C<u>H</u>CH_2), 6.94 (*d*, *J*=10.3, 1H, H-2), 6.92 (*d*, *J*=10.3, 1H, H-3), 5.67 (*dd*, *J* =17.4, *J* =1.4, 1H, CHC<u>H</u>$_2$), 5.47 (*dd*, *J* =17.4, *J* =1.4, 1H, CHC<u>H</u>$_2$).

^{13}C-NMR (125 MHz, $CDCl_3$, δ/ppm): 186.7(C-4), 185.0(C-1), 140.6(C-9), 140.4(C-3), 137.0(C-2), 137.0(<u>C</u>HCH_2), 136.4(C-5), 134.0(C-6), 133.4(C-7), 126.7(C-8), 127.9(C-10), 118.3(CH<u>C</u>H_2).

MS (70eV, m/z): $M^{+\cdot}$ 184(50), 183(100), 155(35).

mp. : 82-84 ^{0}C

4. Photochemical Studies

Continuous irradiation: Solutions of 5-(2-bromoethyl)-1,4-naphthoquinone (**BrNQ**), acetic acid 2-(5,8-dioxo-5,8-dihydronaphthalen-1-yl)-ethyl ester (**AcNQ**) and phosphoric acid 2-(5,8-dioxo-5,8-dihydronaphthalen-1-yl)-ethyl ester diethyl ester (**PsNQ**) were irradiated with monochromatic light at either 254, 313 or 365 nm. The progress of the photolysis was followed by UV-VIS spectroscopy and the final spectrum was compared with the spectrum of an independently synthesized sample of 5-vinyl-1,4-naphthoquinone (**VinNQ**). The experiments were performed in neutral water, in buffered water solutions (pH = 7.8 – 8.1), dilute perchloric acid and acetonitrile (Table 1).

Solvent	Experiment №		
	BrNQ	**PsNQ**	**AcNQ**
H_2O	4.1.1.1	4.2.1.1	4.3.1.1
CH_3CN	4.1.1.2	4.2.1.2	4.3.1.2
10^{-2} M $HClO_4$	4.1.1.3	4.2.1.3	4.3.1.3
Buffer (pH = 8.1)	4.1.1.4	4.2.1.4	4.3.1.4

Table 1. Photolysis experiments performed in different solvents

Product studies: HPLC analysis of the photolysis mixture was used to follow the progress of the irradiation and some of the photoproducts were identified by co-injection with authentic materials. In several cases preparative irradiation of 5-10 mg of starting material was performed and the photoproducts were isolated and identified by standard analytical techniques (NMR, GC-MS, MS).

Laser flash photolysis experiments were performed in acetonitrile and water. They helped us identify transient intermediates and measure the rate constants of release of the protected substrate.

Time-resolved FTIR was used to obtain structural information on the reaction intermediates.

Quantum efficiencies of liberating the protected substrates, being important characteristics of a ppg, were measured either spectrophotometrically or by HPLC.

4.1 Photorelease from 5-(2-bromoethyl)-1,4-naphthoquinone

4.1.1 Continuous Irradiation and Product Studies

4.1.1.1 In Water

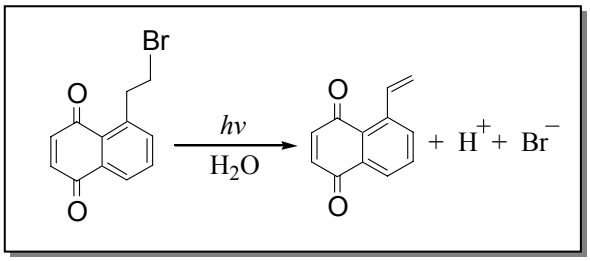

BrNQ was irradiated at 313 or 365 nm and the progress of the photoreaction was followed by recording UV-VIS spectra at different irradiation times (Figure 7). According to the absorption spectra, the photolysis afforded the expected 5-vinyl-1,4-naphthoquinone (VinNQ). UV-VIS monitoring of the reaction revealed a uniform and clean conversion, exhibiting several isosbestic points at 225, 238, 292 and 371 nm. The spectrum of authentic VinNQ is shown in blue. When compared with the spectrum taken after 75 s of irradiation, it clearly indicates that the reaction yields one major product. Preparative photolysis followed by NMR and GS-MS analysis unequivocally proved the presence of VinNQ as a single photoproduct.

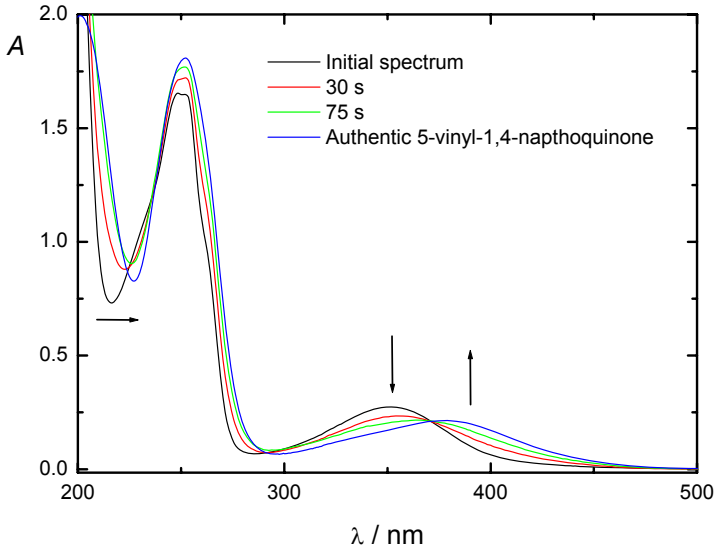

Figure 7. BrNQ irradiated at 365 nm in water. Black arrows indicate the change of absorbance during the irradiation period

4.1.1.2 In Acetonitrile

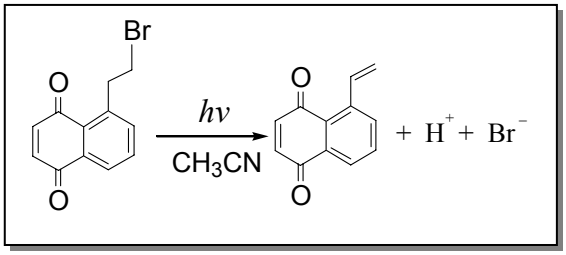

At short irradiation times the photo transformation proceeded cleanly, exhibiting several isosbestic points. Up to 10 s of irradiation an increase of absorbance around 380-400 nm was observed. Later, the reaction progressed mainly with an increase in the region of 320-340 nm. Apparently, the acid released in the beginning of the process played a role in later stages of the photolysis. Interestingly, similar behavior was absent in water. However, preparative irradiation in acetonitrile was carried out and showed one major photoproduct, namely VinNQ. Some additional signals in the NMR spectrum indicated other by-products but their amounts were not sufficient for characterization.

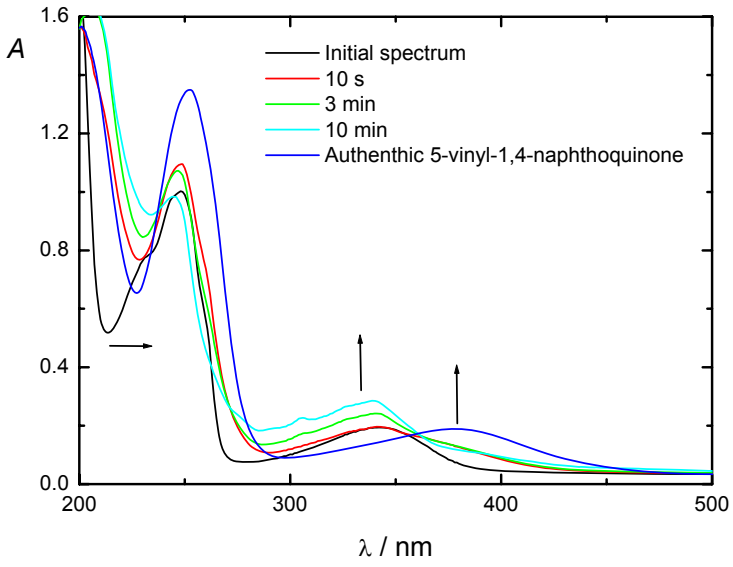

Figure 8. BrNQ irradiated at 365 nm in acetonitrile. Black arrows indicate the change of absorption during the irradiation period

4.1.1.3 In Dilute Perchloric Acid

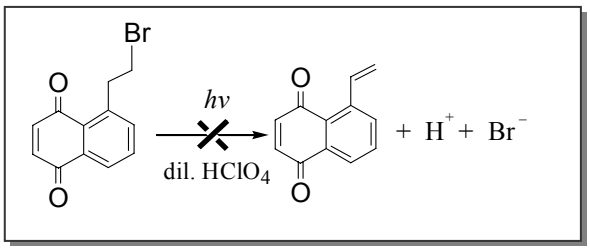

The absorption changes upon irradiation of BrNQ in 0.01 M $HClO_4$ indicated an efficient and uniform conversion of the starting material. The spectral changes showed isosbestic points at 247, 278, and 347 nm (Figure 9). The end spectrum differed substantially from the spectrum of VinNQ and was very similar to the spectrum of naphthalene-1,4-diol[38]. TLC of the irradiated solution showed a mixture of 5-7 products, some of which were unstable to oxygen and/or to Si-gel, consistent with the general instability of naphthalene-1,4-diols towards oxidation. Additional evidence for the formation of naphthol derivatives was the constantly increasing blue luminescence as the irradiation progressed. Preparative photolysis and product analysis were not undertaken since this was done in the case of AcNQ and the spectral changes are qualitatively the same. (see Experiment 4.1.3.1).

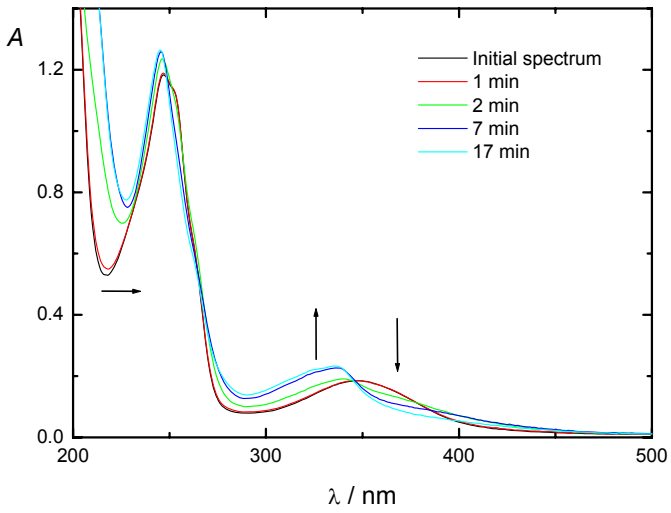

Figure 9. BrNQ irradiated at 365 nm in dilute $HClO_4$

2.1.1.4 In Buffered Aqueous Solution

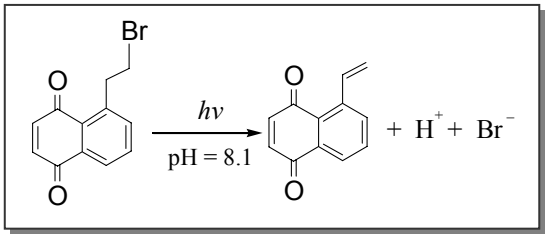

When photolysed in slightly basic water solution (borate buffer, pH=8.1), BrNQ exhibited practically the same behavior as in the case of neutral water solution (Figure 10). Since the photoproducts in water had already been identified (exp. 4.1.1.1) as VinNQ and HBr, product analysis was not carried out. Experiments in basic aqueous solutions are generally difficult, because the 1,4-naphthoquinone chromophore is chemically unstable towards bases.

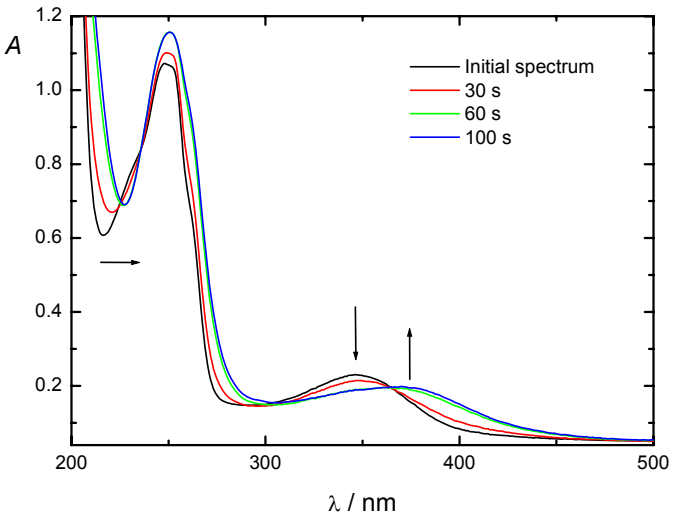

Figure 10. BrNQ irradiated at 313 nm in borate buffer

4.1.2 Laser Flash Photolysis

Laser flash photolysis of BrNQ in acetonitrile gave a strong transient signal in the range of 450 nm to 650 nm, λ_{max}= 560 nm, (Figure 11). The transient absorption was formed within the duration of the laser pulse (ca. 25 ns). Based on previous work[37] this signal was assigned to a photoenol formed as a result of fast H-atom transfer of one of the methylene protons to the adjacent carbonyl group of the 1,4-naphtohoquinone moiety. The quantum efficiency of this primary photochemical process was not measured, but comparison between the intensity of the signal produced by the parent MeNQ (see introduction: "Photochemistry of 5-methyl-1,4-naphthoquinone") and BrNQ, suggested that the photoenolization occurs very efficiently.

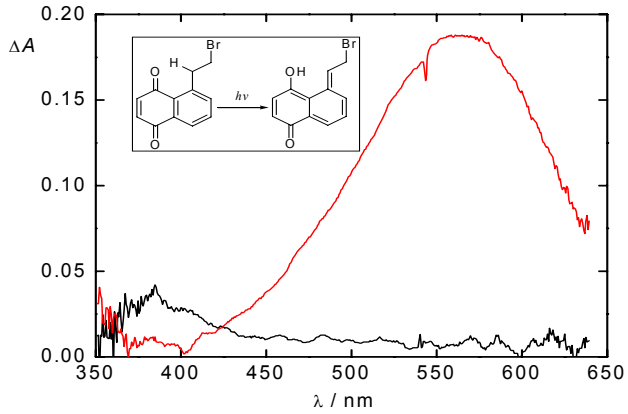

Figure 11. Transient absorption spectra of BrNQ in acetonitrile: — 30 ns and — 150 µs delay after excitation. The inset shows the [1,5]-hydrogen shift to the carbonyl group upon irradiation.

The signal observed at 550 nm decayed to zero and another weak transient, centered at 385, was formed concomitantly. Transient spectra taken at longer delay times after the laser flash proved that the absorption at 385 nm is stable indefinitely (> 100 s). It was attributed to the product of elimination, VinNQ. This was confirmed by the spectral changes associated with the appearance of VinNQ, observed in the steady state photolysis experiments.

Kinetic traces recorded at 570 nm and 385 nm are shown in Figure 12. Kinetic analysis by a least-squares procedure showed that the 570-nm-transient decays with the same rate constant as the growth at 385 nm is formed. (Table 2). Small

differences in the rates can be attributed to uncertainties associated with the biexponential fit of the relatively weak absorption growth at 385 nm.

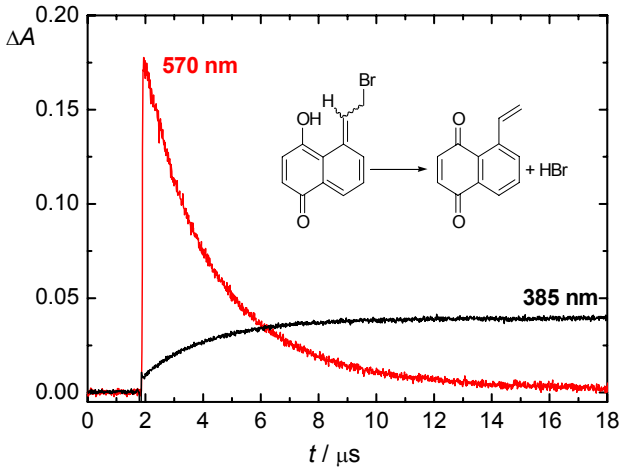

Figure 12. Kinetic traces of the transient signals produced from BrNQ in acetonitrile.

The kinetic curves were best fitted with a combination of two exponents, suggesting a parallel decay of two species with similar absorption spectra. At first, this fact was surprising as the decay of the parent MeNQ in acetonitrile and in several other organic solvents was strictly monoexponential. Taking into account the structural features of the photoenol derived from BrNQ, it became apparent that two isomers are possible with respect to the exocyclic C=C bond. A slight difference in their reactivity would give rise to a biexponential decay rate constants. Since both isomers should have essentially the same absorption spectra, it was not possible to find a wavelength that would allow for discrimination between them.

	Rate constants in CH_3CN, s^{-1}	**Rate constants in H_2O, s^{-1}**
Photoenol decay	$(5.30 \pm 0.07) \times 10^5$ $(2.18 \pm 0.04) \times 10^5$	$(2.13 \pm 0.03) \times 10^7$ $(1.57 \pm 0.02) \times 10^6$
VinNQ formation	$(4.20 \pm 0.10) \times 10^5$ $(2.53 \pm 0.04) \times 10^5$	$(1.48 \pm 0.06) \times 10^7$ $(2.32 \pm 0.20) \times 10^6$

Table 2. Rate constants of the transient signals of BrNQ in acetonitrile. Constants are obtained after a least-squares fit of a biexponential function.

LFP in neat water solution showed transient signals with the same shape. Their maxima were bathochromically shifted due to the greater polarity of the solvent. Kinetic traces at 590 nm and 390 nm afforded rate constants in the submicrosecond time range (Table 2). Acceleration of the photoenol decay and the release rate constants was not the only change upon going from acetonitile to water (Figure 13). The signal decayed exponentially in the first few microseconds and was followed by an additional slow decay that appeared to obey a second order decay law. The fast part of this decay corresponds to the rate constant of deprotection of HBr at 390 nm. Non-exponential rate constants were measured in the case of MeNQ in neutral and slightly basic water solutions, and were attributed to an attack of the deprotonated photoenol on the starting material. When the concentration of the starting material was increased, the decay rate constant raised 1.5 to 2-fold. (Figure 14 and Table 3).

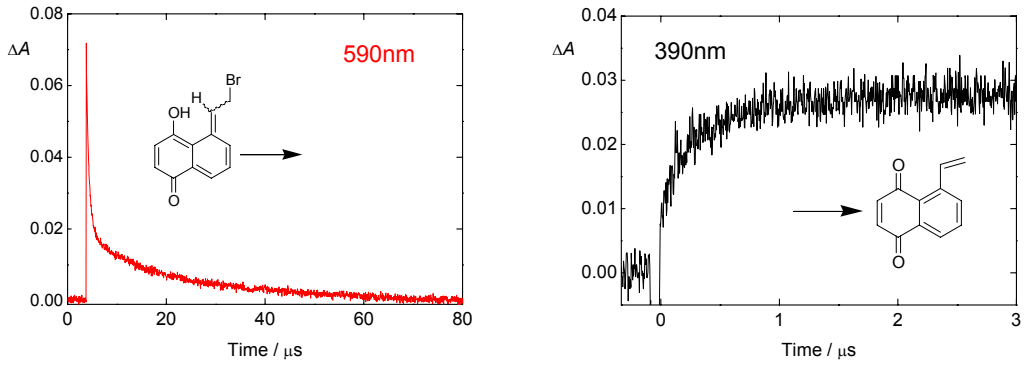

Figure 13. Kinetic traces of the transient signals produced from BrNQ in water. Left panel: decay of the photoenols. Right panel: formation of the expected photoproduct (VinNQ).

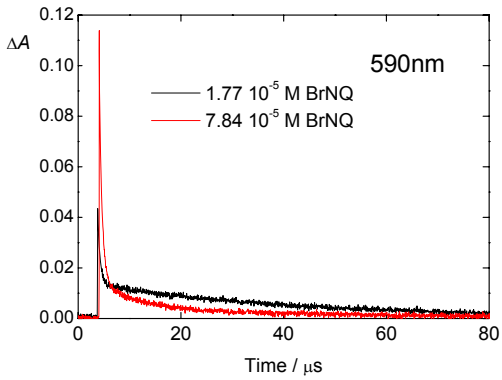

[BrNQ], M	^{2}k, $M^{-1}s^{-1}$
7.84×10^{-4}	$(1.48 \pm 0.04) \times 10^{5}$
3.53×10^{-4}	$(6.11 \pm 0.10) \times 10^{4}$
1.77×10^{-4}	$(2.25 \pm 0.06) \times 10^{4}$

Figure14. The rate constant of the slow decay depends on the concentration of the BrNQ.

Table 3. Second order rate constants of the 590-nm transient at different concentrations of BrNQ.

4.1.3 Reaction Quantum Yield Determination

The goal here was to determine the quantum yield of release of HBr, as being an important characteristic of a photoremovable protecting group. The released HBr possesses no absorption in the near ultraviolet and visible range of the light spectrum. Therefore we have chosen to determine spectrophotometrically the quantum yield of VinNQ formation, which is equal to the quantum yield of acid release. The spectrophotometric quantum yield determination was especially suitable for the BrNQ derivative as its photolysis turned out to be clean and uniform. In contrast, photolysis of AcNQ produces numerous side products, which prevented us from using the same method.

BrNQ (2.11×10^{-4} M) was irradiated with monochromatic light at 313 nm in acetonitrile and neutral water solutions. The irradiation equipment is described in the section "Experimental" of this work. The progress of the reaction was followed by absorption spectroscopy at 400 nm (see the spectra in 4.1.1). The absorbance change for a simple photoreaction **A**→**B** is described by a kinetic equation (1):

$$\frac{\mathrm{dA}}{\mathrm{dt}} = -I\varphi_B \varepsilon'_B F(A - A_{\inf}) \qquad (1)$$

Integration of (1) yields:

$$\ln \frac{A_j^B - A_{\inf}}{A_{j+1}^B - A_{\inf}} = I\varphi_B \varepsilon'_B F(t_{j+1} - t_j) \qquad (2)$$

where:

$\mathbf{A^B_j}$ is the absorbance of **B** at a time $\mathbf{t_j}$. Since **A** and **B** absorb at 400 nm, a simple relation between the absorbance of the two components was used (3):

$$A_j^B = \frac{A_j^{meas} - \varepsilon_A C^{tot}}{\varepsilon_B - \varepsilon_A} \qquad (3)$$

where ε_A and ε_B are the extinction coefficients of **A** and **B** at the observation wavelength; C^{tot} is the initial concentration of BrNQ; A_j^{meas} is the measured absorbance at a time t_i.

A_{inf} = absorbance at the wavelength of observation when the reaction is complete. It was calculated from the spectrum of pure VinNQ with the same concentration like BrNQ.

φ_B = quantum yield of formation of **B** (or quantum yield of disappearance of **A**)

ε'_B = extinction coefficient of B at the irradiation wavelength

I = intensity of the irradiation light source

F' = photokinetic factor, $F' = \frac{1-10^{-A'}}{A'}$

Where **A'** = absorbance at the wavelength of irradiation. Equation **1** can be integrated only if the photokinetic factor **F'** is considered constant and equal to the averaged value between two measurements at time t_j and t_{j+1}.

The intensity of the irradiation light source **I** was measured by chemical actinometry with azobenzene as recommended by IUPAC[46]. Measurements were performed before and right after the photolysis of BrNQ in order to check the stability of the light source. Pure trans-azobenzene (6.4×10^{-4} M in methanol) was irradiated at 313 nm at conditions of total absorption and the change of absorbance was measured at 358 nm. The initial value of the absorbance was ca. 1 and by the end of the irradiation period (30 – 40 min) ca. 0.9. The values of **A** were read off at equal intervals of time, usually 5 min. A linear relation between ΔA and the time of irradiation Δt exists (Equation 4):

$$\Delta A = \frac{I}{W(\lambda)' 10^3} \Delta t \qquad (4)$$

The factors $W(\lambda)'$ are dependent on the wavelength of irradiation and are given in the literature[46], W(313nm) = 5.30×10^{-6} einstein.cm^{-2}. Using a simple linear regression, the intensity of the light source **I** = 3.489×10^{-7} [mol.cm.l^{-1}s^{-1}] was calculated.

The quantum yields of release of HBr from BrNQ are **0.35 ± 0.06** in neat water and **0.47 ± 0.07** in acetonitrile.

4.2 Photorelease from phosphoric acid 2-(5,8-dioxo-5,8-dihydronaphthalen-1-yl)-ethyl ester diethyl ester

4.2.1 Continuous Irradiation and Product Studies

4.2.1.1 In Water

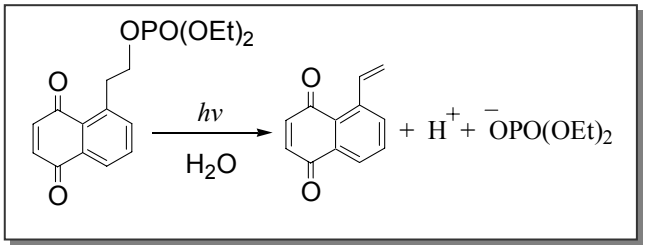

The absorption changes were qualitatively the same as in the case of BrNQ and suggested a clean photolytic conversation (isosbestic points at 238, 308 and 371 nm) of PsNQ to VinNQ and diethylphosphoric acid. Nevertheless, a deviation of the isosbestic points was seen at longer irradiation times. Parallel with the absorption spectra, small portions of the solution were injected in an HPLC system and analyzed. As expected from the UV-VIS spectra, the conversion proceeded mainly with formation of VinNQ, which was identified by co-injections with authentic samples. Minor amounts of one side product, which most likely accounts for the deviations observed at longer irradiation times, were also detected but identification was not attempted. Preparative photolysis followed by an NMR and GC-MS analysis unequivocally proved that VinNQ and the diethyl phosphate are the major photoproducts.

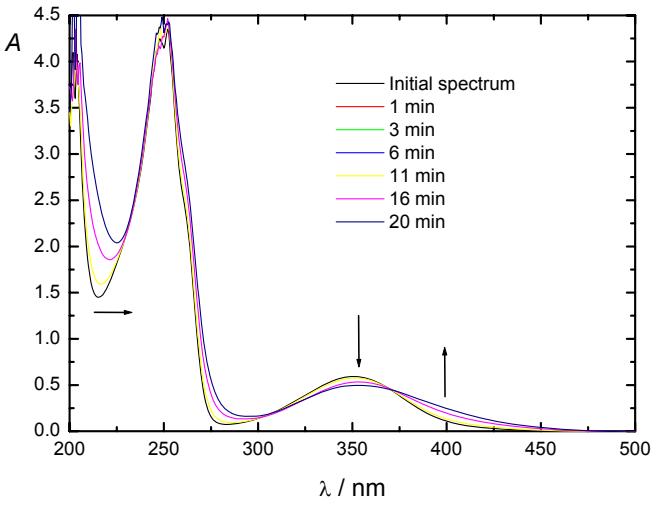

Figure 15. PsNQ irradiated at 313 nm in water. Black arrows indicate change of absorption during the irradiation period

4.2.1.2 In Acetonitrile

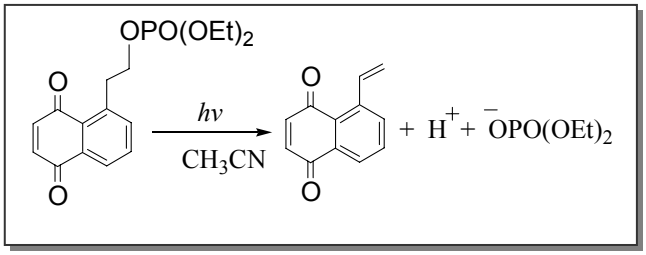

Photolysis of PsNQ in acetonitrile gave essentially the same UV-VIS spectroscopic changes (Figure 16) as in the case of water and was completed with a full liberation of the protected phosphate. In contrast with the BrNQ, the diethyl phosphate derivative was photolysed cleanly to full chemical conversion of the starting material. Attempts to follow the reaction by ^{1}H NMR failed. PsNQ (8 mg) was dissolved in 0.8 ml CD_3CN in an NMR tube and irradiated with a laser (351 nm). The ^{1}H NMR spectrum initially displayed only the starting material that after periodical irradiation pulses, eventually dissolved into broad and difficult to interpret signals. In contrast, photolysis of the same amount of PsNQ at the same conditions but in larger volume of acetonitrile (200 ml) resulted in a clean conversion to the VinNQ and diethylphosphoric acid. Commercially available diethyl phosphate and independently synthesized VinNQ were added to the NMR tube and the signal of the photoproducts increased in intensity, thus firmly proving their structures. The difference observed here was an indication of a concentration dependence of the photoreaction.

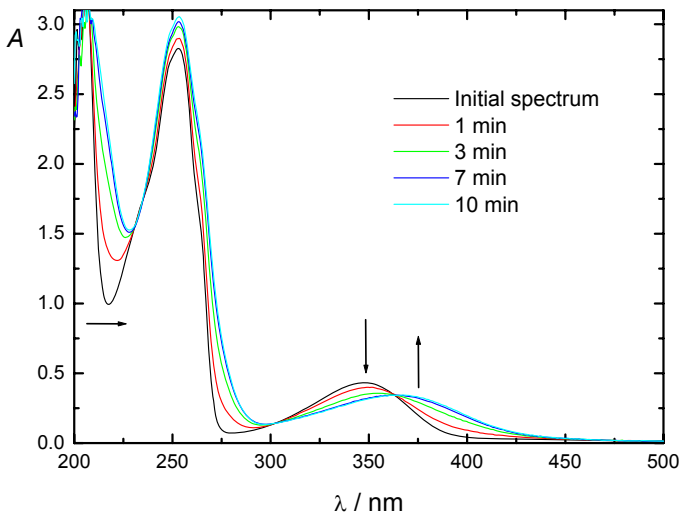

Figure 16. PsNQ irradiated at 313 nm in acetonitrile. Black arrows indicate change of absorption during the irradiation period

4.2.1.3 In dilute perchloric acid

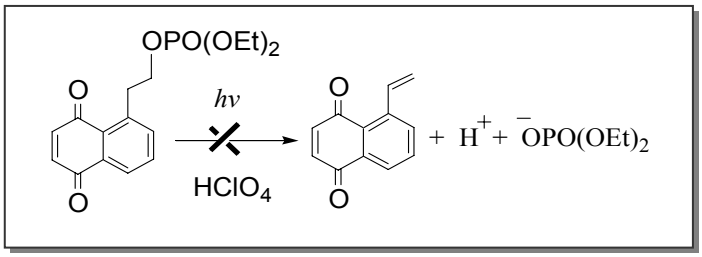

The absorption changes upon irradiation of PsNQ in 0.01 M $HClO_4$ indicated an efficient and uniform conversion of the starting material, closely resembling the case of BrNQ. The spectral changes showed the same isosbestic points at 247, 278, and 347 nm. A preparative photolysis and product characterization was not done as it was evident that deprotection of the phosphate had not occurred. The progress of the photoreaction at these conditions was the same with all three derivatives (BrNQ, PsNQ and AcNQ).

4.2.1.4 In buffered aqueous solution

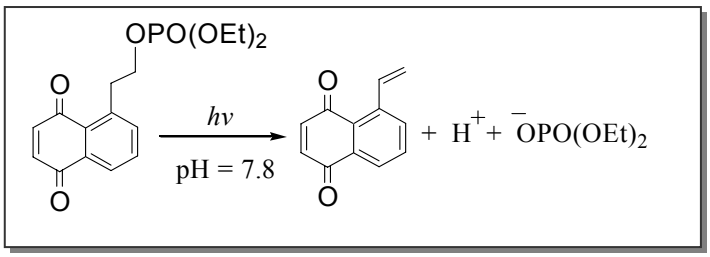

When photolyzed in slightly basic water solution (Phosphate buffer, pH=7.8), PsNQ exhibited practically the same behavior as in the case of neutral water solution (see Figure 15). Since the product of this reaction had already been identified as VinNQ, product analysis was not carried out.

4.2.2 Laser Flash Photolysis

Laser flash photolysis of PsNQ in acetonitrile and water gave an immediate and strong transient signal (Figure 17) in the range of 450 to 650 nm, λ_{max}= 550 nm (CH_3CN) and 590 nm (H_2O). The transient absorption at 550 nm was assigned to the photoenols derived from PsNQ as no significant difference to the signal produced from BrNQ was observed (for a detailed discussion on this process, see 1.2). Single wavelength kinetic traces (Figure 17, right) afforded the rate constants of the photoenol decay and formation of diethyl phosphoric acid. They are summarized in table 4. The decay rate of the photoenols strictly matched the reaction of elimination. In contrast with the BrNQ, no complications of the reaction kinetics in water were observed. The photoenols decayed by first order kinetics and so, was the VinNQ formed.

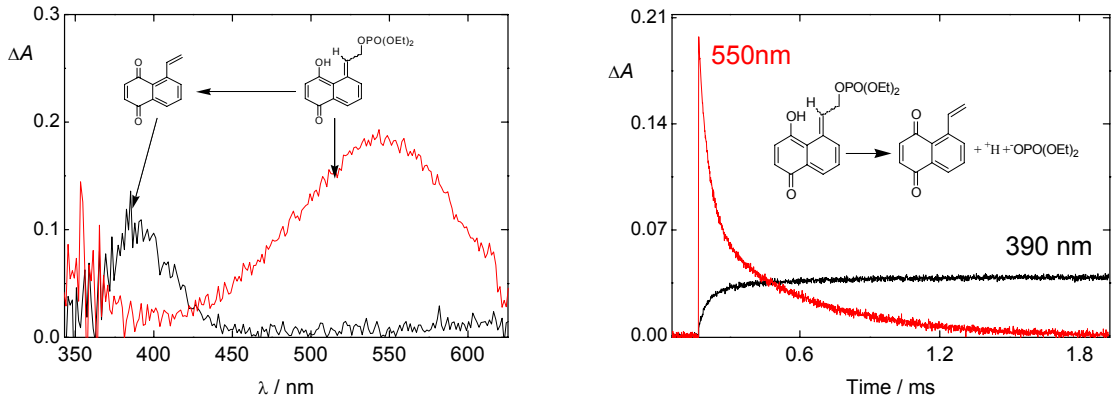

Figure 17. Left: transient absorption spectra of PsNQ in acetonitrile: — 150 ns and — 10 min delay after laser excitation; right: Kinetic traces of the transient signals in acetonitrile

	Rate constants in CH_3CN, s^{-1}	**Rate constants in H_2O, s^{-1}**
Photoenol decay	$(2.23 \pm 0.02) \times 10^4$ $(2.36 \pm 0.02) \times 10^3$	$(3.33 \pm 0.20) \times 10^4$ $(1.06 \pm 0.02) \times 10^4$
VinNQ formation	$(2.35 \pm 0.10) \times 10^4$ $(2.77 \pm 0.13) \times 10^3$	$(1.48 \pm 0.06) \times 10^4$ $(2.32 \pm 0.20) \times 10^4$

Table 4. Rate constants of the transient signals of PsNQ in acetonitrile. Constants are obtained after a least square fit of a biexponential function.

4.2.3 Reaction Quantum Yield Determination

The steady-state photolysis experiments as well as the LFP results showed that the photolytic reaction of PsNQ can be described by a simple model reaction **A** → **B + C**, where **B** is the VinNQ and **C** is the diethyl phosphoric acid. **C** has no absorption in the visible part of the spectrum and that is why we have chosen to determine the quantum yield of VinNQ formation. Its amount, formed per mole of photons absorbed, is equal to the amount of liberated **B** and they are equal to the efficiency of disappearance of the starting material. Reaction quantum yields were measured spectrophotometrically and actinometry was done with azobenzene before and right after the photolysis. Detailed description of the procedure can be found in 4.1.4.

The quantum yields of release of diethyl phosphate from PsNQ are **0.70 ± 0.08** in neat water and **0.61 ± 0.07** in acetonitrile.

4.2.4 Step-Scan FTIR Experiments

Time-resolved IR spectroscopy has been used in conjunction with LFP in investigating the mechanism of several protecting groups. An informative example is the ATP release from the nitrobenzyl ppg[47]. In general, this method permits a precise monitoring of the chemical bond being cleaved and the new ones formed. Various kinetic techniques have been developed for both dispersive and Fourier-transform IR spectrometers. In the present study a step-scan method for a FTIR spectrometer was used in order to obtain more structural information on the transient intermediates and on the kinetics of the occurring reactions. For detailed description of the TR-FTIR set-up and the methodology used, refer to chapter “Experimental” of the present work.

Time dependent difference IR spectra were obtained by 355-nm excitation of solutions of PsNQ (10 mM in CD_3CN) and the spectrum, taken 250 ns after excitation, is shown in Figure 18. The strong negative peak at 1663 cm^{-1} is due to depletion of the quinone carbonyl stretching vibration of PsNQ. The initial bleaching was beyond the time resolution of the spectrometer (50 ns) and the signal recovered within 1 ms. The initial spectrum showed several positive bands in the region

between 1650 and 1350 cm^{-1} (Table 5) and, on the basis of the LFP results and the vibrations predicted by DFT calculation, was attributed to the photoenols of PsNQ.

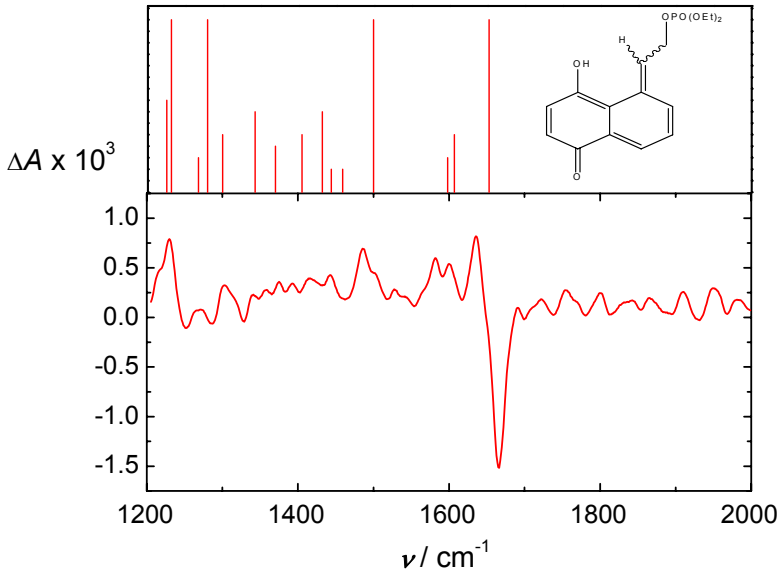

Figure 18. Upper panel: predicted IR vibrations of the photoenols (only one of the isomers was calculated); Lower panel: difference spectrum taken 250 ns after laser excitation of PsNQ

Assignment	***Measured***	***Calculated***
$\nu_{C=O}$	1636	1684
$\nu_{C(ar)=C(ar)}$	1600	1589
$\nu_{C(ar)=C(ar)}$	1582	1545
δ_{C-H}	1486	1500
ν_{CO-O}	1228	1230

Table 5. IR band positions (cm^{-1}) for the photoenols and their assignment to a specific vibrational mode

A comparison between the IR spectra of the PsNQ, VinNQ and free diethyl phosphate is shown in Figure 19. It is evident that the three spectra overlapped in most of the accessible region and discrimination between them would be possible only in the part between 1150 and 1350 cm^{-1}. A photochemical elimination of diethyl phosphate would give growth kinetics at 1226 cm^{-1} due to a newly formed vibrational

mode of the free phosphate. At the same time a parallel bleaching at 1275 cm^{-1} is to be expected due to depletion of the starting material. None of the expected spectral changes was observed.

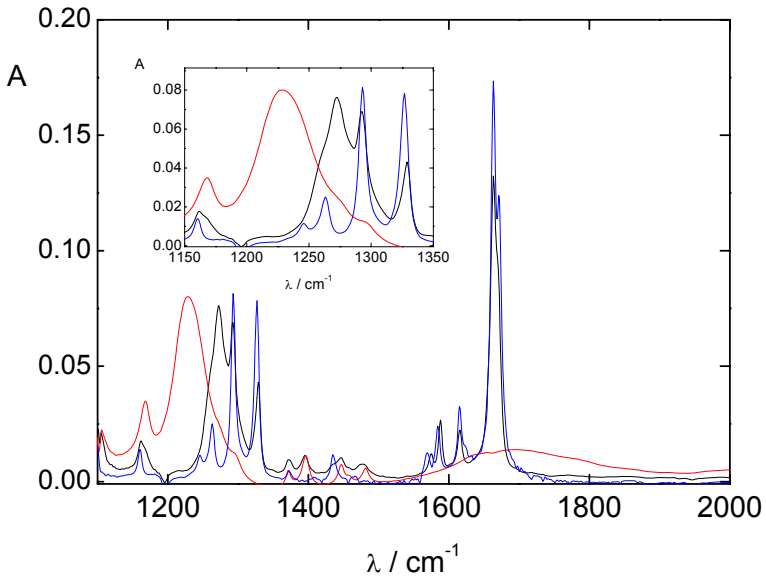

Figure 19. IR spectra of PsNQ (black), VinNQ (blue) and diethyl phosphoric acid (red) in acetonitrile. The inset shows the region from 1150 cm^{-1} to 1350 cm^{-1}.

Apart from structural information of intermediates, the TR-FTIR experiments usually supply valuable knowledge on the kinetics of the reactions as the products and the starting materials have different IR signatures and their time development can be followed independently. Unfortunately, in our case no particularly useful information was obtained. The time evolution of the primary spectrum was rather complicated and any interpretation would have been highly speculative. The kinetics of the primary photoproducts was either of second order or it was a sum of two or more single exponents. Factor analysis of the data failed to give any clear idea of what is behind these changes.

Even though these results looked quite discouraging as they brought only a firm structural establishment of the photoenol, they are in line with other observations and are addressed specifically later in the same chapter.

4.3 Photorelease from acetic acid 2-(5,8-dioxo-5,8-dihydro naphthalene-1-yl)-ethyl ester

4.3.1 Continuous Irradiation and Product Studies

4.3.1.1 In Water

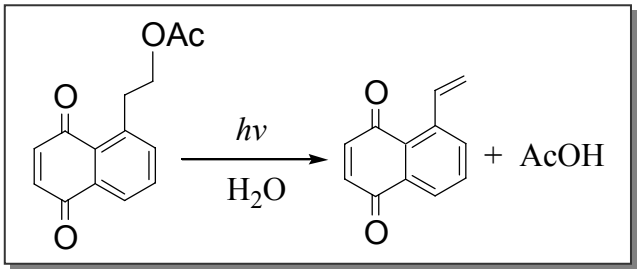

The progress of the irradiation is shown in Fig 20. The reaction did not appear to be clean and uniform as in the case of BrNQ and PsNQ. The slight increase of absorption at around 420 nm suggested formation of the VinNQ along with some other species absorbing at around 300-320 nm. The absorption changes resembled to a large degree the ones seen with BrNQ and PsNQ in dilute perchloric acid. This fact suggests an inefficient liberation of acetic acid and appearance of spectral signals due to other by-products, having the characteristics of 1,4-naphthalendiols.

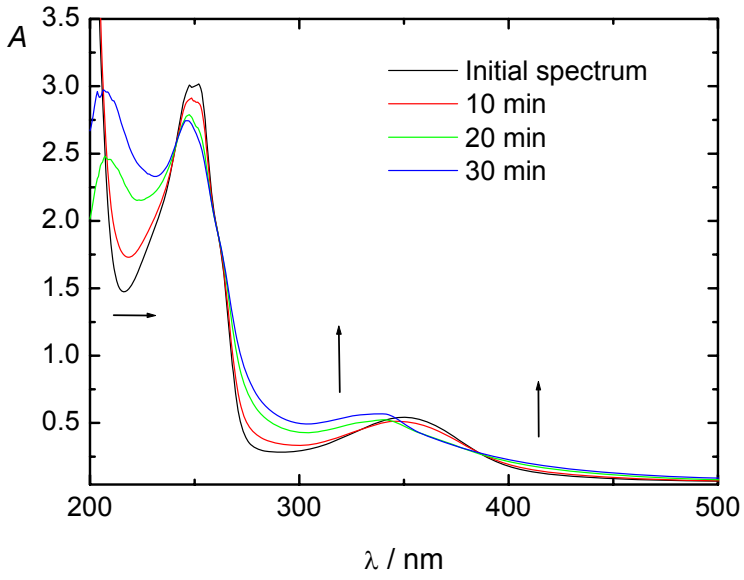

Figure 20. AcNQ irradiated at 313 nm in water. Black arrows indicate change of absorption during the irradiation period

Solution of AcNQ (30 mM) in degassed D_2O was placed in an NMR tube and irradiated with laser pulses at 351 nm. At short photolysis times the characteristic signals of the VinNQ were detected as a minor product whereas at prolonged photolysis none of it was present. This is consistent with the fact that the VinNQ was found to be light sensitive. Another preparative irradiation of AcNQ (0.1 mM) in water, furnished a mixture of six compounds, which was subjected to flash chromatography. Unfortunately, enough material for analysis was obtained only for one of the components. The rest appeared to be unstable in the conditions of our work up. Its structure was assigned by NMR and MS and is shown below.

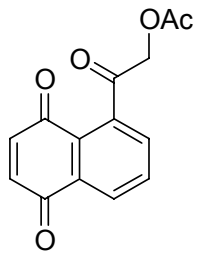

Figure 21. Acetic acid 2-(5,8-dioxo-5,8-dihydro-naphthalen-1-yl)-2-oxo-ethyl ester

HPLC analysis of samples irradiated at 351 nm with different number of flashes showed a complex mixture of 10 products, one of which was identified as VinNQ by co-injections with the authentic compound. Information concerning the chemical structure of the other components was obtained from their UV-VIS spectra. It turned out that most of them have spectra characteristic for 1,4-naphthalendiols and only two are naphthoquinones. An exact structural determination was not attempted.

Oxygen has an effect on the reaction. In degassed conditions the absorption on set at around 340 nm is much more pronounced. This fact is not surprising, taking into account that 1,4-naphthalendiols are easily oxidized by air to naphthoquinones.

4.3.1.2 In Acetonitrile

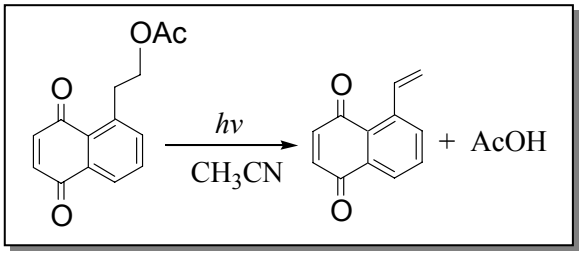

AcNQ was irradiated in acetonitrile by monochromatic light either at 254 or 313 nm. The irradiation progressed with an increase of absorption at around 400 and 290 nm (Figure 22a). As the absorption changes indicated, deprotection of the acetic acid occurred along with formation of other products (see the HPLC chromatogram, Figure 22b). The peak at 10.72 min was identified as VinNQ by co-injections.

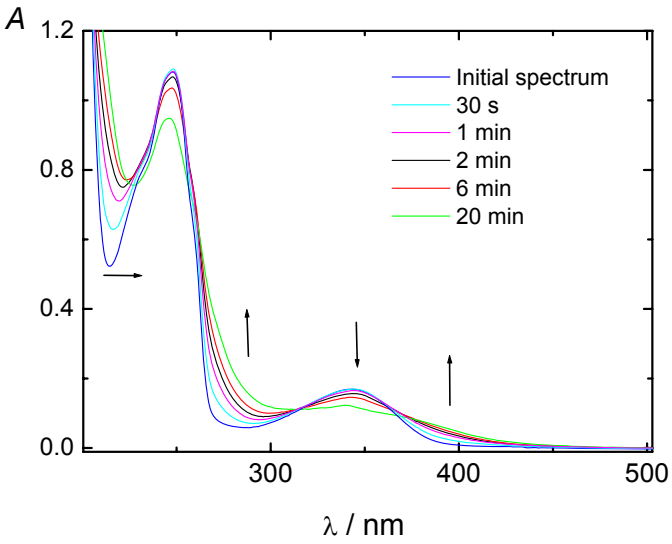

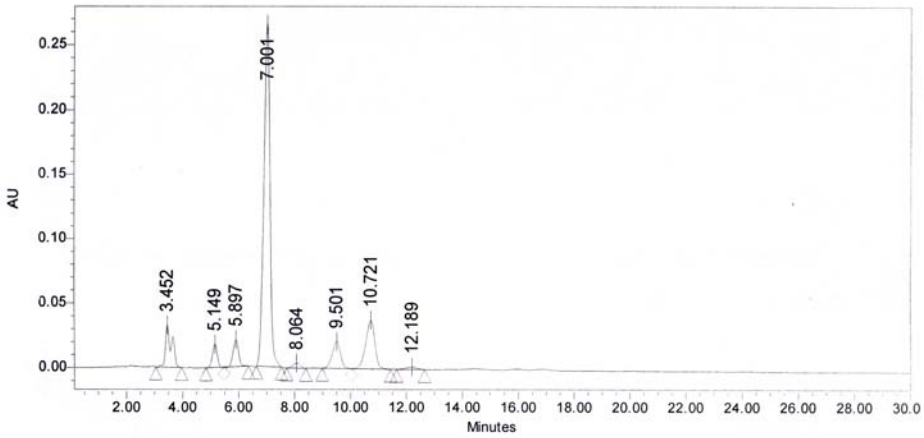

Figure 22. a) Absorption changes of AcNQ irradiated at 254 nm in acetonitrile. b) HPLC analysis of the photolysis mixture (after 150 laser flashes at 351 nm)

4.3.1.3 In Dilute Perchloric Acid

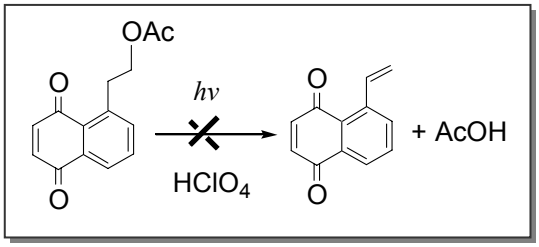

The absorption changes upon irradiation of AcNQ in 0.01 M $HClO_4$ were practically the same as in the case of BrNQ and PsNQ. No VinNQ was detected after preparative photolysis. The final spectrum in Figure 24 resembles the spectrum of 1,4-naphthalendiol[38]. Irradiating 10 mg of AcNQ in slightly acidic, degassed D_2O furnished a mixture of 6 or 7 components. Surprisingly, the NMR signals of those components were not superimposed and some partial characterization, using 2D correlation techniques was possible. The main photoproducts were acetic acid 2-(5,8-dihydroxy-naphthalen-1-yl)-ethyl ester (**1**), acetic acid 2-(5,8-dihydroxy-naphthalen-1-yl)-2-oxo-ethyl ester (**2**) and acetic acid 2-(5,8-dihydroxy-naphthalen-1-yl)-2-hydroxy-ethyl ester (**3**).

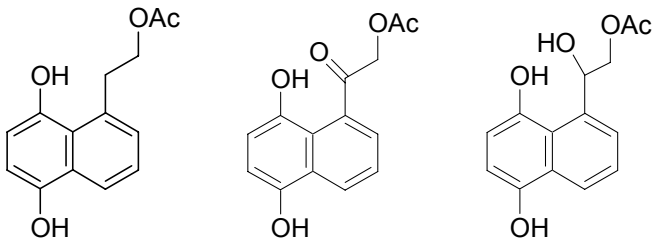

Figure 23. Characterized photoproducts from the photolysis of AcNQ in dilute perchloric acid

Preparative irradiation of larger amounts of AcNQ yielded a mixture of products that was sensitive to the conditions of the work up. Isolating the individual components and characterizing them turned out to be very difficult as some of the components underwent chemical transformation most likely due to oxidation by air or other components of the reaction mixture and, therefore, no additional characterization was attempted.

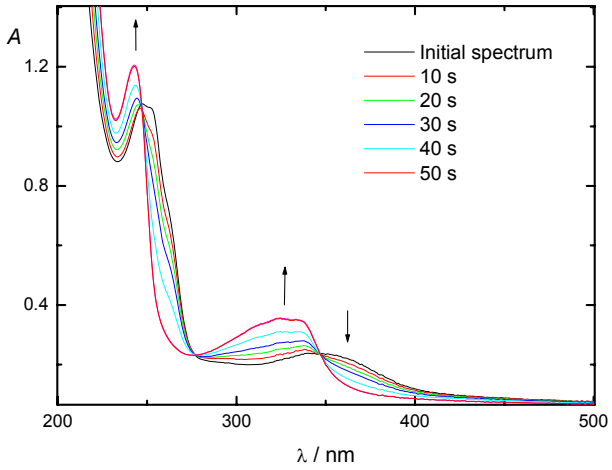

.

Figure 24. AcNQ irradiated at 254 nm in dilute perchloric acid

4.3.1.4 In Buffered Aqueous Solution

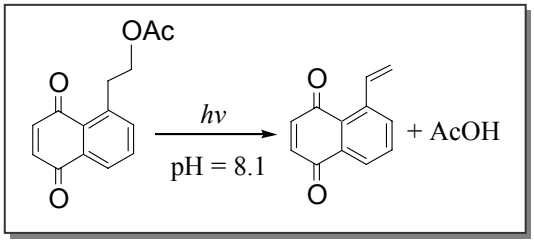

AcNQ was photolysed in slightly basic water solution (borate buffer, pH 8.1) at 313 nm. The reaction proceeded with an increase at around 390 nm and at 290 nm (Figure 25). An apparent difference between the neutral water solution and the slightly basic one was seen. In the Figure below the spectrum of VinNQ is shown for comparison.

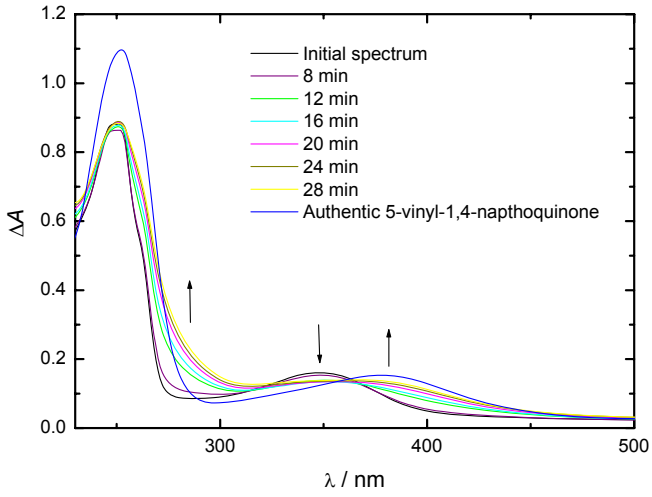

Figure 25. Irradiation of AcNQ in buffer (pH = 8.1)

4.3.2 Laser Flash Photolysis

As in the case of BrNQ and PsNQ, a transient absorption signal was detected in the range of 450 to 650 nm, λ_{max}= 550 nm (CH_3CN) and 590 nm (H_2O) and attributed to the photoenols formed after an intramolecular hydrogen shift. Single wavelength kinetic traces (Figure 26, left panel) afforded the rate constants of the photoenol decay and liberation of acetic acid in acetonitrile (Table 6).The photoenols decayed by two first order kinetics and so was the VinNQ formed. Unlike the PsNQ and BrNQ, the intensity of the signal at 390 nm, attributed to the formation of VinNQ, was very weak and reliable kinetic fits were not possible. This fact is not surprising, taking into account that the quantum yield of VinNQ formation amounts to < 5% (see "Determination of reaction quantum yields").

In neutral water solutions, the photoenols decayed somewhat faster compared to acetonitrile, as expected from PsNQ and BrNQ and no growth kinetics was observed at 390 nm (Figure 26, right panel). The decay kinetics at this wavelength is due to tailing of the absorbance of the photoenols, extending towards 400 nm. The fact that the kinetic curve has a negative Δ*A* is due to disappearance of the starting material at this wavelength.

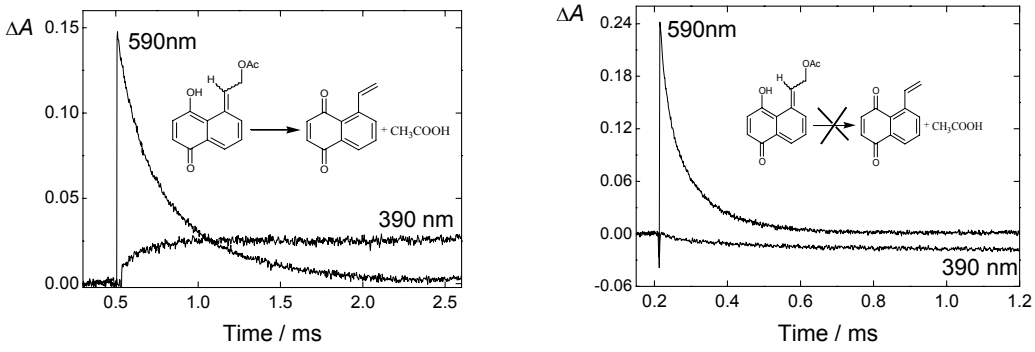

Figure 26. Transient kinetics at 390 and 590 nm in acetonitrile (left) and water (right)

	Rate constants in CH_3CN, s^{-1}	Rate constants in H_2O, s^{-1}
Photoenol decay	$(1.72 \pm 0.05) \times 10^3$ $(4.94 \pm 0.05) \times 10^2$	$(1.47 \pm 0.03) \times 10^4$ $(2.82 \pm 0.02) \times 10^3$
VinNQ formation	$(1.39 \pm 2.80) \times 10^3$ $(5.48 \pm 1.40) \times 10^3$	----------

Table 6. Rate constants of the transient signals of AcNQ in acetonitrile and in water.

4.3.3 Determination of Reaction Quantum Yields

Photolysis of AcNQ produces a large array of side products, which prevented us from using a spectroscopic determination of the quantum yield. In order to determine the amount of VinNQ produced per mole of photons absorbed, we chose to use an HPLC analysis of the photolysis mixture.

AcNQ (3-8 mM) was irradiated with an excimer laser at 351 nm in a standard quartz UV-cell. Acetonitrile, neutral water solutions and an aqueous borate buffer (pH = 8.1) were used as solvents. The transmittance of the solutions, at these concentrations, was essentially zero and the laser flash was fully absorbed by the sample. Samples were flashed with a frequency of 1Hz and stirred continuously. Small aliquots (usually 100 µL) were taken at every 50 to 100 laser flashes and analyzed by a reverse phase HPLC (MeOH/0.1%H_3PO_4=60/40). The HPLC chromatogram recorded after 150 laser flashes in acetonitrile is shown in (Figure 27). The peak with retention time 11.42 min was identified as VinNQ by co-injection with authentic material. The concentration of VinNQ was calculated from the area under the peak after a certain number of flashes. In addition, the concentration of AcNQ as a function of the number of flashes was calculated and the quantum yield of disappearance was determined. The resulting data are summarized in table 7.

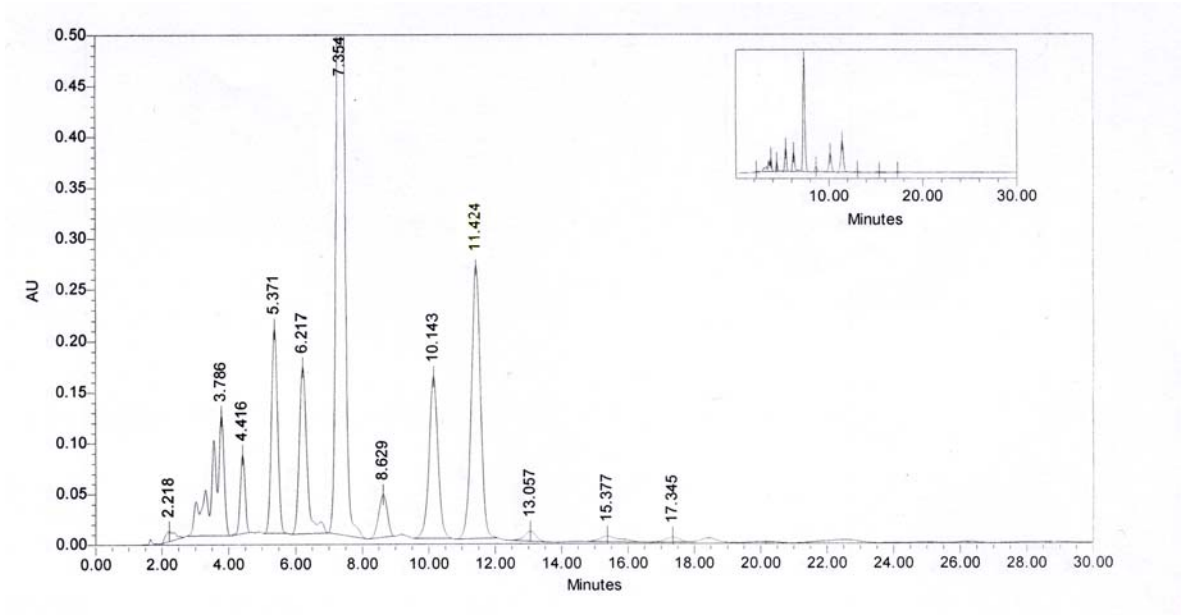

Figure 27. HPLC chromatogram of the photolysis mixture of AcNQ in acetonitrile. Peaks at 7.35 min and 11.42 min are due to AcNQ and VinNQ, respectively.

Solvent	N of flashes	$C_{VinNQ}\,10^{4}$ * [M]	$C_{AcNQ}10^{3}$ ** [M]	Φ_{VinNQ} [%]	Φ_{AcNQ} [%]
CH_3CN	50	1.96	1.53	**5.26**	**41.03**
CH_3CN	100	3.80	2.90	**4.97**	**37.94**
CH_3CN	150	5.35	3.95	**4.65**	**34.35**
H_2O	150	0.95	2.23	**0.83**	**19.39**
H_2O	250	1.07	2.41	**0.06**	**12.50**
Buffer pH = 8	50	1.10	1.98	**2.95**	**53.10**
Buffer pH = 8	100	1.69	2.80	**2.21**	**36.64**

Table 7. Quantum yields of formation of VinNQ. * Formed VinNQ, ** Converted AcNQ

Azobenzene actinometry was used for measuring the intensity of the laser pulse. Commercially available *trans*-azobenzene ($1.174\text{x}10^{-3}$M in MeOH) was repeatedly flashed at 351 nm at full absorption of the laser pulse and its absorbance was measured at 436 nm. A linear relationship between the number of flashes and the absorbance change was established. The extinction coefficients of azobenzene at 436 nm in methanol are ε^{trans} = 490 $M^{-1}cm^{-1}$ and ε^{cis} = 1140 $M^{-1}cm^{-1}$ [48] and were used to calculate the amount of *cis*-Azobenzene formed per flash. A simple relationship between the amount of formed *cis*-azobenzene, the amount of VinNQ and the quantum yield of *trans*→*cis* isomerization of azobenzene was used to calculate the quantum efficiencies (Equation 5).

$$\Phi_{VinNQ} = \frac{\Delta C_{VInNQ}}{\Delta C_{AZB}} \Phi_{AZB} \qquad (5)$$

where: Φ_{VinNQ} is the quantum yield of VinNQ formation

ΔC_{VinNQ} is the concentration of VinNQ

ΔC_{AZB} is the concentration of *cis* Azobenzene

Φ_{AZB} = 0.14 is quantum yield of *trans*→*cis* isomerization[46]

4.3.4 Step-Scan FTIR Experiments

Time dependent difference IR spectra were obtained by 355-nm or 266-nm excitation of solution of AcNQ (10 mM in CD_3CN). All results were quantitatively the same as in the case of PsNQ. In order to avoid unnecessary repetition, the reader is refered to section 4.2.4 of the present work.

5. Discussion

The three naphthoquinone derivatives, which were studied in the present work, behave very similarly and it is possible to put forward a common reaction mechanism of their photochemistry. However, they appear to have some differences, which will be addressed on an individual basis in the discussion.

Photolysis and product studies:

UV-VIS and HPLC monitoring of the progress of the photoreaction revealed that VinNQ (**3**, Scheme 20) is formed in all cases except in acidified water solutions. UV-VIS spectroscopy in the visible part of the light spectrum does not allow for detection of the acid release but we were able to detect them (CH_3COOH and $HOPO(OEt)_2$) by HPLC and NMR analysis. VinNQ is readily observed by absorption spectroscopy and we used this fact to signal the acid liberation.

In water:

The overall photolytic conversion of BrNQ and PsNQ (**1**→**3**) is a clean and uniform process with quantum efficiency of deprotection of 0.35±0.06 for BrNQ, and 0.70 ± 0.08 for PsNQ. In addition, the quantum yield of photodecomposition of VinNQ was found to be less than 0.020 ± 0.006. Apparently, the VinNQ is much less photoreactive than the BrNQ and PsNQ and thus allows for exhaustive irradiation of the BrNQ and PsNQ with nearly no secondary photolysis. In sharp contrast with BrNQ and PsNQ, was the photolysis of the AcNQ. It liberates acetic acid with an efficacy of less than 1% and produces a mixture of several compounds. Their structures were not explicitly elucidated because of their instability. Nevertheless, sufficient evidence was collected to show that most of them have naphthol chromophores. A naphthoquinone with a keto group at the benzylic position was isolated, suggesting that oxidation of the naphthols occurs during the work up and providing an indirect proof for the formation of naphthols. It is interesting to note that the absorbance changes of AcNQ during photolysis in water resemble the reaction in dilute perchloric acid.

In perchloric acid:

$HClO_4$ (0.01M) completely changes the mechanism of the photolytic reaction, giving rise to formation of substituted 1,4-napthols. It "switches off" the elimination reaction (**1**→**3**) and favors formation of naphthols with oxygen functions (OH or C=O) at the benzylic position (**1**→**5**). Therefore it is reasonable to assume that the photoreaction in acidic water solution and in water for the AcNQ follows predominantly the reaction pathway **1**→**2**→**2**$^+$→**4**→**5**. The same reaction pathway was discovered in the parent MeNQ[38].

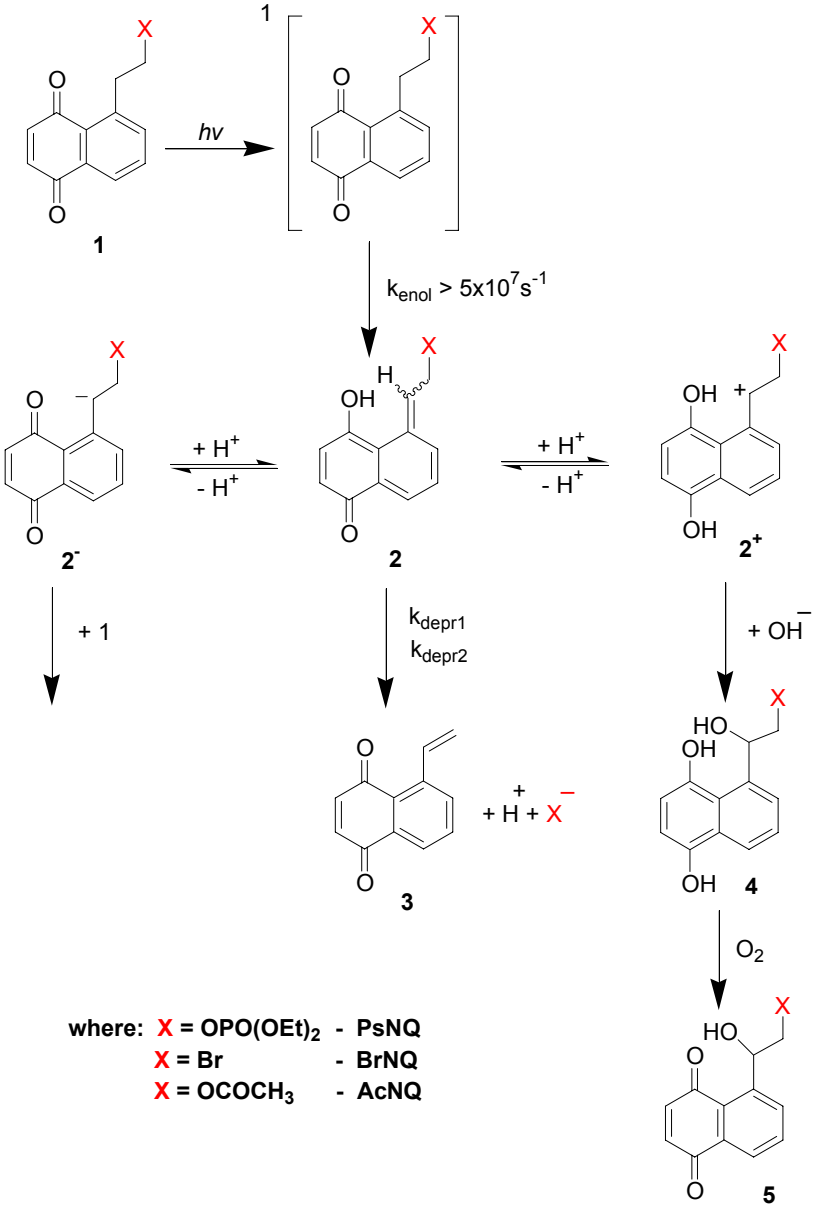

Scheme 20. Proposed photochemical mechanism of BrNQ, PsNQ and AcNQ.

In basic solution:

Irradiation in buffered aqueous solutions (pH ~ 8) does not have any influence on the reaction mechanism of the BrNQ and PsNQ. According to the absorption changes, they form the expected VinNQ and liberate the protected acid. Unfortunately, quantum yields of deprotection at these conditions can not be reliably determined as naphthoquinones are unstable to aqueous bases.

In acetonitrile:

When acetonitrile is used as a solvent for photolysis, PsNQ is the only compound that shows a clean transformation to VinNQ with a quantum yield of 0.61±0.08. The BrNQ also releases the protected acid but only at short irradiation times ($\Phi = 0.47 \pm 0.07$). Upon prolonged illumination, another reaction sets in. As the irradiation progresses, the pH of the irradiated solutions rises and changes the reaction mechanism. It is surprising that similar behavior is not observed in neat water. Equilibrium **2**→**2**$^+$ may be more shifted towards **2**$^+$ in acetonitrile than in water, thus funneling the reaction in manifold **1**→**2**→**2**$^+$→**4**→**5.**

The AcNQ photolysis was not clean and a mixture of products was formed. A slight increase of the quantum yield of liberation, compared to Φ in water, to around 5% is observed.

Measurements of the efficiency of disappearance of VinNQ in water (0.020 ± 0.004) show that complications due to secondary photolysis of VinNQ are easily avoided due to its low photoreactivity.

LFP and TR-FTIR results:

Laser flash photolysis and time resolved FTIR experiments provide solid evidence for the structure of a transient intermediate **2**. All three derivatives produce efficiently photoenol **2** within 25 ns of laser excitation either in water or in acetonitrile. Although sub-nanosecond experiments were not performed, it is very likely that the photoenolization occurs from a singlet excited state as it was observed for the parent MeNQ. Two isomers with respect to the exocyclic double bond are formed and this is reflected in the biexponential rate constant of the transient signals of **2** and **3**.

TR-FTIR usually provides very useful information on the kinetics of processes like **2**→**3** but unfortunately in our case, it failed to do so. We attribute this fact to the high concentration of starting material, needed to perform such a TR-FTIR experiment. Apparently, the photoenols reacted with the starting material and essentially no acid deprotection was observed. Our attempts to conduct those experiments at lower concentrations failed as in that case very weak IR signals were recorded.

In acetonitrile:

The rate constants of the decays of BrNQ- and PsNQ-derived photoenols match the one of VinNQ formation. The rate constants of deprotection are different for the diethyl phosphoric acid (2.23×10^4 s^{-1} and 2.36×10^3 s^{-1}) and the HBr (2.53×10^5 s^{-1} and 4.20×10^5 s^{-1}). This fact is due to differences in the pK_a values of the hydrobromic and phosphoric acid diethyl phosphate (pK_a(HBr)=-9, *vs* .pK_a($HOPO(OEt)_2$=1.39)[49]. The higher the acidity of the conjugated acid of the leaving group, the faster the release rates are.

Let us assume that the photoenolization (**1**→**2**) takes place with efficiency close to unity. If **3** is the only product of the photolysis, then only a back re-ketonization (**2**→**1)** would account for overall quantum yields of release of 50% to 60%. This is, though, not surprising as the recovery of the starting material via back H-atom transfer was observed in organic solvents in the case of the MeNQ.

Due to the low quantum yield of acetic acid released, the formation of **3** from AcNQ has a signal with a very low intensity and exponential fits do not give reliable rate constants. Nevertheless, rate constants of liberation are found to be ca. 10^3 s^{-1}.

In water:

The PsNQ-photoenols show practically the same behavior as in acetonitrile. The only difference is the acceleration of reaction **2**→**3** in going from acetonitrile to water. The rate constants of deprotection in AcNQ are impossible to measure. Its quantum yield (Φ<0.01) is so low, that practically no signal is detected. It seems that the photoenols of AcNQ decay largely in reaction manifolds **1**→**2**→$\mathbf{2^+}$→**4**→**5** and **1**→**2**→$\mathbf{2^-}$→**.** Wirz and Kresge[38] have found that the photoenol of MeNQ is an amphoteric intermediate. Presumably photoenols **2** also have about the same acidity

constants. It is, then, not surprising that the reaction of AcNQ proceeds via fast deprotonation or protonation and subsequent reactions of the cations $\mathbf{2}^{+}$ and the anions $\mathbf{2}^{-}$. That is the case when a poor leaving group like AcO^{-} is released, whereas good nucleofuges like Br^{-} and $^{-}OPO(OEt)_2$ provide an efficient deactivation pathway for **2**. In the case of BrNQ, **2** have more complex decay kinetics, which could be fitted with a combination of two first order rate laws and one second order. The two first order rate constants ((2.32 ± 0.20) x 10^6 s^{-1}, (1.48 ± 0.2) x $10^7 s^{-1}$) correspond to the constants obtained at 390 nm and are attributed to the release of HBr. The slow decay represents about 15% of the initial signal and is accelerated by increasing the concentration of the BrNQ. For the time being, the origin of this signal remains unknown.

6. Conclusions

5-(2-Bromoethyl)-1,4-naphthoquinone and phosphoric acid 2-(5,8-dioxo-5,8-dihydronaphthalen-1-yl)-ethyl ester diethyl ester release the corresponding substrates (HBr and $HOPO(OEt)_2$) in the sub- and fast-microsecond time domain with prominently high quantum yields (Φ = 0.3 - 0.7), therefore they could be applied for producing rapid pH jumps and for caging ATP or caged cyclic nucleotides (cAMP, cGMP, *etc*.). Advantageous is their relatively high extinction coefficient at 350 nm, allowing for irradiation with light, harmless for the biological environment.

Acetic acid 2-(5,8-dioxo-5,8-dihydronaphthalen-1-yl)-ethyl ester liberates acetic acid with a disappointingly low efficiency, in the slow-microsecond time range. Moreover, in water it generates numerous side products, illustrating that poor leaving groups can not be efficiently released by this phototrigger. The strong pH dependence of the reaction mechanism and the general instability of the naphthoquinones towards bases, restrict the use of this protecting group to neutral pH values.

7. Experimental

7.1 Irradiation

Solutions were irradiated in a quartz UV-cell. with a Hanau medium pressure mercury lamp. Band-pass filters were used to isolate the desired line. The solutions had concentrations in the range from 10^{-3} to 10^{-4} M and were continuously stirred. Absorption spectra were recorded on a Perkin Elmer Lambda 19 spectrometer.

7.2 Laser Flash Photolysis

The experiments were performed using a setup that has been described previously[50]. Solutions were placed in quartz cells (4.5 cm long and 1 cm wide) and excited by one of the following excitation sources: a Lambda-Physik EMG 101 excimer laser operating at 308 nm (XeCl) or Lambda-Physik Compex 205 at 248 nm (KrF) / 351 nm (XeF) with a pulse energy of ca. 100 mJ and a pulse width of ca. 20 ns. Fresh samples were exposed only to one shot due to the high photochemical decomposition of the naphthoquinones.

The probing light was provided by a pulsed Xe-arc lamp and it was directed perpendicular to the excitation source. This allowed excitation in 1 cm path-length and monitoring of the transient absorption in 4.5 cm path-length.

The detection system allowed for the capture of the kinetics at a given wavelength (using a Tektronix TDS 540 transient digitizer) and of the transient spectrum at a given time delay after excitation. The transient spectrum was captured by an intensified CCD camera (IStar 720, Andor Tech.). The optical resolution was 2 nm and the time of accumulation 20 ns. Care was also taken to minimize exposure of the samples to the monitoring light by using light shutters and appropriate filters.

7.3 Time-Resolved FTIR

Measurements were carried out on a Bruker IFS 66v/s Fourier transform infrared spectrometer equipped with a glowbar IR source, a KBr beam splitter and a nitrogen-cooled MCT detector (KV-100-1-B-7/190). The transient signal was amplified by a DC-coupled preamplifier from Kolmar, Inc (KA020-E6/MU/B). The spectral IR region was restricted to 2257–1130 cm^{-1} by using a cut on/cut off filter combination (LOT Oriel). The second or the third harmonic from a Nd–YAG laser (266/355 nm) were used for excitation. Deuterated acetonitrile solutions of starting material were used with optical density of 0.3-0.5 at the wavelength of excitation and were flowed through a cell (CaF_2 windows, 200 μm path-length) in order to avoid re-irradiation of transient intermediates and products. Experiments were carried out with a spectral resolution of 8 cm^{-1}. Raw experimental data were baseline corrected, truncated and factor analyzed in the region 1200 cm^{-1} and 2000 cm^{-1}.

7.4 Analytical Equipment

NMR spectroscopy: Bruker AVANCE 400 (400 MHz), Bruker DRX500 (500 MHz) were used for recording NMR spectra. The chemical shifts (δ) are given in ppm and referred to tetramethylsilane (δ = 0.0) or to the partially deuterated nucleus of d_1-chloroform (δ = 7.26). The chemical shifts in ^{13}C NMR are given in ppm and are referred to the signal of deuterated chloroform (δ = 77.0). Coupling constants are given in Hz. 2D experiments (COSY, HMBC, HMQC) were performed by Dr.Klaus Kulicke at the Basel University.

Analytical HPLC: The instrument was from Waters Alliance with a photodiode array detector (PDA). The column was reverse phase, Lichro-spher 100 Rp-18e (5μm), dimensions 250 mm x 4 mm, and the flow 1 mL/min. All runs were performed with a solvent mixture of CH_3OH / 0.1% H_3PO_4 = 68/32.

Mass Spectroscopy: Mass spectrometer VG70-250 and Finnigan MAT 312. Mass spectra were carried out by Dr. H. Nadig at the Institute for Organic Chemistry at the University of Basel. The ion generation was achieved by electron impact (EI) or bombardment with fast xenon atoms (FAB). Nitrobenzyl alcohol was used as a matrix and sodium chloride as an additive. The data are given in mass units per charge (m/z) and the intensities of the signals are indicated in percent of base peak in brackets.

Gas-Chromatography-Mass Spectroscopy: Samples for GS-MS analysis were dissolved in diethyl ether or chloroform (approx. 1% by mass) and were analyzed on a HP 5890 Series II gas chromatograph coupled with mass selective detector HP 5971. Two types of columns were used: a) 25 m Dimethylsilicone (OV-1, OV-101, SE-30) or b) 25 m, 5% Phenyl-methylsilicon (OV-3, SE-52). Valves were set to ca. 1 ml/min flow and 20:1 split.

Elemental Analysis: The instruments are Leco CHN-900 (C-, H-detection), Leco RO-478 (O-detection). The elemental analyses were carried out by W. Kirsch at the Institute for Organic Chemistry at the University of Basel. The data are indicated in mass percents.

DFT Calculations: Density functional calculations were done using the B3LYP functional with the 6-31G* basis set, as provided in the Gaussian 98 program package. All structures were fully optimised. Frequencies were scaled with a factor of 0.9614[51].

8. References

(1) G. Bochet, C., Photolabile protecting groups and linkers. *J. Chem. Soc., Perkin Trans. 1* 2002, 125-142.

(2) P. Kocienski, *Protecting groups,* 3ed. 2004.

(3) T. W. Greene and P. G. M. Wuts, *Protective groups in organic synthesis*., 1999, *3rd ed., New York*.

(4) V. N. R. Pillai, Photoremovable protecting groups in organic synthesis., *Synthesis,* 1980, 1-26.

(5) V. N. R. Pillai, *Organic Photochemistry,* 1987, ***9***, 225.

(6) A. P. Pelliccioli and J. Wirz., Photoremovable protecting groups: Reaction mechanism and applications, *Photochem. Photobiolog. Sci.,* 2002, **1**, 441-458.

(7) J. H. Kaplan, B. Forbush III and J. F. Hoffman, Rapid photolytic release of adenosine 5'- triphosphate from a protected analogue: Utilization by the Na:K pump of human red blood cells ghosts, *Biochemistry,* 1978, **17**, 1229-1935.

(8) M. Goeldner and R. Givens (ed.), *Dynamic studies in Biology*, Wiley-VCH: 2005.

(9) S. R. Adams and R. Y. Tsien, Controlling cell chemistry with caged compounds, *Annu. Rev. Physiol.,* 1993, **55**, 755-784.

(10) G. Marriott (ed.), Caged compounds, *Methods in Enzymolology,* 1989, 291.

(11) J. A. McCray and D. R. Trentham, Properties and uses of photoreactive caged compounds, *Annu. Rev. Biophys.Biophys.Chem,* 1989, **18**, 239-270.

(12) C. Rajesh, R. Givens and J. Wirz, Kinetics and mechanism of phosphate photorelease from benzoin diethyl phosphate: Evidence for adiabatic fission to an -keto cation in the triplet state, *J. Am. Chem. Soc.,* 2000, **122**, 611-618.

(13) Y. Shi, J. E. T. Corrie and Peter Wan, Mechanism of 3',5'-Dimethoxybenzoin ester Photochemistry: Heterolytic cleavage intramolecularly assisted by the dimethoxybenzene ring is the primary photochemical step, *J. Org. Chem.,* 1997, **62**, 8278-8279.

(14) R. S. Rock and S. I. Chan, Preparation of a water-soluble "cage" based on 3',5'-dimethoxybenzoin, *J. Am. Chem. Soc.,* 1998, **120**, 10766-10767.

(15) J. C. Sheehan, R. M. Wilson and A. W. Oxford, Photolysis of methoxy-substituted benzoin esters. Photosensitive protecting group for carboxylic acids, *J. Am. Chem. Soc.,* 1971, **93**, 7222-7228.

(16) R. S. Givens, A. Jung, C.-H Park, J. Weber and W Bartlett, New photoactivated protecting groups, 7. *p*-Hydroxyphenacyl: A phototrigger for excitatory amino acids and peptides, *J. Am. Chem. Soc.,* 1997, **119**, 8369-8370.

(17) R. S. Givens, J. F. W. Weber, P. G. II Conrad, G. Orosz, S. L.Donahue and S. A.Thayer, New Phototriggers 9: *p*-Hydroxyphenacyl as a c-terminal photoremovable protecting group for oligopeptides, *J. Am. Chem. Soc.,* 2000, **122**, 2687-2697.

(18) K. Kandler, L. C. Katz and J. A. Kauer, Focal photolysis of caged glutamate produces long-term depression of hippocampal glutamate receptors, *Nat. Neurosci.,* 1998, 1, 119-123.

(19) X. Du, H. Frei and S-H. Kim, Comparison of nitrophenylethyl and hydroxyphenacyl caging groups, *Biopolymers,* 2001, **62**, 147-149.

(20) P. G. II Conrad, R. S. Givens, B. Hellrung, C. S. Rajesh, M. Ramseier and J. Wirz, *p*-hydroxyphenacyl phototriggers: The reactive excited state of phosphate photorelease, *J. Am. Chem. Soc.,* 2000, **122**, 9346-9347.

(21) P. G. II Conrad, R. S. Givens, J. F. W. Weber and K. Kandler, New phototriggers: Extending the p-hydroxyphenacyl π-π^* absorption range, *Organic Letters* 2000, **2**, 1545-1547.

(22) J. C. Anderson and C. B. Reese, A photo-induced rearrangement involving aryl participation, *Tetrahedron Letters* 1962, **3**, 1-4.

(23) Y. Kamdzhilov, J. Wirz, *Unpublished work*.

(24) D. Geißler, Y. N. Antonenko, R. Schmidt, S. Keller, O. O. Krylova, B. Wiesner, J. Bendig, P. Pohl and V. Hagen, (Coumarin-4-yl)methyl esters as highly efficient, ultrafast phototriggers for protons and their application to acidifying membrane surfaces, *Angew. Chem. Int. Ed.* 2005, **44**, 1195-1198.

(25) B. Schade, V. Hagen, R. Schmidt, R. Herbrich, E. Krause, T. Eckardt, and J. Bendig, Deactivation behavior and excited-state properties of (Coumarin-4-yl)methyl derivatives. 1. Photocleavage of (7-methoxycoumarin-4-yl)methyl-caged acids with fluorescence enhancement. *J. Org. Chem.,* 1999, **64**, 9109-9117.

(26) T. Furuta, S. S.-H. Wang, J. L. Dantzker, T. M. Dore, W. J. Bybee, E. M. Callaway, W. Denk, and R. Y. Tsien, Brominated 7-hydroxycoumarin-4-ylmethyls: Photolabile protecting groups with biologically useful cross-sections for two photon photolysis, *Proc. Natl. Acad. Sci. USA,* 1999, **96**, 1193-1200.

(27) G. P. Hess, H. Ulrich, H-G. Breitinger, L. Niu, A. M. Gameiro, C. Grewer, S. Srivastava, J. E. Ippolito, S. M. Lee, V. Jayaraman and S. E. Coombs, Mechanism-based discovery of ligands that counteract inhibition of nicotinic acetylcholine receptor by cocaine and MK-801, *Proc. Natl. Acad. Sci. USA,* 2000, **97**, 13895-13900.

(28) U. B. Kaupp, J. Solzin, E. Hildebrand, J. E. Brown, A. Helbig, V. Hagen, M. Beyermann, F. Pampaloni, and I.Weyand, The signal flow and motor response controlling chemotaxis of sea urchin sperm, *Nature Cell Biology,* 2003, **5**, 109-117.

(29) L. J. Hofseth, S. P. Hussain, G. N. Wogan and C. C. Harris, Nitric oxide in cancer and chemoprevention, *Free Radical Biol. Med.,* 2003, **34**, 955-968.

(30) T. Yonemura, J. Nakata, M. Kadota, M. Hasegawa, K.-i. Okamoto, T. Ama, H. Kawaguchi and T. Yasui, Photoinduced denitrosyl dinuclearizing reaction of dinitrosyl-molybdenum [Mo(didentate-N,S)$_2$(NO)$_2$] complexes, *Inorg. Chem. Commun.,* 2001, **4**, 661-663.

(31) S. Namiki, T. Arai and K. Fujimori, High-performance caged nitric oxide: A new molecular design, synthesis, and photochemical reaction, *J. Am. Chem. Soc.,* 1997, **119**, 3840-3841.

(32) K. C. Hansen, R. S. Rock, R. W. Larsen and S. I. Chan, A method for photoinitating protein folding in a nondenaturing environment, *J. Am. Chem. Soc.,* 2000, **122**, 11567-11568.

(33) C. G. Bochet, Wavelength-selective cleavage of photolabile protecting groups, *Tetrahedron Letters,* 2000, **41**, 6341-6346.

(34) Y. Tatsu, Y. Shigeri, S. Sogabe, N. Yumoto and S. Yoshikawa, Solid-phase synthesis of caged peptides using tyrosine modified with a photocleavable protecting group: Application to the synthesis of caged neuropeptide Y, *Biochem. and Biophys. Res. Commun.,* 1996, **227**, 688-693.

(35) A. Dussy, C. Meyer, E. Quennet, T. A. Bickle, B. Giese and A. Marx, New light-sensitive nucleosides for caged DNA strand breaks, *ChemBioChem,* 2002, **3**, 54-60**.**

(36) G. Bendz, 5-Methyl-1,4-naphthoquinone. Synthesis and ultraviolet absorption spectrum, *Arkiv för kemi,* 1951, **4**, 163-167.

(37) E. Rommel and J. Wirz, The photoenol tautomer of 5-methyl-1,4-naphthoquinone, *Helvetica Chimica Acta,* 1977, **60**, 38-42.

(38) Y. Chiang, J. Kresge, B. Hellrung, P. Schünemann and J. Wirz, Flash photolysis of 5-methyl-1,4-naphthoquinone in aqueous solution: Kinetics and mechanism of photoenolization and enol trapping, *Helvetica Chimica Acta,* 1997, **80**, 1106-1121.

(39) M.-A. Hangarter, A. Hörmann, Y. Kamdzhilov and J. Wirz, Primary photoreactions of phylloquinone (vitamin K_1) and plastoquinone-1 in solution**,** *Photochem. Photobiolog. Sci.,* 2003, **2**, 524-535.

(40) H. Görner, Photoreactions of *p*-benzo-, *p*-naphtho- and *p*-anthraquinones with ascorbic acid, *Photochem. Photobiol. Sci.*, 2004, **3**, 933-938.

(41) O. Brahmia and C. Richard, Phototransformation of 1,4-naphthoquinone in aqueous solution, *Photochem. Photobiol. Sci.*, 2003, **2**, 1038-1043.

(42) W. N. Atemnkeng, L. D.-II Louisiana, P. K. Yong, B. Vottero and A. Banerjee, 1-[2-(2-Hydroxyalkyl)phenyl]ethanone: A new photoremovable protecting group for carboxylic acids, *Organic Letters,* 2003, **5**, 4469-4471.

(43) S. Mashraqui and P. Keehn, Active MnO2. Oxidative dehydrogenations, *Synthetic communication,* 1982, **12**, 637-645.

(44) R. V. Stevens, R. E. Cherpeck, B. L. Harrison, J. Lai and Richard Lapalme, Studies on the synthesis of vitamine B12. 2. Synthesis of the "Southern" half, *J. Am. Chem. Soc.,* 1976, **98**, 6317-6321.

(45) M. E. Jung and S. J. Miller, Preparation of N-alkadienyl N-E-2-arylethenylcarbamates via sulfoxide elimination in a synthetic approach to lycorine, *HETEROCYCLES,* 1990, **30**, 839-853.

(46) H. J. Kuhn, S. E. Braslavsky and R. Schmidt, Chemical actinometry (IUPAC technical report), *Pure and Applied Chemistry,* 2004, **76**, 2105-2146.

(47) A. Barth, J. E. T. Corrie, M. J. Gradwell, Y. Maeda, W. Mantele, T. Meier and D. R. Trentham, Time-resolved infrared spectroscopy of intermediates and products from photolysis of 1-(2-nitrophenyl)ethyl phosphates: Reaction of the 2-nitrosoacetophenone byproduct with thiols, *J. Am. Chem. Soc.,* 1997, **119**, 4149-4159.

(48) G. Gauglitz and S. Hubig, Chemical actinometry in the UV by azobenzene in concentrated solution: A convenient method, *Journal of Photochemistry,* 1985, **30**, 121-125.

(49) W. D. Kumler and J. J. Eiler, The acid strength of mono and diesters of phosphoric acid. The n-alkyl esters from methyl to butyl, the esters of biological importance, and the natural guanidine phosphoric acids, *J. Am. Chem. Soc.,* 1943, **65**, 2355-2361.

(50) E. Leyva, M. S. Platz, G. Persy, J. Wirz, Photochemistry of phenyl azide: The role of singlet and triplet phenylnitrene as transient intermediates, *J. Am. Chem. Soc.,* 1986, **108**, 3783-3790.

(51) A. P. Scott and L. Radom, Harmonic vibrational frequencies: An evaluation of Hartree-Fock, Møller-Plesset, quadratic configuration interaction, density functional theory, and semiempirical scale factors, *J. Phys. Chem.,* 1996, **100**, 16502-16513.

9. Summary

The aim of this work was to synthesize a new photoremovable protecting group for acids and phosphates, and to investigate its reaction mechanism. We based our idea on a fast and efficient process of photoenolization, occurring in 5-methyl-1,4-naphthoquinones. An efficient and fast elimination of **X** (Scheme 21) should occur due to the strong re-aromatization driving force of photoenol **2**.

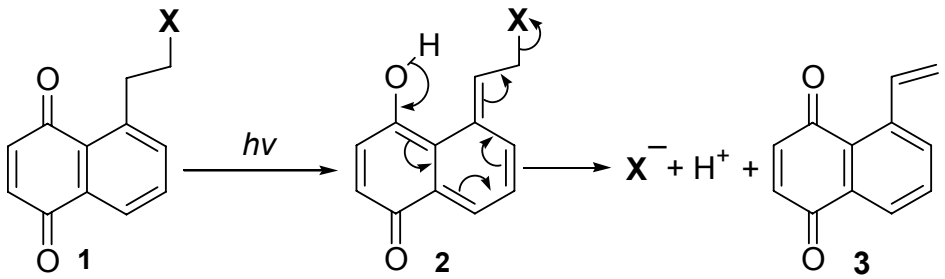

Scheme 21. Proposed mechanism of liberation of **X**

Three derivatives (**X** = Br, $OPO(OEt)_2$ and $OCOCH_3$) were synthesized using a four-step synthetic route based on [4+2] cycloaddition of an appropriately designed diene and p-benzoquinone. Subsequent oxidation of the Diels-Adler adduct yielded the desired compounds.

The photochemical reaction mechanism of these derivatives was elucidated by employing time-resolved absorption spectroscopy, step-scan FTIR spectroscopy and product analysis. The reactive intermediate **2** was observed. Our mechanistic studies provided rate constants and quantum efficiencies of release for all three derivatives in two different solvents (CH_3CN and H_2O). 5-(2-Bromoethyl)-1,4-naphthoquinone (**X** = Br) and phosphoric acid 2-(5,8-dioxo-5,8-dihydronaphthalen-1-yl)-ethyl ester diethyl ester (**X** = $OPO(OEt)_2$) liberate **X** within microseconds with high quantum yields (Φ = 0.3-0.7). When **X** is $OCOCH_3$, the quantum efficiency of release is negligible and many side products are formed, suggesting that poor leaving groups should not be caged by this phototrigger.

A part of this work was presented at the *SGPP-Graduate Student Symposium, Fribourg, Switzerland, 11/12 April, 2003.* A manuscript is currently in preparation.

10. Annex

During my PhD studies at the University of Basel I have worked on several other projects, which are briefly summarized below. Published results are not described here (see Appendix).

Project I. Photochemistry of a New Probe for Photoaffinity Labelling

Photoaffinity labelling is an efficient method for studying interactions between biologically relevant molecules and their receptor proteins. A few years ago Prof. Peng and co-workers designed a new photoaffinity probe for studying the modes of action of the promising antiviral drug EICAR. They synthesized azidoimidazole **1**, which upon irradiation with light, should form a reactive nitrene. We scrutinized the photochemical mechanism of this reaction.

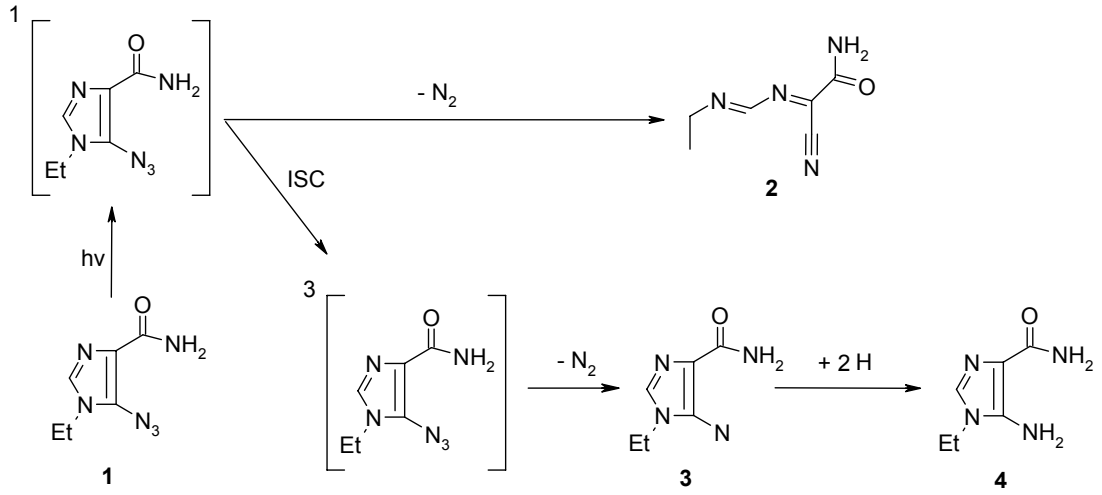

Scheme 22. Photochemistry of a probe for photoafinity labeling

Irradiation of the **1** gives predominantly cyanoformamidine **2** via fast and efficient ring-opening. Its structural identification is based on low temperature NMR experiments. Laser flash photolysis (20 ns) and pumb-probe spectroscopy (200 fs) failed to detect directly the triplet nitrene **3** but proved to be very useful in observing the mono-radical derived from it. Opposite to the initial expectation, the H-abstraction **3→4** is a minor process. Our findings are important in view of future applications of the probe in photoaffinity labeling and a manuscript is currently in preparation.

Project II. p-Hydroxyphenacyl Protecting Group: The Fate of the Spirodienedione Intermediate.

Spirodienedienone **2** is an intermediate that has escaped detection in all published studies on the photochemistry of pHP **1**. Our work was aimed specifically at this putative intermediate. Knowledge on its chemistry would add the missing piece to the mechanistic scheme of one of the promising photolabile protecting groups.

We employed several time-resolved spectroscopic techniques (LFP, TR-FTIR) as well as product studies in our quest for **2**. A precursor of p-quinonemethide **4** was synthesised and used to prove the formation of **4**.

More about our findings is given in the introductory chapter of the present thesis (The p-hydroxyphenacyl group).

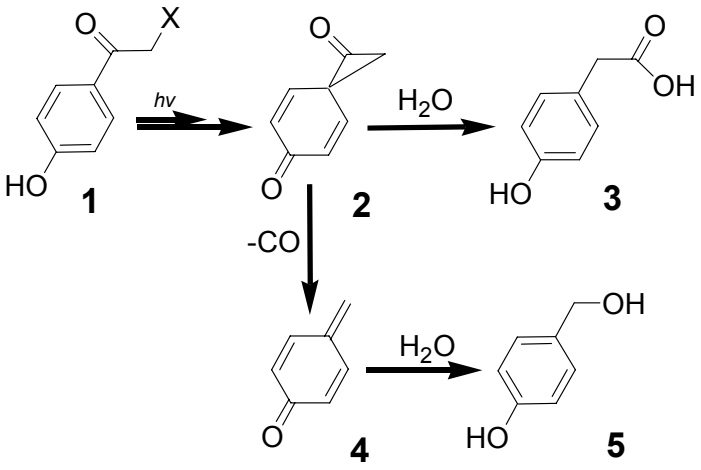

Scheme 23. The fate of the spirodienedione intermediate

A part of this project was presented at the *XX IUPAC Symposium on Photochemistry, Granada, Spain, 17-22 July, 2004* and we intend to publish the results in the near future.

Project III. Synthesis and Photochemistry of 5,8-Dioxo-5,8-dihydronaphthalene-1-carbaldehyde

The [1,5]-hydrogen shift occurring upon photolysis of 5-substituted-1,4-naphthoquinones is a remarkable reaction. Its efficiency and rate can be utilized in designing new phototriggering systems. We discovered that the same reaction takes place in 5,8-Dioxo-5,8-dihydronaphthalene-1-carbaldehyde **1** (Scheme 24), generating a highly reactive ketene intermediate **2**. This noteworthy transformation was studied by laser-flash photolysis and product analysis.

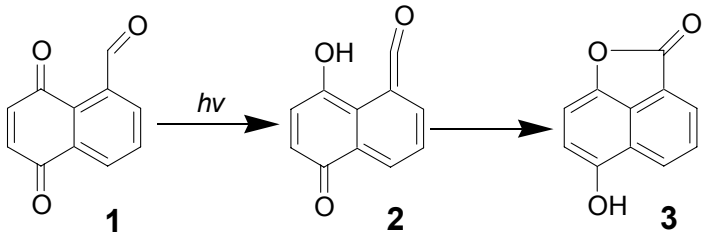

Scheme 24. Photochemistry of 5,8-Dioxo-5,8-dihydronaphthalene-1-carbaldehyde (**1**)

Compound **1** was synthesized by using a sequence of reactions, very similar to the one employed in the synthesis of BrNQ, AcNQ and PsNQ (Scheme 25).

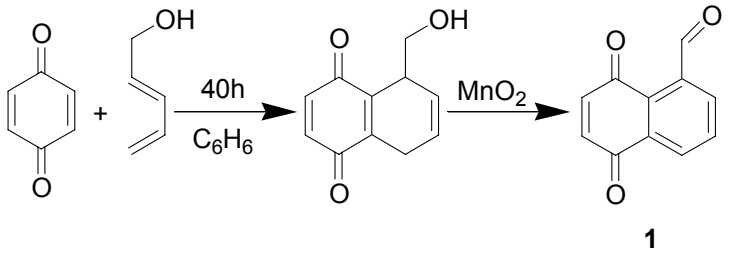

Scheme 25. Synthesis of 5,8-Dioxo-5,8-dihydronaphthalene-1-carbaldehyde (**1**)

11. Curriculum Vitae

Personal

Name	Yavor Kamdzhilov
Date of birth	December, 27 1977
Nationality	Bulgarian

Education

- PhD in Chemistry / Basel University, Switzerland
  Thesis title "A new photoremovable protecting group – synthesis and reaction mechanism"; Advisor: Prof.J.Wirz **2001- 2005**

- MSc in Organic Synthesis / University of Chemical Technology and Metallurgy, Sofia, Bulgaria.
  Thesis title: "Synthesis of novel derivatives of 1,4-anthraquinones", Advisor: Prof.L.Natova **1998-2000**

- Chemical Engineer / University of Chemical Technology and Metallurgy, Sofia, Bulgaria **1995-2000**

- High school with emphasis "Chemistry and Biology" **1992-1995**
  Sofia, Bulgaria

Teaching/research appointments

- **Teaching Assistant** at the Department of Chemistry, Basel University.
  "General and Inorganic chemistry for Biologists and Nanoscientists" **2004-2005**

- **Research assistant** at the University of Chemical Technology and Metallurgy, Sofia, Laboratory of HPLC and GC-MS analysis **1998-2000**

During my studies at the University of Basel I attended courses by the Professors: J.Wirz, B.Giese, W.-D. Woggon, G.Gescheidt, E.D.Pelloquin, J.Seelig.

12. Appendix

J|A|C|S
COMMUNICATIONS

Published on Web 00/00/0000

Photorelease of Alcohols from 2-Nitrobenzyl Ethers Proceeds via Hemiacetals and May Be Further Retarded by Buffers Intercepting the Primary *aci*-Nitro Intermediates

Bruno Hellrung, Yavor Kamdzhilov, Markus Schwörer, and Jakob Wirz*

Departement Chemie der Universität Basel, Klingelbergstrasse 80, CH-4056 Basel, Switzerland

Received April 9, 2005; E-mail: j.wirz@unibas.ch

Photoremovable protecting groups are used, inter alia, to determine physiological response times to bioactive compounds. To this end, the release must be faster than the response time of interest.[1] It was recently found that the release of alcohols from 1-(2-nitrophenyl)ethyl ethers proceeds via hemiketal intermediates that, under physiological conditions, have lifetimes around 10 s.[2,3] Therefore, they cannot be used for time-resolved work.

For 2-nitrobenzyl ethers **1**, the reaction via the formation of a hemiacetal intermediate **C** (Scheme 1) was explicitly excluded in an investigation of the glycolic acid ether **1** (R = CH_2CO_2H).[2] Yet, we identified[3] the decay of **C** as the rate-limiting step for the release of methanol from the methyl ether (**1**, R = Me) in aqueous solutions, pH < 8. Here, we show that the release of glycolic acid from **1** (R = CH_2CO_2H) also proceeds via a hemiacetal **C** and, moreover, that buffers can trap the primary *aci*-intermediates **A**, thereby further retarding alcohol release.

Scheme 1

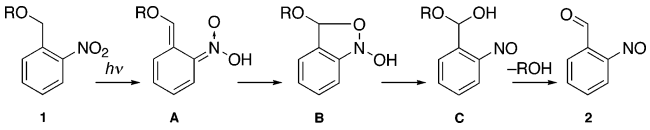

Intermediates of type **A**, **B**, and **C** had been observed by nanosecond laser flash photolysis (248 nm, 25 ns) of **1** (R = Me) in aqueous solution.[3] Quite similar results were obtained here with **1** (R = CH_2CO_2H), Table S1.[4] In the pH range of 2−6, the formation of 2-nitrosobenzaldehyde (**2**) was sufficiently slow to be monitored on a conventional spectrophotometer. The reaction is associated with a characteristic[3] increase in absorbance at 236 nm (Figure S1).[4] Surprisingly, these absorbance changes were best fitted by a biexponential rate law. In contrast, the reaction with R = Me had obeyed a first-order rate law with rate constants close to those of the faster component, k_1, of the glycolic acid ether reaction. The second component, k_2, is an order of magnitude slower. The ratio of the two 236-nm amplitudes, $A(k_1)/A(k_2)$, depends strongly on pH (Table S2 and Figure S2).[4] It is minimal at pH 3−4, which indicates that the reaction via the longer-lived intermediate predominates in this pH range.

Time-resolved infrared (TRIR) experiments provide direct evidence for the presence of functional groups (−C═O, −N═O) in the observed reactive intermediates. A solution of **1** (R = CH_2CO_2H, ca. 20 mM) in CD_3CN containing 20% D_2O and 0.01 M DCl in a CaF_2 cell of 200 μm path length was irradiated for 3 s with the frequency-quadrupled output of a Nd:YAG laser (266 nm, 10 Hz, 5 mJ/pulse). IR spectra (scan duration 70 ms) were then recorded repeatedly for 60 s. The resulting difference spectra (spectrum at delay t − spectrum prior to irradiation) were subjected to factor analysis. The spectra were reproduced, within experimental error, by linear combination of the two major spectral components, providing a reduced set of data. The rate constant obtained by global

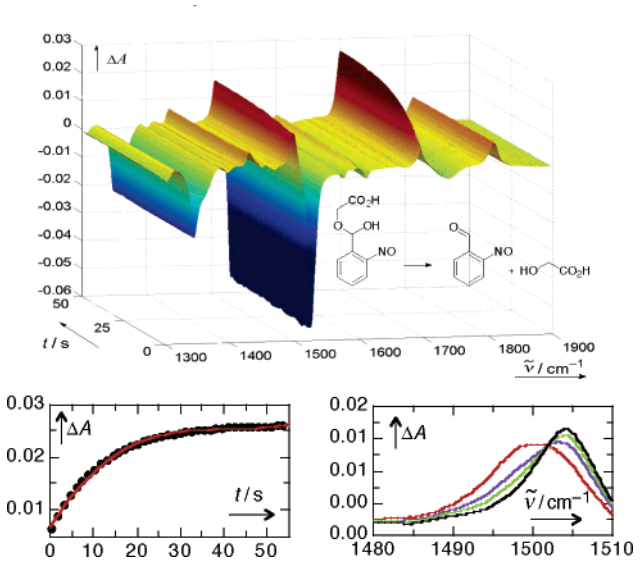

Figure 1. TRIR spectra of **1** in CD_3CN with 20% D_2O and 0.01 M DCl. The lower panels show a kinetic trace of the growth of the 1698-cm^{-1} band (left) and a detailed view of the shift of the nitroso stretching vibration from 1500 to 1505 cm^{-1} during the observation period (right).

least-squares fitting of a first-order rate law to the reduced data (Figure 1), $k = (8.5 \pm 0.2) \times 10^{-2}$ s^{-1} (35 °C), is in satisfactory agreement with that determined by the absorbance growth at 236 nm in the same, but nondeuterated solvent mixture, $k_1 \approx 5 \times 10^{-2}$ s^{-1} (25 °C). The lower panels of Figure 1 display a kinetic trace for the appearance of a C═O band at 1698 cm^{-1} (left) and the concomitant shift of the N═O band from initially 1500 to 1505 cm^{-1} (right). These observations leave no doubt that the faster process observed by UV and IR is the reaction **C** → **2** + ROH (R = CH_2CO_2H).

In addition to the variable features in the sequence of spectra (Figure 1), a positive band at 1809 cm^{-1} is present throughout the 60 s covered by the scans. Thus, another compound, which is stable for at least 60 s, is formed in addition to **C** by the laser flash. The yield of the new compound was higher in a solution containing more water but no acid (75% D_2O, 25% CD_3CN, ca. 2 mM of **1**). Here, the depletion of absorbance in the region of the free carboxyl group of **1** (1730 cm^{-1}) and the intensity of the positive band at 1809 cm^{-1} were much more pronounced, while the growth amplitude of the 1698-cm^{-1} C═O band of **2**, $k = (4.1 \pm 0.6) \times 10^{-2}$ s^{-1}, was substantially reduced.

The position of the 1809-cm^{-1} band suggested that the new compound might be a dioxolanone.[5] To obtain NMR spectra of this product, a solution of **1** (R = CH_2CO_2H, 10 mg) in 0.7 mL of CD_3CN/D_2O (1:1 by vol.) was irradiated for 15 min in a quartz NMR tube with the frequency-quadrupled output of a Nd:YAG laser (266 nm, 10 Hz, 5 mJ/pulse). Irradiation produced new signals that

10.1021/ja052300s CCC: $30.25

Scheme 2. Thermal Reactions of the Primary *aci*-Tautomers (only the *E* Isomer Is Shown) Formed by Irradiation of **1** (R = CH_2CO_2H)

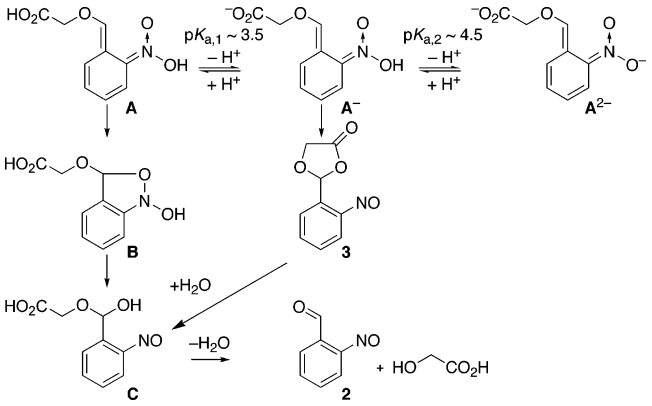

belong to three different compounds, two of them being the expected 2-nitrosobenzaldehyde (**2**) and glycolic acid, which were identified by comparison with the ^{1}H NMR spectra of authentic samples in the same solvent mixture. The new compound was identified as 2-(2′-nitrosophenyl)-1,3-dioxolan-4-one (**3**) on the basis of its NMR spectral data.[4] These spectra exhibited all features characteristic for an ortho-substituted nitrosobenzene,[5,6] especially the unusual upfield shifts of C_3 and H_3. Most of the heteronuclear correlations expected for **3** were also detected.

To determine the stability of **3**, another solution of **1** (R = CH_2CO_2H, 5 mg) in 0.7 mL of CD_3CN/D_2O (4:6 by vol.) with no added acid was irradiated for 15 min with the Nd:YAG laser, and ^{1}H NMR spectra were recorded 15, 250, 500, and 1400 min after irradiation. The decay of the CH_2 and CH signals of **3** at δ 4.62 and 8.19 ppm, respectively, as well as the concomitant growth of the CH_2 signal due to released glycolic acid, δ 4.07 ppm, all obeyed a first-order rate law, $k = (1.0 \pm 0.1) \times 10^{-4}$ s^{-1}. 2-Nitrosobenzaldehyde (**2**) is not quite stable under the reaction conditions: the NMR signals of **2** exhibited growth, $k_{growth} \approx 1.1 \times 10^{-4}$ s^{-1}, followed by decay, $k_{decay} \approx 3 \times 10^{-5}$ s^{-1}.

The difference between the rate constants for the reaction **3** → **2** determined by H NMR (40% CD_3CN), $k = (1.0 \pm 0.1) \times 10^{-4}$ s^{-1}, and that determined by absorption spectroscopy in wholly aqueous solution, $k_2 = 6 \times 10^{-3}$ s^{-1}, is due to the cosolvent. The optical measurements showed that the reaction is strongly retarded by addition of acetonitrile to water, $k_2 = 2 \times 10^{-3}$ s^{-1} (10%) and $k_2 < 1 \times 10^{-3}$ s^{-1} (20% CH_3CN). The hydrolysis of **3** requires formation of an ionic intermediate and is strongly inhibited by even small amounts of acetonitrile.

Dioxolanone **3** was a minor product in strongly acidic and in neutral aqueous solutions (Table S1 and Fig. S2), but dominated at the expense of intermediate **C** in the absence of added acid or buffer. Such solutions were still slightly acidic, pH ≈ 3.2, due to the presence of 2 mM of the carboxylic acid **1** (R = CH_2CO_2H). Cyclization to form **3** should be most favorable from the monoanion of the *aci*-intermediate $\mathbf{A}^-$, as shown in Scheme 2. The concentration of $\mathbf{A}^-$ is expected to peak around pH 4, because the pK_a of the carboxylic acid function should be about 3.5,[7] that of the nitronic acid function about 4.5.[3] Indeed, the relative amount of **3** is maximal in the pH range of 3−4 (Table S1).[4] The lifetime of the hemiacetal **C** is about 10 s at pH < 6 and low buffer concentrations, as expected from previous work.[3]

Buffer concentrations were kept low (≤0.03 M). At high buffer concentrations the yield of **C** is reduced. For example, an increase of the acetic acid buffer concentration to 1 M (buffer ratio 1:1) reduced the amplitude of the reaction **C** → **2** by a factor of 4. This indicates that the free acetate also adds to the benzylic position of the *aci*-nitro intermediate **A**. The resulting addition product was not identified, but is expected to have a lifetime similar to that of **3**, i.e., trapping of **A** by the buffer is also likely to delay the release of the alcohol.

We have shown that the nitroso intermediates **3** and **C** are formed in dilute, wholly aqueous solutions and that they hydrolyze with rate constants of about 6×10^{-3} s^{-1} and 0.25 s^{-1}, respectively (pH = 7, 20 °C). Why, then, were NO bands not detected in the previous TRIR investigation of the same compound,[2] leading the authors to exclude reaction via hemiacetal **C**?

As the pH of aqueous solutions approaches 7, the slow UV-spectral changes observed after irradiation are no longer consistent with a clean formation of **2**. Slightly above pH 7 the absorption spectra become featureless and GC−MS analysis of the irradiated solution indicates a highly complex mixture containing products of high molecular weight. The previous time-resolved IR study of **1** (R = CH_2CO_2H)[2] was done at pH 8.5 and with a high buffer concentration (200 mM bicine). Therefore, the nitroso compounds **3** and **C** did not accumulate under the reaction conditions. Remarkably, the same authors did observe an absorbance rise at 740 nm (pH 7, 20 °C, $k = 590$ s^{-1}), which they attributed to formation of an aromatic nitroso compound.

In summary, the hemiacetal **C** is formed from 2-nitrobenzyl ethers **1** (R = CH_2CO_2H or Me), and hydrolysis of **C** does limit the release rate of the corresponding alcohols in wholly aqueous solutions at pH values ≤7. In view of these results it is surprising that photolysis of 2-nitrobenzyl-caged D-glucose (**1**, R = D-glc) induced chemotaxis of *Escherichia coli* bacteria with response rates as fast as 15 s^{-1}.[8,9] A finding that may well be relevant to nitrobenzyl-protected compounds, in general, is that interception of the *aci*-intermediates **A** by buffers may further retard release of the desired alcohol. The formation of dioxolanone **3** with a lifetime of 3 min in wholly aqueous solution is an intramolecular example for the trapping of **A** by a "buffer", providing structural proof of concept.

Acknowledgment. This work was supported by the Swiss National Science Foundation, Project No. 20020-105219. We thank Dr. J. E. T. Corrie, NIMR, London, for a gift of compound **1** (R = CH_2CO_2H) and for helpful discussions.

Supporting Information Available: NMR spectral data of **3** and kinetic data for the intermediates **A**−**C** formed by excitation of **1** (R = CH_2CO_2H). This material is available free of charge via the Internet at http://pubs.acs.org.

References

(1) (a) Pellicioli, A.-P.; Wirz, J. *Photochem. Photobiol. Sci.* **2002**, *1*, 441−458. (b) Goeldner, M., Givens, R. S., Eds. *Dynamic Studies in Biology*; Wiley-VCH: Weinheim, 2005.
(2) Corrie, J. E. T.; Barth, A.; Munasinghe, V. R. N.; Trentham, D. R.; Hutter, M. C. *J. Am. Chem. Soc.* **2003**, *125*, 8546−8554.
(3) Il'ichev, Y. V.; Schwörer, M. A.; Wirz. J. *J. Am. Chem. Soc.* **2004**, *126*, 4581−4595.
(4) Supporting Information.
(5) Pearson, W. H.; Cheng, M.-C. *J. Org. Chem.* **1987**, *52*, 1353−1355.
(6) Gowenlock, B. G.; Cameron M. *Can. J. Chem.* **1994**, *72*, 514−518.
(7) The pK_a (I = 0.1 M, 25 °C) of methoxyacetic acid is 3.5: Headley, A. D.; Starnes, S. D.; Wilson, L. Y.; Famini, F. G. *J. Org. Chem.* **1994**, *59*, 8040−8046.
(8) Lux, R.; Munasinghe, V. R. N.; Castellano, F.; Lengeler, J. W.; Corrie, J. E. T.; Khan, S. *Mol. Biol. Cell* **1999**, *10*, 1133−1146.
(9) A fraction of the glucose might be released directly from intermediate **B**, **B** → **2** + D-glc. This shortcut could be favored by the steric bulk of D-glc. Whether alcohol release from 2-nitroveratryl ethers also proceeds via long-lived hemiacetal intermediates is not known, but the frequently adopted assumption that the release rate is equal to the decay rate of the readily observable *aci*-nitro transients is clearly not safe at this point.

JA052300S

FULL PAPER

PPS www.rsc.org/pps

Photochemical reaction mechanisms of 2-nitrobenzyl compounds: 2-Nitrobenzyl alcohols form 2-nitroso hydrates by dual proton transfer†‡

Martin Gaplovsky, Yuri V. Il'ichev,*§ Yavor Kamdzhilov, Svetlana V. Kombarova,§ Marek Mac,¶ Markus A. Schwörer and Jakob Wirz*

Departement Chemie der Universität Basel, Klingelbergstr. 80, CH-4056 Basel, Switzerland. E-mail: J.Wirz@unibas.ch; Fax: +41 61 267 38 55; Tel: +41 61 267 38 42

Received 30th June 2004, Accepted 29th July 2004
First published as an Advance Article on the web 11th August 2004

Irradiation of 2-nitrobenzyl alcohol (**1**, R = H) and 1-(2-nitrophenyl)ethanol (**1**, R = Me) in various solvents yields 2-nitroso benzaldehyde (**4**, R = H) and 2-nitroso acetophenone (**4**, R = Me), respectively, with quantum yields of about 60%. The mechanism of this reaction, known since 1918, was investigated using laser flash photolysis, time-resolved infrared spectroscopy (TRIR), and ^{18}O-labeling experiments. The primary *aci*-nitro photoproducts **2** react by two competing paths. The balance between the two depends on the reaction medium. Reaction *via* hydrated nitroso compounds **3** formed by proton transfer prevails in aprotic solvents and in aqueous acid and base. In water, pH 3–8, the classical mechanism of cyclization to benzisoxazolidine intermediates **5**, followed by ring opening to carbonyl hydrates **6**, predominates. The transient intermediates **3** and **6** were identified by TRIR. Potential energy surfaces for these reactions were mapped by density functional calculations.

Introduction

2-Nitrobenzyl compounds have found numerous applications as photoremovable protecting groups.[1] Their photoreactions are initiated by an intramolecular 1,5-H shift yielding *aci*-nitro protomers as primary photoproducts. Cyclisation to short-lived benzisoxazolidines is generally assumed to be the next step (Scheme 1, path a). In a recent paper[2] we reported the first direct observation of such a cyclic intermediate. Here we show that a different reaction path exists for 2-nitrobenzyl alcohols **1** (R = H or Me). The primary *aci*-nitro intermediates **2** form nitroso hydrates **3** by proton transfer. Dehydration of **3** yields the 2-nitrosobenzoyl products **4**[3] (path b). Partitioning between the classical reaction *via* path a (cyclization to **5** followed by ring opening to the carbonyl hydrate **6**) and path b (proton transfer) depends strongly on the reaction medium.

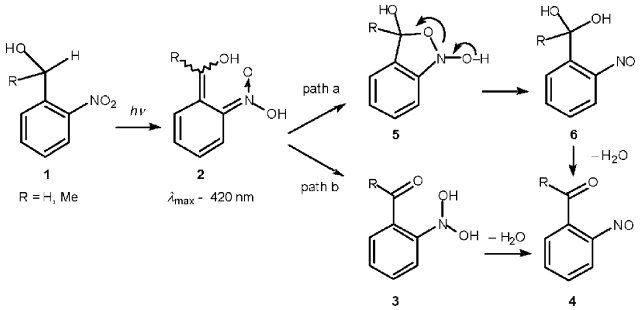

Scheme 1

Both reaction paths shown in Scheme 1 do not release the R group. Nevertheless, Tsien *et al.*[4] observed fast photoinduced release of Ca^{2+} from a 2-nitrobenzyl alcohol derivative of BAPTA (1,2-bis(*o*-aminophenoxy)ethane-*N*,*N*,*N*′,*N*′-tetraacetic acid), 'nitr-5'. The photoreaction lowers the Ca^{2+} affinity of the BAPTA ligand by replacing the electroneutral benzhydrol **1** with an electronegative phenone **4**.

Experimental

Methods

The apparatus used for nanosecond LFP and TRIR as well as the methods of data analysis have been described.[2] Neither the amplitudes nor the kinetics of the transient absorptions were influenced by degassing. Therefore, most measurements were done with air-saturated solutions.

Quantum yields for the formation of the nitroso compounds **4** were determined by spectrophotometric monitoring of the absorbance changes. A medium-pressure mercury lamp equipped with a 365 nm band-pass filter was used as a light source. Actinometry was done with a solution of azobenzene in methanol.[5]

Picosecond pump–probe spectroscopy was done with a Ti:Sa laser system Clark MXR CPA-2001 (775 nm, pulse energy 0.8 mJ, full width at half maximum 150 fs, operating frequency 426 Hz). Part of the beam was fed into a Clark-MXR NOPA. The output at 540 nm was frequency-doubled to 270 nm, and after the compression provided pump pulses with an energy of 1 μJ and <100 fs pulse width. A probe beam continuum (300–680 nm) was produced by focusing part of the 775 nm beam 1 mm in front of a CaF_2 crystal of 2 mm path length. The detection system has been described.[6] Two-photon absorption is observed when the pump and probe pulses coincide at the sample. The FWHM of the two-photon absorption in water was 250 fs, which provides a measure of the time resolution of the detection system. Typically, several hundred spectra were collected and averaged for each delay. The translation stage allowed for a maximum time delay of 1.8 ns for the probe beam.

† Dedicated to Professor Hiroshi Masuhara on the occasion of his 60th birthday.

‡ Electronic supplementary information (ESI) available: Coordinates and energies of all optimised structures, original rate data and calculated frequencies. See http://www.rsc.org/suppdata/pp/b4/b409927c/

§ Present address: Wichita State University, Department of Chemistry, 317 McKinley Hall, 1845 Fairmount, Wichita, KS 67260-0051, USA. E-mail: Yuri.Ilitchev@wichita.edu.

¶ Present address: Jagiellonian University, Krakow, Poland.

DOI: 10.1039/b409927c

Materials

2-Nitrobenzyl alcohol (**1**, R = H, Fluka) was purified by recrystallisation from ethanol. 1-(2-Nitrophenyl)-ethanol (**1**, R = Me) was prepared by reduction of 2-nitroacetophenone (Aldrich) with $NaBH_4$.[7] 2-Nitrosobenzaldehyde (**4**, R = H) was synthesised from anthranil.[2] Bidistilled water was used to prepare aqueous solutions. All other solvents were of spectroscopic grade and were used as received. The absorbance of the neat solvents at 248 nm was less than 0.01 at 1 cm path length.

Isotopic labelling of the alcohol oxygen atom of **1** (R = H) was done as follows. 2-Nitrobenzaldehyde (0.5 g, Fluka) in 14 ml of acetonitrile was mixed with a solution of 0.15 ml 70% $HClO_4$ in 7.5 ml $^2H_2{}^{18}O$ (about 75 % ^{18}O). The solution was kept at room temperature for 2 h, neutralised with $NaHCO_3$, and extracted with methylene chloride. The organic extract was dried over $MgSO_4$, filtered and evaporated to dryness, leaving 0.425 g of a white solid, mp 43 °C. The isotopic purity of the resulting labelled 2-nitrobenzaldehyde was about 70%, as estimated from the ratio of the mass peaks at m/z = 123 and 121. Reduction with $NaBH_4$[7] gave **1** (R = H). Its isotopic purity was determined as 65 ± 1% ^{18}O from the ratios of the mass peaks at 150/152, 135/137 and 105/107.

Calculations

Density functional theory (DFT) calculations were performed with the GAUSSIAN 98[8] package of programs. All geometries were fully optimised at the B3LYP level of theory with the 6-31G(d) basis set. Starting geometries were those optimised at the HF/6-31G(d) level. Wavefunction stability was tested for all energy minima, and vibrational frequencies were calculated by using analytical second derivatives. All quoted energies include zero-point vibrational energy corrections that were scaled with a factor of 0.9806.[9] For comparison with IR spectra a scaling factor of 0.9613 was used.[9] This level of theory gave satisfactory results in previous related studies.[10] For all molecules, single-point energies were computed using B3LYP functionals with the 6-311+G(2d,p) basis set at the B3LYP/6-31G(d) geometries. Transition states were located with the Gaussian implementation of the STQN method. Reaction pathways were followed using the 'intrinsic reaction coordinate' (IRC) approach to verify the correspondence between the transition states and the minimum-energy structures. Self-consistent reaction field (SCRF) calculations with the polarized continuum model (PCM) of Tomasi *et al.*[11] were utilized to estimate solvent effects. Aqueous acidity constants were calculated using the approach of Pliego and Riveros[12] at the level of DFT described above. This method predicts pK_a values within about 2 units, *e.g.*, pK_a values of 2.5 for formic acid (exp: pK_a = 3.75)[2] and 4.3 for the *aci*-form of 2-nitrotoluene (3.6).[13] Electronic excitation energies were calculated using the random phase approximation for a time-dependent DFT calculation[14] with the B3LYP/6-311+G(2d,p) basis set. A list of the coordinates and energies of all optimised structures is available as supplementary material.‡

Results

Continuous irradiations and quantum yields

Irradiation of 2-nitrobenzyl alcohol (**1**, R = H) in hexane at 365 nm induced the formation of new absorption bands at 234 and 282 nm and a very weak band with a maximum at 760 nm that is characteristic for nitroso compounds. The initial absorbance changes indicated a clean formation of 2-nitrosobenzaldehyde (**4**, R = H), which was identified by comparison of its IR and mass spectra with an authentic sample.[2] The electronic spectrum of (**4**, R = H) was determined with the authentic sample in hexane solution with 0.3% $CHCl_3$: λ_{max} = 234 nm, $\varepsilon \approx 17000\ M^{-1}\ cm^{-1}$, 282 nm, $\varepsilon \approx 7500\ M^{-1}\ cm^{-1}$, shoulder at *ca.* 310 nm, $\varepsilon \approx 3000\ M^{-1}\ cm^{-1}$. Product **4** (R = H) is also sensitive to irradiation, so that complete photoconversion of **1** (R = H) and isolation of **4** (R = H) from the reaction mixture was not attempted.

Similar spectral changes were observed upon irradiation of 1-(2-nitrophenyl)ethanol (**1**, R = Me) in hexane. In this case, the photoproduct 2-nitrosoacetophenone (**4**, R = Me) was sufficiently stable under the irradiation conditions to allow near-complete photoconversion. The final absorption spectrum obtained in this manner agrees with that of **4** (R = Me).[15]

The spectral changes observed upon irradiation of acidic aqueous solutions of **1** (R = H, Fig. 1a) and of **1** (R = Me, Fig. 1b) with UV light were similar to those in hexane solutions. The rise of absorption at 780 nm indicated the formation of **4** (R = Me) upon irradiation, Fig. 1c.

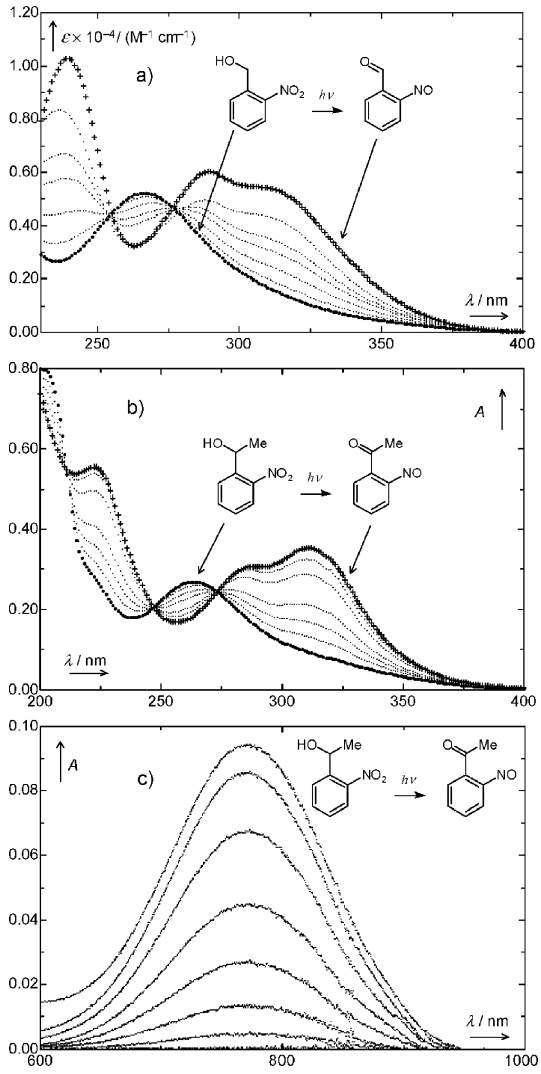

Fig. 1 (a) Absorption spectra of **1** (R = H, 7.0 × 10^{-5} M) in 1 mM aqueous HCl recorded before (···) and after irradiation at 365 nm. Irradiation times between measurements were 1, 3, 6, 9, and 19 min. A spectrum of authentic 2-nitrosobenzaldehyde (**4**, R = H) is also shown (+++). (b) Absorption spectra of **1** (R = Me, 6.4 × 10^{-5} M) in 1 mM aqueous HCl recorded before (···) and after irradiation (+++) at 365 nm. Irradiation times: 1.5, 3.5, 6.5, 15.4, 25.0, 50.0, and 65.2 min. (c) Absorption spectra recorded before and after irradiation of **1** (R = Me, 3.4 × 10^{-3} M) in hexane at 365 nm. Irradiation times: 12.5, 38.0, 85.0, 165.1, 305.3, 496.3, and 2067 min.

The progress of the photoreaction **1** → **4** was determined spectrophotometrically assuming a clean reaction at low conversions. The quantum yields for irradiation at 365 nm were estimated by using the linear interpolation method[5] or by direct numerical integration of the rate equation. Consistent results were obtained by the two methods. The quantum yields were essentially independent of the solvent and of pH in water:

$\phi = 0.52 \pm 0.05$ for **1** (R = H) in hexane, acetonitrile, ethanol, 1 mM aqueous HCl, and 50 mM aqueous phosphate buffer ($Na_2HPO_4/NaH_2PO_4 = 1:1$), and $\phi = 0.67 \pm 0.10$ for **1** (R = Me) in the same solvents. Quantum yields could not be determined in aqueous base due to instability of the nitroso compounds **4** in this medium.

Photodehydration of ^{18}O-labeled 1 (R = H)

Solutions of ^{18}O-labelled **1** (R = H, *ca.* 1×10^{-3} M, $65 \pm 1\%$ ^{18}O isotopic purity at the alcohol function) in hexane, abs. ethanol, acetonitrile, and abs. methanol were irradiated for 2 h (40–70% conversion) with the 254 nm line of a mercury arc lamp. The isotopic purity of product **4** (R = H) was determined by GC–MS using the 135/137 mass peak ratio. The ^{18}O isotopic purity determined for **4** (R = H) after irradiation in hexane was 62.8 ± 1.3 (4 batches), indicating essentially complete retention ($96.6 \pm 2.5\%$). Retention in polar solvents was lower, 60% in acetonitrile and 36% in methanol. However, a control experiment showed that noticeable ^{18}O-depletion occurred within minutes even in 'dry' acetonitrile ($\leq$0.014% H_2O), apparently due to exchange of the carbonyl oxygen of **4** *via* reversible hydration[16] by traces of water. Hence, the retention data determined for acetonitrile and methanol solutions must be considered as lower limits.

Laser flash photolysis (LFP)

Aprotic solvents. LFP of **1** (R = H) in hexane gave a broad transient absorption (320–500 nm, $\lambda_{max} \approx 400$ nm, initial absorbance $A_0 \approx 0.1$) due to an *aci*-nitro intermediate **2**, which was formed within the duration of the laser pulse (25 ns, 248 or 308 nm). The decay of **2** accurately obeyed a second-order rate law, $1/A_t = 1/A_0 + kt/(\varepsilon d)$. A_0 and A_t are the transient absorbances observed immediately after the flash ($t = 0$) and at time t, respectively, ε is the decadic molar extinction coefficient of the transient intermediate at the observation wavelength, and $d = 4.3$ cm is the cell path length. The applicability of second-order kinetics (as opposed to a sum of exponentials) was established by varying the initial transient concentration by an order of magnitude. The fit parameters $kA_0/(\varepsilon d)$ of 13 decay traces were directly proportional to the initial transient absorbances A_0 with a slope of $k/\varepsilon d = (1.22 \pm 0.03) \times 10^6$ s^{-1}. Assumption of $\varepsilon \approx (2–4) \times 10^3$ M^{-1} cm^{-1} for the extinction coefficient of the quinonoid *aci*-nitro intermediate[17] gives $k \approx (1–2) \times 10^{10}$ M^{-1} s^{-1}, a diffusion-controlled reaction rate. An explanation for this fast bimolecular reaction of **2** is given in the discussion.

Transient kinetics at 320 nm showed an unresolved step ($\Delta A = 0.02$), followed by a fast partial decay ($\Delta A = 0.005$) due presumably to the blue edge of the *aci*-nitro transient, and finally a very slow growth to an end absorbance, $\Delta A_\infty \approx 0.04$, with a rate constant of about 1.5 s^{-1}.

The decay of the *aci*-nitro transient **2**, $\lambda_{max} \approx 390$ nm, formed by LFP of **1** (R = Me) in hexane obeyed a first-order rate law. However, the rate constant increased linearly with the concentration of the starting material, and a bimolecular rate constant of $k \approx 6 \times 10^8$ M^{-1} s^{-1} was determined from the slope of this concentration dependence. At an observation wavelength of 320 nm, a weak step and partial decay, due presumably to the blue edge of the 400 nm transient, was followed by a very slow growth in absorbance with a rate constant of about 1 s^{-1}.

The decay of the *aci*-nitro transient, $\lambda_{max} = 425$ nm, formed by LFP of **1** (R = H) in acetonitrile required fitting with a bi-exponential rate law. A slight shift of the transient absorption maximum from 425 to 415 nm was observed during the decay of the fast component, $k \approx 4.5 \times 10^5$ s^{-1}. The slow component had a larger amplitude, $A_{slow}/A_{fast} = 2.8$, and a decay rate constant of about 2×10^4 s^{-1}. Although the rate constants could be determined accurately and reproducibly for a given sample, their values varied considerably when different batches of solvent were used. This was found to arise from variations in the water (or acid) content of different solvent batches. The second rate constant increased markedly upon addition of water: 6×10^4 s^{-1} (5% v/v), 1.4×10^5 s^{-1} (10%), 5×10^5 s^{-1} (20%), 1.3×10^7 s^{-1} (40%). The two transients merged to a single first-order decay, $k = 2.2 \times 10^6$ s^{-1}, in a solution containing 20% water, but a slower decay, $k \approx 7 \times 10^4$ s^{-1}, reappeared at water contents exceeding 80%. At 320 nm, a fast initial step, $\Delta A/A_{max} = 0.14$, was followed by a bi-exponential growth in absorbance with rate constants of about 2×10^5 s^{-1} (relative amplitude $\Delta A/A_{max} = 0.1$) and 20 s^{-1} ($\Delta A/A_{max} = 0.76$).

LFP of **1** (R = Me) in dry acetonitrile also gave a double exponential decay, $k_1 = 1.1 \times 10^6$ s^{-1}, $k_2 = 2.7 \times 10^4$ s^{-1} at 415 nm. These rates were also found to be very sensitive to water, particularly that of the the slower decay. After addition of 1% (v/v) water these rate constants were $k_1 = 1.2 \times 10^6$ s^{-1}, $k_2 = 2.6 \times 10^5$ s^{-1}. They merged to a single first-order decay, $k = 2.2 \times 10^6$ s^{-1}, in a solution containing 5% water and reached the detection limit, $k \approx 5 \times 10^7$ s^{-1}, in the presence of 20% water. In contrast, the resolved growth observed at 320 nm was slowed down by the addition of water. The growth curves were best fitted by a bi-exponential function with rate constants of $k_1 = 24$ s^{-1}, $k_2 = 480$ s^{-1} (0% water), $k_1 = 2.3$ s^{-1}, $k_2 = 41$ s^{-1} (5% water), and $k_1 = 1.7$ s^{-1}, $k_2 = 7.5$ s^{-1} (10% water).

Protic solvents. LFP of **1** (R = H) in methanol, ethanol or water with a 248 nm laser pulse induced the fast (<20 ns) formation of *aci*-nitro transients absorbing in the range of 340–540 nm, $\lambda_{max} \approx 425$ nm. Their decay required fitting with a bi-exponential function. The faster decay was accompanied by slight ($\approx$20 nm) hypsochromic shift of the absorption maximum. A step-and-growth of absorption was observed in the range 300–330 nm. The rate constants determined in methanol and ethanol were similar to those in unbuffered aqueous solution.

Flash photolysis of **1** (R = H) at 248[18] or 308 nm in aqueous solutions was done over a pH range of 1–13 that was adjusted with HCl, NaOH, or buffers. Ionic strength was kept constant at $I = 0.1$ M by addition of NaCl. Kinetic traces obtained in 10 mM aqueous phosphate buffer, pH = 6.8, are shown in Fig. 2. The decay of the *aci*-transient, 410 nm, was biexponential. The relative amplitude of the faster component was larger at longer wavelengths of observation (470 nm). In the traces recorded at 320 nm, the amplitude ratio of step and growth increased with pH, from $A_{step}/A_{growth} \approx 0.1$ (0.1 M $HClO_4$), ≈ 0.3 (acetic acid buffers), ≈ 1 (carbonate buffers), and ≈ 10 (0.1 M NaOH). In acetic acid buffers the growth curves at 780 nm were consistent with those observed at 330 nm, which proved that the growth kinetics determined in the UV represents the formation of a nitroso compound. Finally, on time scales of s to min, a strong increase in absorbance at 230 nm associated with a partial decay of the absorbance at 320 nm occurred. These spectral changes were very similar to those of the decay of the hemiacetal formed from 2-nitrobenzyl methyl ether (Fig. 6 of ref. 2). They are attributed to dehydration of the carbonyl hydrate **6**. The product **4** (R = H) was unstable in basic solutions ($\tau \approx 2$ min in 0.01 M NaOH).

The observed rate constants of both transient decays at 420 nm, and of the growth of product absorption at 320 nm depended linearly on total buffer concentration. Bimolecular rate coefficients for buffer catalysis were determined from the linear dependencies of the observed first-order rate constants on total buffer concentrations. Buffer slopes for the faster decay component at 420 nm could not be determined accurately. Buffer slopes obtained for different buffer ratios were plotted against the mole fraction of the acidic buffer component, x_{HA}, to determine the catalytic coefficients of the acid (HA) and base (A^-) components of the buffers from the intercepts at $x_{HA} = 1$ and 0, respectively. The resulting rate coefficients for the acid and base components of the buffers are given in Table 1. Both general acid and general base catalysis was found for the *aci*-decay, but only general base catalysis was significant for the growth of the 320 nm absorption (k^{NO}).

Table 1 Catalytic coefficients for general acid and base catalysis on the slow component of the *aci*-decay (420 nm) and of the growth at 320 nm

		Second *aci*-component		NO formation
Buffer	$pK_{a,c}$[a]	$k_B/(M^{-1}\ s^{-1})$	$k_{HB}/(M^{-1}\ s^{-1})$	$k_B/(M^{-1}\ s^{-1})$
HAc/NaAc	4.57	$\sim 1 \times 10^8$	$(5 \pm 1) \times 10^8$	$(1.1 \pm 0.2) \times 10^4$
$H_2PO_4^-/HPO_4^{2-}$	6.78	$(2.2 \pm 0.2) \times 10^7$	$(2.2 \pm 0.1) \times 10^7$	$(9 \pm 3) \times 10^5$
HCO_3^-/CO_3^{2-}	9.91	$(4 \pm 1) \times 10^8$	4×10^7	3×10^8

[a] Buffer acidity quotients at 25 °C, ionic strength $I = 0.1$ M.[19]

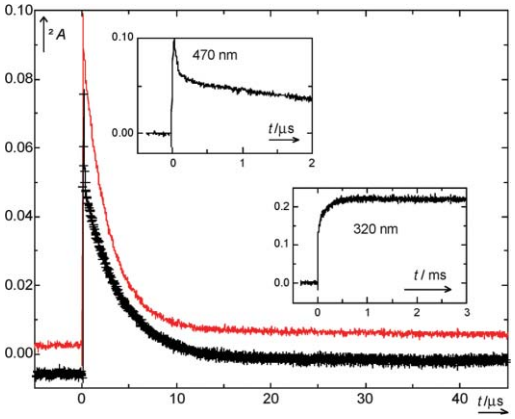

Fig. 2 Kinetic traces recorded by 248 nm excitation of **1** (R = H) in 10 mM aqueous phosphate buffer (1 : 1, pH = 6.78, $I = 0.1$) at 410 nm (— upper trace) and at 470 nm (+–+ lower trace). Upper left inset: 470 nm trace at higher time resolution. Lower right inset: 320 nm trace.

Rate constants for wholly aqueous solutions (Table 2) were obtained by linear extrapolation to zero buffer concentration. The resulting pH–rate profiles are depicted in Fig. 3. The solid lines were obtained by nonlinear least-squares fitting of eqn. (1) to the data points for the second component of the *aci*-decay (k_2^{aci}), and of eqn. (2) to those for reactions **5** → **6** (k^{NO}) and **6** → **4** (k^{CO}). The resulting values for the fit parameters are given in Table 3 and the parameters are identified in the Discussion.

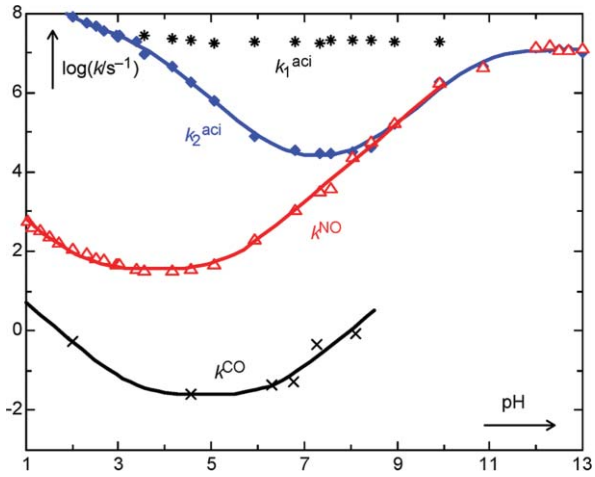

Fig. 3 pH–rate profile for the transient kinetics obtained by LFP of **1** (R = H) in wholly aqueous solution. The two upper series of data points (* * * and ◆–◆–) represent the two components of the bi-exponential decay of the *aci*-transient **2** at 420 nm (k_1^{aci} and k_2^{aci}). The middle trace (Δ–Δ–Δ) shows the resolved growth in absorbance at 320 nm (k^{NO}) due mostly to formation of **6** from **5**. The bottom trace (×–×–×) shows the slow partial decay of absorbance at 320 nm (k^{CO}) attributed to formation of **4** by dehydration of **6**. The solid lines show the fitted eqn. (1) and (2).

LFP of 2-nitrophenyl ethanol (**1**, R = Me) in water gave no transient absorption attributable to an *aci*-nitro intermediate at any pH, in sharp contrast to **1** (R = H). As the reaction quantum yields of both compounds are about the same, we suspected that only the fast, pH-independent component of the *aci*-transients is formed, and that it escaped detection by nanosecond LFP of **1** (R = Me). Indeed, pump–probe spectroscopy of **1** (R = Me) in water produced a strong transient intermediate, $\lambda_{max} \approx 420$ nm, that was formed with a rate constant of $(9 \pm 1) \times 10^{11}\ s^{-1}$ and decayed on the subnanosecond time scale, $k = (3.8 \pm 0.2) \times 10^9\ s^{-1}$.

Table 2 Decay rate constants obtained by 248 nm excitation of **1** (R = H) in aqueous solution ($I = 0.1$ M)[a]

pH[b]	k_1^{aci}/s^{-1}	k_2^{aci}/s^{-1}	k^{NO}/s^{-1}	k^{CO}/s^{-1}[h]
1.00			596	
1.15			399	
1.30			330	
1.52			220	
1.70			156	
2.00		7.80×10^7	108	0.54
2.30		5.85×10^7	83.5	
2.52		4.64×10^7	66.7	
2.70		3.70×10^7	57.4	
2.95		2.62×10^7	43.0	
3.00		2.59×10^7	43.3	
3.03		2.62×10^7	43.0	
3.38		1.92×10^7	34.0	
3.56[c]	2.61×10^7	9.01×10^6	32.5	
4.16[c]	2.23×10^7	4.66×10^6	30.7	
4.56[c]	2.16×10^7	1.87×10^6	33.5	2.58×10^{-2}
5.07[c]	1.81×10^7	6.25×10^5	43.5	
5.93[d]	1.93×10^7	7.90×10^4	194	
6.30[d]				4.42×10^{-2}
6.78[d]	1.92×10^7	3.39×10^4	1.02×10^3	5.33×10^{-2}
7.36[d]	1.79×10^7	2.89×10^4	3.21×10^3	0.47
7.57[d]	2.09×10^7	2.96×10^4	3.75×10^3	
8.04[e]	2.01×10^7	3.23×10^4	2.21×10^4	
8.12[g]				0.88
8.43[e]	2.06×10^7	4.07×10^4	5.48×10^4	
8.95[f]	1.82×10^7	1.67×10^5	1.65×10^5	
9.91[f]	1.84×10^7	1.87×10^6	1.74×10^6	
10.86		4.56×10^6	4.08×10^6	
12.00		1.35×10^7	1.34×10^7	
12.30		1.27×10^7	1.41×10^7	
12.48		1.21×10^7	1.14×10^7	
12.70		1.21×10^7	1.09×10^7	
13.00		1.03×10^7	1.21×10^7	

[a] Solutions were adjusted to an ionic strength $I = 0.1$ M by addition of NaCl. All measurements were done at ambient temperature, 20 ± 1 °C. [b] pH ≤ 3.5: nominal HCl concentrations. 10.0 ≤ pH ≤ 13.0: calculated from nominal NaOH concentrations using K_w ($I = 0.1$ M, 20 °C) = 1.08×10^{-14} M^2. [c] Acetic acid buffer ≤ 0.05 M. [d] Sodium phosphate buffer ≤ 0.08 M. [e] $Na_2B_4O_7$/HCl buffer ≤ 0.022 M. [f] $Na_2CO_3/NaHCO_3$ buffer ≤ 0.05 M. [g] Tris buffer ≤ 0.1 M. [h] Dilute buffer solution were used to minimize buffer catalysis. Rate constants did not change significantly in the buffer concentration ranges indicated. The original rate data are available as supplementary material.‡

$$\log(k_2^{aci}/s^{-1}) = \log[\{k_H[H^+]^3 + k_0[H^+]^2 + k_0'K_{a,1}[H^+] + k_0''K_{a,1}K_{a,2}\}/(M^2\ s^{-1})] - \log[\{[H^+]^2 + K_{a,1}[H^+] + K_{a,1}K_{a,2}\}/M^2] \quad (1)$$

$$\log(k^{NOorCO}/s^{-1}) = \log[(k_0 + k_H[H^+] + k_{OH}K_w/[H^+])/s^{-1}] \quad (2)$$

LFP of 2-nitrophenyl ethanol (**1**, R = Me) in water gave no transient absorption attributable to an *aci*-nitro intermediate at any pH, in sharp contrast to **1** (R = H). As the reaction quantum

Table 3 Parameters obtained by fitting of eqn. (1) to the rate constants for reaction **2** → **5** (R = H) and eqn. (2) to those for **5** → **6**/**3** → **4** (k^{NO}) and **6** → **4** (k^{CO}) in wholly aqueous solution (Table 2 and Fig. 3)[a]

coefficient	k_2^{aci}, eqn. (1)	k^{NO}, eqn. (2)	k^{CO}, eqn. (2)
$k_H/(M^{-1}\ s^{-1})$	$(5 \pm 2) \times 10^9$	$(6.3 \pm 0.6) \times 10^3$	52 ± 32
k_0/s^{-1}	$(3.5 \pm 0.9) \times 10^7$	34 ± 3	$(2.3 \pm 1.3) \times 10^{-2}$
$k_{OH}/(M^{-1}\ s^{-1})$		$(1.1 \pm 0.1) \times 10^{10}$	$(6.3 \pm 0.3) \times 10^5$
k_0'/s^{-1}	$(1.9 \pm 0.3) \times 10^4$		
k_0''/s^{-1}	$(1.2 \pm 0.1) \times 10^7$		
$K_{a,1}/M$	$(5 \pm 2) \times 10^{-4}$		
$K_{a,2}/M$	$(1.3 \pm 0.2) \times 10^{-12}$		

[a] Mechanistic assignments of these coefficients are given in the Discussion (see Scheme 7).

The longer-lived transient intermediates observed by LFP of **1** (R = Me) were similar to those described above for **1** (R = H). Step-and-growth kinetic traces were obtained at 330 nm (*cf.* the lower inset of Fig. 2). The ratio of the amplitudes, A_{step}/A_{growth}, increased strongly with pH, from 0.1 in 0.01 M $HClO_4$ ($k_{growth} = 1.0 \times 10^2\ s^{-1}$) and in acetic acid buffer (buffer ratio 0.05 M CH_3CO_2H/0.01 M CH_3CO_2Na, pH = 3.87, $k_{growth} = 88\ s^{-1}$), to 0.4 ($k_{growth} = 2.0 \times 10^2\ s^{-1}$) in non-buffered water, to 8 ($k_{growth} = 1.1 \times 10^7\ s^{-1}$) in 0.1 M aqueous NaOH. These rate constants are close to those determined for **1** (R = H). Finally, formation of the product **4** (R = Me) was observed on a time scale of seconds to minutes (pH 1–8) by an absorbance increase at 230 nm and partial absorbance decay at 320 nm.

Time-resolved infrared (TRIR) measurements

A solution of 36.5 mg 2-nitrobenzyl alcohol (**1**, R = H) in 22 ml acetonitrile-d_3 was photolysed with 6 ns, 266 nm pulses from a Nd:YAG laser. The changes induced in the IR spectra were monitored by the step–scan technique. A 3D plot of the time-dependent spectra is shown in Fig. 4.

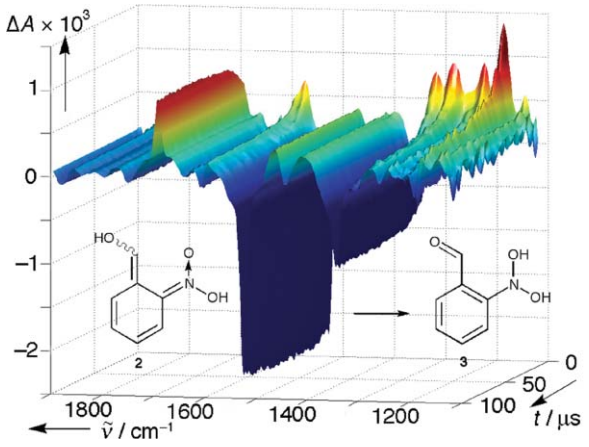

Fig. 4 Step–scan IR difference spectra generated by irradiation of **1** (R = H) in CD_3CN/CN.

The initial difference spectrum (1 μs after the laser flash) is dominated by bleaching of the absorption bands of **1** at 1348 and 1527 cm^{-1}, and new absorption bands at 1190, 1223, 1290, 1319, 1573 (asymm. stretch C=C–O), and 1619 cm^{-1} (asymm. stretch C=N–O) that are due to the formation of an *aci*-nitro compound **2** (R = H). The assignments are based on the results of DFT calculations, which were done for each of the four geometrical isomers of **2**.[20] Moreover, a strong absorption band at 1695 cm^{-1} is present in the first spectrum. It is attributed to the C=O stretch of **3**. The spectrum lacks absorption near 1500 cm^{-1}, indicating the absence of a nitroso group. In the subsequent spectra, the C=O band increases further, concomitant with the decay of the *aci*-nitro bands.

Component analysis of the difference spectra, Fig. 4, indicated the presence of two significant spectral components, *i.e.*, a uniform conversion **2** → **3**. The latter was persistent up to 100 μs. Least-squares fitting of a single exponential function to the reduced data set left residuals within the noise level and gave a rate constant of $(6.7 \pm 0.4) \times 10^4\ s^{-1}$ (*ca.* 30 °C). Prominent features of the final spectrum are the bands at 1184 (1170, ring stretch), 1416 (1380, OH bend), 1466 (1433, OH bend), 1695 (1692, C=O stretch) cm^{-1}. The wavenumbers and assignments given in brackets were obtained by DFT calculations for **3** (R = H). LFP of **1** (R = H) in acetonitrile solution gave bi-exponential decay traces at $\lambda_{max} = 420$ nm, $k_1^{aci} = 6 \times 10^5\ s^{-1}$ (about 15% of the amplitude), and $k_2^{aci} = 2 \times 10^4\ s^{-1}$, in satisfactory agreement with the kinetics determined by TRIR.

Dehydration of intermediate **3** (R = H) to the end product 2-nitrosobenzaldehyde (**4**, R = H) did not occur in CD_3CN within the upper time limit of the step–scan method (1 ms). To accelerate dehydration, 5 mM of D_2SO_4 were added. The hydrate **3** (R = H) was now formed within 1 μs and the dehydration to **4** (R = H) was observed with a rate constant of $k = (3.6 \pm 0.4) \times 10^3\ s^{-1}$ (30 °C, Fig. 5). The reaction **3** → **4** is characterised by the appearance of the N=O stretch band at 1504 cm^{-1}. At the same time, the C=O stretch frequency shifts from 1695 (**3**) to 1700 cm^{-1} (**4**). The final spectrum with prominent absorption bands at 1182, 1268 (1242, ring stretch), 1432, 1504 (1540, N=O stretch), 1699 (1721, C=O stretch) cm^{-1} was equal to a difference spectrum generated with authentic samples of **1** (R = H) and **4** (R = H).

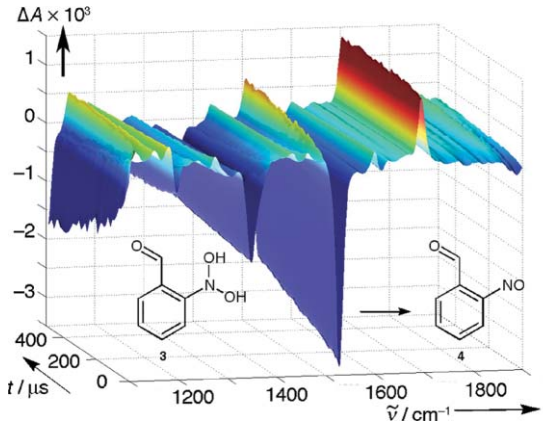

Fig. 5 Step–scan IR spectra obtained by irradiation of **1** (R = H) in CD_3CN/5 mM D_2SO_4.

The spectra shown in Fig. 4 and 5 above document the formation and dehydration of intermediate **3** (path b of Scheme 1) in anhydrous acetonitrile solution. The addition of 1% water suffices to direct the reaction predominantly *via* path a. A fast-scan IR measurement with a CD_3CN solution of **1**-^{18}O (R = H) containing 1% H_2O (Fig. 6) showed that the formation of the nitroso band of **6** (R = H) was largely complete within 1 s. The carbonyl bands at 1670 (C=^{18}O) and 1699 cm^{-1} (C=O, intensity ratio 4:6), rose with a first-order rate constant of $k = (2.0 \pm 0.1) \times 10^{-3}\ s^{-1}$ (dehydration of **6**). Over the same time period, the N=O band was shifted from 1498 to 1503 cm^{-1}.

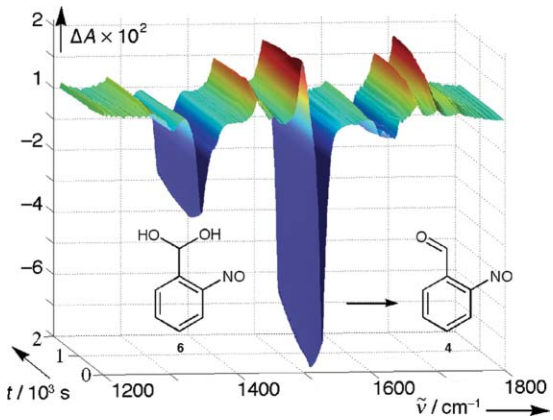

Fig. 6 Fast–scan IR spectra taken between 1 and 2000 s after excitation of ^{18}O-labeled **1** (R = H) in CD_3CN with 1% H_2O.

IR measurements in wholly aqueous solutions (Fig. 7) are more difficult to perform, because strong absorption by the solvent demands the use of very short path lengths. Measurements in D_2O were feasible with a path length of 25 μm, necessitating a 10 mM concentration of **1** (R = H) to achieve sufficient absorption of the laser pulse (266 nm). This produced a rather high concentration of the nitroso products (1496 cm^{-1}), which then disappeared, presumably by forming nitroso dimers, with a half-life of about 15 s. However, only about 30% of the C=O band at 1700 cm^{-1} appears within 1 s after excitation. The major part of the C=O band grows in with a first-order rate constant of 2.8×10^{-2} s^{-1}. As the *aci*-nitro intermediate **2** decays with a rate constant of about 1×10^4 s^{-1} in neutral aqueous solution, this observation indicates that the major fraction reacts *via* the long-lived carbonyl hydrate **6** (path a), which then forms NO dimers under the conditions of the IR experiment. Finally, dehydration of the hemiacetal functions is responsible for the slow appearance of the C=O band.

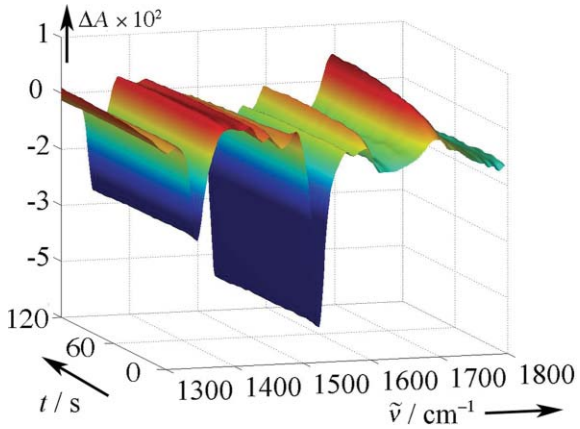

Fig. 7 Fast-scan IR spectra obtained by irradiation of **1** (R = H) in D_2O.

DFT calculations

2-Nitrobenzyl alcohol (1, R = H) and its isomers. The potential energy surface for isomerisation of **1** (R = H) was explored by DFT. The energies of the most stable conformers of **1**, *syn*-**1** and *anti*-**1** are shown in Scheme 2.

An intramolecular hydrogen bond renders the *syn*-conformer slightly more stable than *anti*-**1** despite some repulsive interactions in the former: The nitro group in *syn*-**1** is twisted out of the ring plane by 21°, but is coplanar in *anti*-**1**. SCRF calculations indicate that the conformational equilibrium shifts towards the *anti*-isomer in polar solvents. Both conformers have the same energy in acetonitrile, and *anti*-**1** is favoured by 7.6 kJ mol^{-1} in water (PCM). Both *anti*- and *syn*-**1** are well disposed

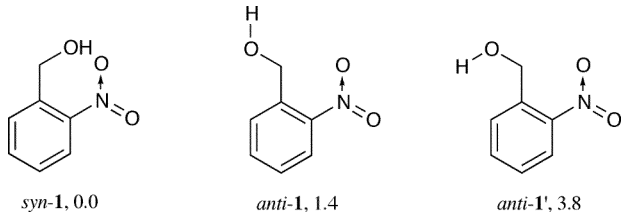

Scheme 2 ZPE-corrected energies of **1** (R = H) in kJ mol^{-1} relative to the *syn*-conformer as obtained by DFT calculations.

for light-induced intramolecular hydrogen transfer from the methylene to the nitro group upon electronic excitation; the closest nonbonded distance between the H–(CH) and O–(NO) atoms is 2.401 Å in *anti*- and 2.484 Å in *syn*-**1**.

The most stable conformer of each of the four geometrical isomers of the quinonoid *aci*-nitro compound **2** (R = H), *EE*, *ZE*, *EZ* and *ZZ*, is shown in Scheme 3. The backward reaction from *ZE*-**2** to *anti*-**1** encounters an overall barrier of 65 kJ mol^{-1} and proceeds *via* a conformer of *ZE*-**2** with the OH group oriented towards the enol function. Two further isomers of **1** (R = H) were located, namely hydrates of 2-nitrosobenzaldehyde at the nitroso (**3**, R = H) and at the aldehyde function (**6**, R = H).

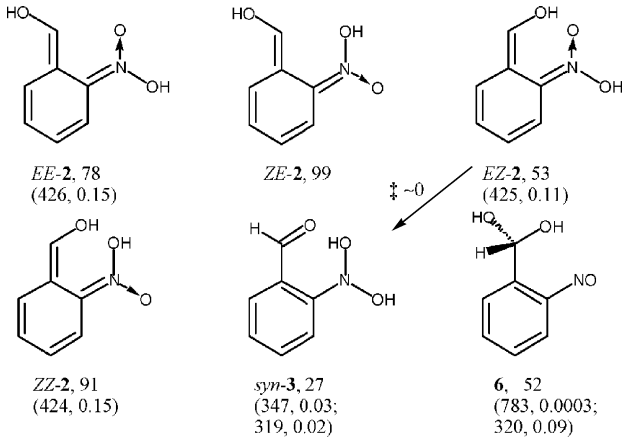

Scheme 3 ZPE-corrected energies in kJ mol^{-1} of **2**, **3**, and **6** (R = H) relative to *syn*-**1**. The calculated positions (λ/nm) and oscillator strengths of the first electronic transition are given in brackets. In *aci*-compounds **2** the first letter *E* or *Z* designates the configuration of OH in the nitronic moiety, the second one that of OH in the enol function.

Formation of the nitroso hydrate *syn*-**3** (R = H) by intramolecular proton transfer from the isomer *EZ*-**2** is calculated to be exothermic by 26 kJ mol^{-1} with a negligible energy barrier.[21] The most stable *anti*-conformer of **3** has an energy of 20 kJ mol^{-1} relative to *syn*-**1**. For the geometric isomers *EE*-**2** and *ZE*-**2**, proton transfer to the nitronic acid function is possible only through the solvent or other proton acceptors. Cyclization of *EZ*-**2** to *trans*-benzisoxazolidine (*trans*-**5**, Scheme 4) is also exothermic by 33 kJ mol^{-1}, but it encounters a large activation barrier of 91 kJ mol^{-1}. The activation barrier for cyclization of *EE*-**2** to *cis*-benzisoxazolidine (*cis*-**5**) is 54 kJ mol^{-1}.

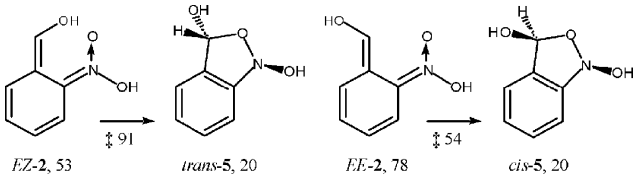

Scheme 4 ZPE-corrected energies in kJ mol^{-1} relative to that of *syn*-**1** and transition state energies.

Anionic species formed by deprotonation. *Aci*-nitro compounds are moderately strong acids that ionise in aqueous

Table 4 Gas-phase deprotonation free energies in kJ mol^{-1} (298 K) and acidity constants in aqueous solution (298 K) calculated at the B3LYP/6-311+G(2d,p) level of theory. Geometries were optimised using the 6-31G(d) basis set for neutral species and the 6-31+G(d) basis set for anions[a]

Reaction	ΔG° (gas phase)	pK_a (water, PCM)
Anti-**1** → *E*-**2**$^-$	1429	17.5
Syn-**1** → *Z*-**2**$^-$	1391	13.8
EE-**2** → *E*-**2**$^-$	1350	4.7
EZ-**2** → *Z*-**2**$^-$	1338	3.4
EE-**2** → *anti*-**3**$^-$	1316	4.9
Anti-**3** → *anti*-**3**$^-$	1363	13.8
Syn-**3** → *syn*-**3**$^-$	1356	10.3

[a] pK_a = $(\Delta_r G^\circ + \Delta\Delta_s G)/(2.303RT)$ + 15.74, where $\Delta_r G^\circ$ is the free energy of the gas-phase reaction AH + OH$^-$ = A$^-$ + H$_2$O, $\Delta\Delta_s G$ is the difference of solvation free energies for the products and reactants, and 15.74 is the pK_a of water.[12]

solution. We performed full geometry optimisation for the anions formed by deprotonation of **1** (R = H) and its isomers at the B3LYP/6-31+G(d) level of theory. Single point energies were computed with the 6-311+G(2d,p) basis set. Deprotonation free energies (gas phase) and pK_a values (aqueous solution) are given in Table 4.

The energies of the most stable conformers of the anions (B3LYP/6-311+G(2d,p)) are given in Scheme 5 relative to that of *E*-**2**$^-$; they are corrected using scaled B3LYP/6-31+G(d) zero-point vibrational energies. We also located two conformers of the deprotonated carbonyl hydrate **6**, **6**$^-$, with energies of −29 and −41 kJ mol^{-1} relative to *E*-**2**$^-$. The enol *E*-**2**$^-$ is calculated to be 32 kJ mol^{-1} higher in energy than the aldehyde *anti*-**3**$^-$. Thus, the enol function of the *aci*-compounds **2** is predicted to be a weaker acid than the nitronic acid function in the gas phase, but the calculated acidity constants in aqueous solution are nearly equal.

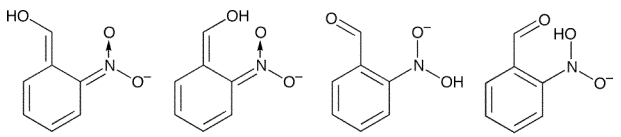

E-**2**$^-$ g: 0, aq: 0 (481, 0.15) | *Z*-**2**$^-$ g: –41, aq: –12 (470, 0.12) | *anti*-**3**$^-$ g: –32, aq: +7 | *syn*-**3**$^-$ g: –48, aq: –15 (457, 0.11)

Scheme 5 ZP-corrected energies of anions **2**$^-$ and **3**$^-$ (R = H, g, 0 K) and free energies (aq, 298 K) in kJ mol^{-1} relative to *E*-**2**$^-$. The calculated positions (λ/nm) and oscillator strengths of the first electronic transition are given in brackets.

1-(2-Nitrophenyl)ethanol (*1*, R = CH$_3$). In the gas phase the *syn*-conformer of **1** (R = CH$_3$) is favoured over the *anti*-conformer by 1.6 kJ mol^{-1}. The relative stability is reversed in acetonitrile and water where *anti*-**1** (R = CH$_3$) is predicted to be below the *syn*-conformer by 0.4 and 6.9 kJ mol^{-1}, respectively. Geometries of two isomers of the *aci*-form (*EZ*-**2** and *EE*-**2**) and one conformer of the hydrate of 2-nitrosoacetophenone (**3**, R = CH$_3$) were also optimised at the B3LYP/6-31G(d) level. Their relative stabilities are similar to those of the corresponding isomers of 2-nitrobenzyl alcohol.

Discussion

2-Nitrobenzyl alcohol (**1**, R = H) and 1-(2-nitrophenyl)ethanol (**1**, R = Me) are cleanly and efficiently dehydrated to the corresponding 2-nitrosobenzoyl compounds **4** by irradiation in various solvents ranging from hexane to water (Fig. 1). This apparent simplicity is deceptive. The present study shows that two different reaction mechanisms prevail in different reaction media. The primary reaction is very fast intramolecular 1,5-hydrogen transfer, $k \approx 1 \times 10^{12}$ s^{-1},[22] leading to *aci*-nitro intermediates **2**. The *aci*-transients exhibit broad absorption around 420 nm and several strong IR peaks in the range of 1190–1320 cm^{-1}.

Four geometrical isomers of the *aci*-nitro intermediates could, in principle, be formed in the primary photoreaction (Scheme 3), and their kinetic behaviour is expected to be quite different. The yield of the different isomeric *aci*-intermediates likely depends on the preferred conformation of the benzyl group of **1** in the ground state (ground state conformational control). Calculations indicate that the *syn*-conformer of **1** is more stable in apolar solvents, and that the *anti*-conformer is favoured in water. In the following, we attempt to assign the configuration of the observed *aci*-nitro transients **2**, and to identify the secondary transient intermediates observed in various media.

Only the *EZ*-isomer of **2** is disposed for direct intramolecular proton transfer to form the nitroso hydrate **3** (Scheme 1, path b). Assistance by amphiphilic molecules is required for the other isomers. The primary photochemical reaction is likely to generate the *ZE*- or *ZZ*-isomers of **2**, in which the proton is transferred to the oxygen atom next to the donating *ortho* substituent.[23] Intramolecular 1,3-proton transfer between the two oxygen atoms of the nitronic acid function (*ZE*-**2** → *EE*-**2** and *ZZ*-**2** → *EZ*-**2**, Scheme 3) is expected to be slow in apolar solvents. The activation barrier for 1,3-proton transfer in the *aci*-form of 2-nitrotoluene was calculated to be 85 kJ mol^{-1}.[10a] However, this barrier is strongly reduced in protic solvents; a B3LYP/6-31+G(d) calculation including a single water molecule for proton transfer and the polarised continuum model for bulk water reduced that barrier to 42 kJ mol^{-1}.

Photodehydration of 1 (R = H or Me) in hexane

To distinguish between the two general reaction mechanisms proposed in Scheme 1, we determined the retention of the ^{18}O label in the alcohol function of (**1**-^{18}O, R = H) in the photoproduct **4**. Reaction by path b would result in complete retention of the label, while reaction by path a would give about 50% retention. Near-complete retention was found by GC-MS of photoproduct **4** after irradiation of **1**-^{18}O (R = H) in hexane, which indicates predominant reaction *via* path b. Consistently, the DFT calculations predict substantial energy barriers for cyclization of *EZ*-**2** and *EE*-**2** (Scheme 4). Unfortunately, rapid loss of the label in the product **4** prohibited a reliable determination of label retention in more polar solvents.

The least-motion path for photoinduced hydrogen transfer from *syn*-**1** (R = H) forms the *aci*-isomer *ZZ*-**2** as the primary photoproduct (Scheme 6). Indeed, the observation of second-order *aci*-decay in hexane suggests that *ZZ*-**2** is observed, which in this solvent requires diffusional encounter with a proton transfer catalyst, in this case a second molecule of *ZZ*-**2**, to promote proton exchange on the nitronic acid function (*ZZ*-**2** → *EZ*-**2**). Once *EZ*-**2** is formed, rapid intramolecular proton transfer gives the nitroso hydrate **3**. Such a reaction sequence is consistent with the decreasing DFT energies of the sequential intermediates, and with the negligible energy barrier calculated for the last step, *EZ*-**2** → *syn*-**3**.

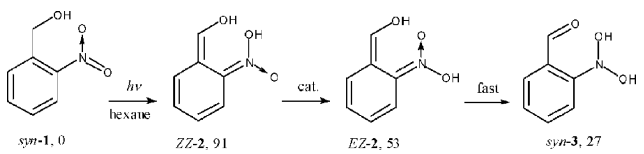

syn-**1**, 0 | *ZZ*-**2**, 91 | *EZ*-**2**, 53 | *syn*-**3**, 27

Scheme 6 Reaction path for **1** (R = H) in hexane and calculated energies in kJ mol^{-1} relative to *syn*-**1** (R = H).

The decay of **2** (R = Me) in hexane obeyed a first-order rate law, but the observed rate constant increased linearly with the concentration of parent **1** (R = Me). In this case, the rate-determining H-shift *ZZ*-**2** → *EZ*-**2** is apparently accelerated

by the protic solute **1** (R = Me). The final dehydration of **3** to **4**, as observed by the growth in absorbance at 320 nm, was quite slow in hexane, $k \approx 1\ s^{-1}$, for both **3** (R = H) and **3** (R = Me).

Taken together, these results indicate that isomer *ZZ*-**2** is the predominant primary photoproduct of **1** (R = H or Me) in hexane solution and that the reaction proceeds by path b of Scheme 1.

Photodehydration of 1 (R = H) in acetonitrile. TRIR experiments show that the reaction in dry acetonitrile also proceeds mostly by path b and that the nitroso hydrate **3** is formed in two waves (Fig. 4). About half of the nitroso hydrate **3** (characterised by the C=O band at 1695 cm^{-1}) is formed within 1 μs. The rest appears in a time-resolved reaction with a rate constant of about $7 \times 10^4\ s^{-1}$. The nitroso band (1504 cm^{-1}) is not formed within 100 μs, unless dehydration of **3** is accelerated by the addition of acid (Fig. 5).

The slight preference of gas-phase DFT calculations for the *syn*-conformer of **1** (R = H) tilts towards the *anti*-conformer in polar media. Photoinduced hydrogen transfer from the latter is expected to yield predominantly *ZE*-**2** as the primary photoproduct. A bi-exponential decay of the *aci*-transient was observed by LFP in acetonitrile with the short-lived component absorbing at somewhat longer wavelengths. This suggests that both *ZZ*-**2** and *ZE*-**2** are formed in the primary photoreaction. The fast component, $k = 2 \times 10^6\ s^{-1}$, may be due to rate-limiting, solvent-assisted transformation of *ZZ*-**2** to *EZ*-**2**, followed by rapid intramolecular proton transfer yielding the nitroso hydrate **3** (R = H). The slower decay, $k = 4 \times 10^4\ s^{-1}$, is attributed to the *ZE*-isomer of **2**. Its isomerisation to the nitroso hydrate **3** requires proton transfer through the solvent.

Small amounts of water in acetonitrile largely suppress reaction *via* the nitroso hydrate **3** (R = H), as indicated consistently by TRIR (Fig. 6) and LFP. We believe that the *anti*-conformation of **1** is favoured by external hydrogen bonding and that excitation of *anti*-**1** leads preferentially to *ZE*-**2**. Alternatively, disruption of the intramolecular H-bond in *EZ*-**2** by water molecules may suppress the tautomerisation to **3**.

In summary, both *ZZ*- and *ZE*-**2** are formed as primary products in anhydrous acetonitrile and the intermediate **3** (path b) appears in two waves. In moist acetonitrile, however, the reaction proceeds predominantly by path a (*ZE*-**2** → *EE*-**2** → **5** → **6**).

pH–rate profiles of transients generated from 1 (R = H) in aqueous solution (Fig. 3). Nitronic acids **2**, $pK_a \approx 4$,[2] ionise to the corresponding nitronate anions $\mathbf{2}^-$. DFT calculations (Table 4) provide a remarkably accurate estimate of the acidity of the nitronic acid function, and they predict that the acidity of the enol moiety, **2** → $\mathbf{3}^-$ + H^+, is about the same. Thus, ionisation of the *aci*-intermediates **2** can take place from either site to give $\mathbf{2}^-$ or $\mathbf{3}^-$. As **2** may be a mixture of isomers, each having two labile protons, the nitronic acid and enol functions, many different proton transfer reactions may be considered for the reaction **2** → **4**. Scheme 7 shows the proton transfer reactions (path b) initiated from *ZE*-**2**, our best bet for the configuration of the primary *aci*-stereoisomer formed in aqueous solution.

The strong base $\mathbf{3}^-$ is expected to be very short-lived and to disappear either by rapid protonation to **3** by water or by elimination of hydroxyl ion yielding **4**. Thus, ionization of the enol function, **2** → $\mathbf{3}^-$ + H^+, would be seen as a decay of *aci*-absorption. In contrast, ionisation of $\mathbf{2}^-$ to $\mathbf{2}^{2-}$ should leave the absorption at 420 nm largely unchanged.

The decay of transient **2** (R = H) at 420 nm was bi-exponential in the pH range of 3–10. The rate constant of the fast component, $k_1^{aci} = 2 \times 10^7\ s^{-1}$, was independent of pH in this range, but was accelerated by buffers. It may be due to deprotonation at the enol function, **2** → $\mathbf{3}^-$ + H^+. Alternatively, cyclisation of **2** prior to ionisation (path a) could compete with ionization to $\mathbf{3}^-$. Methyl substitution at the benzylic position was found to accelerate cyclisation in 2-nitrobenzyl ether.[2] Indeed, the *aci*-decay of **2** (R = Me), $k = 3.8 \times 10^9\ s^{-1}$, is much faster than that of **2** (R = H). However, only reaction **2** → $\mathbf{3}^-$ + H^+ accounts for the partial formation of a nitroso compound within 100 ns (step observed at 330 nm, Fig. 2) and for the increasing yield of this reaction (path b of Scheme 1) at higher pH values.

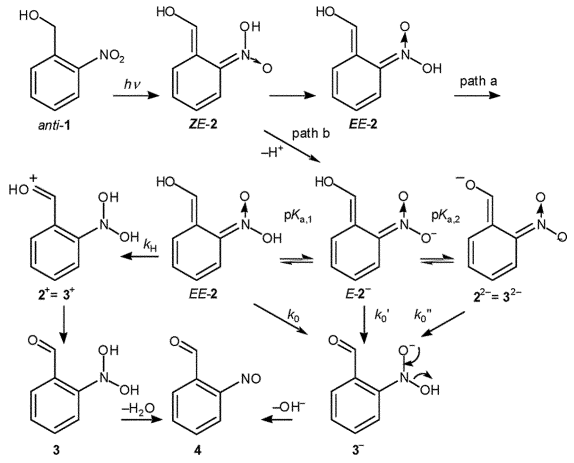

Scheme 7 Proton transfer reactions leading from **2** to **4** (path b).

Nevertheless, the end product **4** is partly formed by the slow dehydration of **6** (path a of Scheme 1). This was established by TRIR spectroscopy with wholly aqueous (D_2O) solutions. Reaction **6** → **4** is also readily observed by conventional UV-spectroscopy of an irradiated aqueous solution of **1** (R = H or Me) in the pH-range of 2–8. The spectral changes (absorbance increase at 230 nm, decay at 316 nm) are quite similar to those associated with the decay of the hemiacetal formed from 2-nitrobenzyl methyl ether (Fig. 6 of ref. 2), and the amplitudes indicate that this reaction, path a, contributes at least 75% to the overall conversion at pH ≈ 5. The rate constants for reaction **6** → **4** (R = H), k^{CO}, are shown in Fig. 3. It should be noted that the equilibrium constant for carbonyl hydration K_h = [**6**]/[**4**] is expected[24] to be on the order of 0.1 for R = H, but four orders of magnitude lower for R = Me.

We conclude that both pathways a and b contribute to the overall reaction in aqueous solution, path b being predominant at pH < 2 and pH > 10, path a in near-neutral solutions.

The pH–rate profile of the longer-lived *aci*-transient (k_2^{aci} in Fig. 3) exhibits five bent regions.[25] Upward curvature is observed around pH 3, 6 and 9, indicating changes of the reaction mechanism. Downward curvatures at pH ≈ 4 and 11.0 suggest rapid ionisation pre-equilibria. The decay of the *aci*-transient is also accelerated by general acids and bases (Table 1). The longer-lived *aci*-transient is attributed to the nitronate anion *E*-$\mathbf{2}^-$, which decays by reprotonation to *EE*-**2** at pH values < 6. Hence the incipient saturation of acid catalysis at pH ≈ $pK_{a,1}$(**2**) = 3.3. However, a second branch of acid catalysis accelerates the decay of *EE*-**2** further at pH < 3. This is attributed to protonation of the nitronic acid yielding $\mathbf{2}^+$. Deprotonation of $\mathbf{2}^+$ at the carbonyl oxygen gives the nitroso hydrate **3**. Protonation of **2** to $\mathbf{2}^+$ becomes faster than cyclisation in strong aqueous acid, so that the amplitude of the slow dehydration of **6** (path a) decreases and is no longer observed at pH < 1.

In contrast to pH–rate profiles observed for the *aci*-transients formed from nitrobenzyl ethers,[2] the decay of the anion $\mathbf{2}^-$ exhibits base catalysis at pH > 7, which saturates at pH = $pK_{a,2}$ ≈ 11. This observation indicates deprotonation of *E*-$\mathbf{2}^-$ by OH^- at the enol site forming the dianion $\mathbf{2}^{2-}$ = $\mathbf{3}^{2-}$. Base catalysis saturates when the equilibrium shifts to $\mathbf{2}^{2-}$. Deprotonation of *E*-$\mathbf{2}^-$ is also indicated by a change in the absorption spectrum of the *aci*-transient, which becomes broader and shifts to λ_{max} ≈ 475 nm at pH > 11. The flat portion in the pH profile of k_2^{aci} around pH 7 is attributed to proton transfer from the enol function of *E*-$\mathbf{2}^-$ through water forming the anion $\mathbf{3}^-$.

To analyse the pH profile of k_2^{aci} on the basis Scheme 7, we assume that the protonation equilibria between **2**, $\mathbf{2}^-$, and $\mathbf{2}^{2-} = \mathbf{3}^{2-}$ are all established prior to the decay of the *aci*-transients. The pre-equilibrium assumption is unlikely to hold for the formation of cation $\mathbf{2}^+$. Here, for simplicity, we assume that protonation of **2** is the rate-determining step. Based on these assumptions Scheme 7 leads to the pH-dependence of k_2^{aci} expressed by eqn. (1). The parameters obtained by nonlinear least-squares fitting of eqn. (1) to the data points are given in Table 3.

No transient absorption above 330 nm is left after the decay of the *aci*-nitro intermediates $\mathbf{2}^-$ (R = H), $\lambda_{max} \approx 430$ nm, that occurs on the microsecond time scale. However, the absorbance at 320 nm rises again on much longer time scales, indicating the presence of an 'invisible' intermediate formed from **2**, which could be **5** or **3**. Both intermediates are formed in aqueous solution. Indeed, the growth curves observed at 320 nm were not accurately mono-exponential at all pH values, but a reliable separation into two first-order processes was not possible. The kinetic traces were thus fitted by a single exponential and the rate constants so obtained were fitted by eqn. (2) (pH-range 1–9), allowing for both acid and base catalysis, as well as a pH-independent contribution. The apparent saturation of base-catalysis at pH > 11 is attributed not to a pre-equilibrium, but to the fact that the decay of $\mathbf{2}^{2-}$ becomes rate-determining for the formation of $\mathbf{3}^-$ at high pH.

The pH-dependent rate constants of the 320 nm growth, k^{NO}, are similar to those observed for ring-opening of the bicyclic intermediate formed from 2-nitrobenzyl methyl ether,[2] which would correspond to the reaction **5** → **6** in the present case. However, dehydration of **3** (R = H) to the nitroso product **4** (R = H) is expected to exhibit similar behaviour. The nitroso hydrates **3** should exhibit little absorption above 300 nm. An absorption maximum of 278 nm, $\varepsilon = 5.5 \times 10^3$ M^{-1} cm^{-1} was reported for the hydrate of 3-nitrosophenol.[26] Henglein *et al.* have determined acid-catalysed rates of dehydration for several arylnitroso hydrates by pulse radiolysis.[27] From their data, the acid-catalysed branch for dehydration of **3** (R = H) may be predicted to exhibit a rate constant of about 1×10^4 M^{-1} s^{-1}. This agrees well with the rate constant of 6.3×10^3 M^{-1} s^{-1} deduced from the pH-rate profile (Fig. 3, Table 3).

The cyclisation of **1** (R = Me) is fast, $k \approx 4 \times 10^9$ s^{-1} (path a). However, part of the reaction still proceeds by path b, presumably by direct deprotonation of one of the *aci*-isomers at the enol function, $\mathbf{2} \rightarrow \mathbf{3}^- + H^+$. No *aci*-transient is observed on the ns time scale, but the kinetics of the slow reactions **3** → **4** and **5** → **6** → **4** are similar to those of **1** (R = H).

A reaction mechanism involving 'proton shuffling' and loss of hydroxyde to the solvent was suggested by Tsien *et al.*[4] to explain the remarkably fast release of Ca^{2+} from the photosensitive 'nitr-5' chelator (**1**, R = aryl). These authors observed two waves of Ca^{2+} release from 'nitr-5', with rate constants of 3000 s^{-1} and 0.17 s^{-1} at pH 7.4, which are close to the rate constants observed here for reactions **3** → **4** and **6** → **4**, respectively.

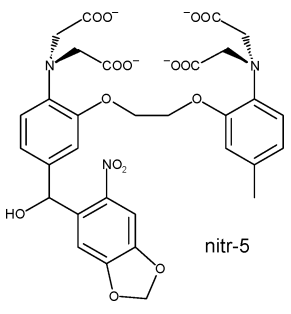

nitr-5

Related mechanisms have been proposed for the photoreactions of 4-nitrobenzyl alcohol[28] and 2-nitrobenzaldehydes.[29]

Conclusions

Aci-nitro intermediates **2** generated by irradiation of the 2-nitrobenzyl alcohols **1** (R = H or Me) have the option of a novel reaction path involving proton transfer from the enol to the *aci*-nitro function forming a nitroso hydrate intermediate **3** (Scheme 1, path b). This mechanism predominates in hexane, dry acetonitrile and in strongly acidic or basic aqueous solutions. The conventional mechanism *via* benzisoxazolidine **5** and carbonyl hydrate **6** (Scheme 1, path a) dominates in wet acetonitrile and in near-neutral aqueous solutions. The dehydration of intermediates **3** and **6** to the nitroso product **4** is orders of magnitude slower than the decay of the *aci*-form. LFP studies of the readily accessible 2-nitrobenzyl alcohols are a convenient method to study the dehydration kinetics of these intermediates, particularly the nitroso hydrates **6**. Nitroso hydrates have, in general, received little attention to date.[27,28]

Acknowledgements

This work is part of project No. 20-68087.02 of the Swiss National Science Foundation. We thank Professor N. Ernsting and his group, HU Berlin, for extensive support in the construction of the pump–probe detection system.

References

1 C. G. Bochet, Photolabile protecting groups and linkers, *J. Chem. Soc., Perkin Trans. 1*, 2002, **2002**, 125–142; A. P. Pelliccioli and J. Wirz, Photoremovable protecting groups: reaction mechanisms and applications, *Photochem. Photobiol. Sci.*, 2002, **1**, 441–458.
2 Y. V. Il'ichev, M. A. Schwörer and J. Wirz, Photochemical reaction mechanisms of 2-nitrobenzyl compounds: methyl ethers and caged ATP, *J. Am. Chem. Soc.*, 2004, **126**, 4581–4595.
3 E. Bamberger, Photochemische Bildungsweise des *o*-Nitroso-benzaldehyds, *Ber.*, 1918, **51**, 606–612.
4 S. R. Adams, J. P. Y. Kao, G. Grynkiewicz, A. Minta and R. Y. Tsien, Biologically useful chelators that release Ca^{2+} upon illumination, *J. Am. Chem. Soc.*, 1988, **110**, 3212–3220.
5 (*a*) G. Gauglitz and S. Hubig, Photokinetische Grundlagen moderner chemischer Aktinometer, *Z. Phys. Chem. (Munich)*, 1984, **139**, 237–246; (*b*) G. Gauglitz and S. Hubig, Chemical actinometry in the UV by azobenzene in concentrated solution: A convenient method, *J. Photochem.*, 1985, **30**, 121–125; (*c*) G. Persy and J. Wirz, Spectrophotometric actinometry with azobenzene, *EPA Newslett.*, 1987, **29**, 45–46.
6 S. A. Kovalenko, A. L. Dobryakov, J. Ruthmann and N. P. Ernsting, Femtosecond spectroscopy of condensed phases with chirped supercontinuum probing, *Phys. Rev. A*, 1999, **59**, 2369–2384.
7 J. H. Kaplan, B. Forbush and J. F. Hoffman, Rapid photolytic release of adenosine 5′-triphosphate from a protected analogue: utilization by the Na:K pump of human red blood cell ghosts, *Biochemistry*, 1978, **17**, 1929–1935.
8 M. J. Frisch, G. W. Trucks, H. B. Schlegel, G. E. Scuseria, M. A. Robb, J. R. Cheeseman, V. G. Zakrzewski, J. A. Montgomery, Jr., R. E. Stratmann, J. C. Burant, S. Dapprich, J. M. Millam, A. D. Daniels, K. N. Kudin, M. C. Strain, O. Farkas, J. Tomasi, V. Barone, M. Cossi, R. Cammi, B. Mennucci, C. Pomelli, C. Adamo, S. Clifford, J. Ochterski, G. A. Petersson, P. Y. Ayala, Q. Cui, K. Morokuma, P. Salvador, J. J. Dannenberg, D. K. Malick, A. D. Rabuck, K. Raghavachari, J. B. Foresman, J. Cioslowski, J. V. Ortiz, A. G. Baboul, B. B. Stefanov, G. Liu, A. Liashenko, P. Piskorz, I. Komaromi, R. Gomperts, R. L. Martin, D. J. Fox, T. Keith, M. A. Al-Laham, C. Y. Peng, A. Nanayakkara, M. Challacombe, P. M. W. Gill, B. G. Johnson, W. Chen, M. W. Wong, J. L. Andres, C. Gonzalez, M. Head-Gordon, E. S. Replogle and J. A. Pople, *GAUSSIAN 98 (Revision A.11)*, Gaussian, Inc., Pittsburgh, PA, 2001.
9 A. P. Scott and L. Radom, Harmonic vibrational frequencies: an evaluation of Hartree–Fock, Møller–Plesset, quadratic configuration interaction, density functional theory, and semiempirical scale factors, *Phys. Chem.*, 1996, **100**, 16502–16513.
10 (*a*) Y. V. Il'ichev and J. Wirz, Rearrangements of nitrobenzyl compounds. 1. Potential energy surface of 2-nitrotoluene and its isomers explored with *ab initio* and density functional theory methods, *J. Phys. Chem. A*, 2000, **104**, 7856–7870; (*b*) Y. V. Il'ichev, Rearrangements of nitrobenzyl compounds. 2. Substituent effects on the reactions of the quinonoid intermediates, *J. Phys. Chem. A*, 2003, **107**, 10159–10170.

11 M. Cossi, V. Barone, R. Cammi and J. Tomasi, *Ab initio* study of solvated molecules: a new implementation of the polarizable continuum model, *Chem. Phys. Lett.*, 1996, **255**, 327–335.
12 J. R. Pliego, Jr. and J. M. Riveros, Theoretical calculation of pK_a using the cluster–continuum model, *J. Phys. Chem.*, 2002, **106**, 7434–7439.
13 M. Schwörer and J. Wirz, 2-Nitrotoluene: thermodynamic and kinetic parameters of the *aci*-tautomer, *Helv. Chim. Acta*, 2001, **84**, 1441–1458.
14 M. E. Casida, C. Jamorski, K. C. Casida and D. R. Salahub, Molecular excitation energies to high-lying bound states from time-dependent density-functional response theory: Characterization and correction of the time-dependent local density approximation ionization threshold, *J. Chem. Phys.*, 1998, **108**, 4439–4449.
15 A. Barth, J. E. T. Corrie, M. J. Gradwell, Y. Maeda, W. Mäntele, T. Meier and D. R. Trentham, Time-resolved infrared spectroscopy of intermediates and products from photolysis of 1-(2-nitrophenyl)ethyl phosphates: reaction of the 2-nitrosoacetophenone byproduct with thiols, *J. Am. Chem. Soc.*, 1997, **119**, 4149–4159.
16 R. A. McClelland and M. Coe, Structure-reactivity effects in the hydration of benzaldehydes, *J. Am. Chem. Soc.*, 1983, **105**, 2718–2725.
17 The extinction coefficient of *o*-benzoquinone is $\varepsilon_{390} = 2200$ M^{-1} cm^{-1} (S. Goldschmidt and F. Graef, Optische Untersuchungen an Chinonen und freien Radikalen, *Ber.*, 1928, **61**, 1858–1869); that of 2,2-dimethylisoindene is $\varepsilon_{400} = 3060$ M^{-1} cm^{-1} (; M. Allan, K. R. Asmis, S. El houar, E. Haselbach, M. Capponi, B. Urwyler and J. Wirz, Triplet energy of 2,2-dimethylisoindene from electron-energy-loss spectroscopy and photoinduced triplet energy transfer, *Helv. Chim. Acta*, 1994, **77**, 1541–1548).
18 Excitation of compounds **1** at 248 nm in aqueous base formed an additional, unidentified intermediate with absorption overlapping the *aci*-nitro transients **2**. This complication was avoided by excitation with 308 nm pulses from the excimer laser operating on XeCl.
19 R. G. Bates, Determination of pH. *Theory and Practice*, Wiley, New York, 1973.
20 Calculated frequencies are available as supplementary material.‡ The predicted band positions and intensities for the four isomers were too similar to warrant an identification of the observed geometrical isomer(s) of **2**.
21 A potential energy minimum was found for *EZ*-**2**, but the energy of the transition state was lower than that of *EZ*-**2** after correcting for the zero-point energies.
22 The rate of formation of the *aci*-transients may depend on the wavelength of excitation: A. Blanc and C. Bochet, Isotope effects in photochemistry. 1. *o*-Nitrobenzyl alcohol derivatives, *J. Am. Chem. Soc.*, 2004, **126**, 7174–7175. Compound **1** (R = Me) was excited at 270 nm in this pump–probe experiment.
23 If the excited-state proton transfer occurs adiabatically from triplet **1** yielding the triplet state of the *aci*-intermediate, then isomerization around the C=N bond might occur: R. Haag, J. Wirz and P. J. Wagner, The photoenolization of 2-methylacetophenone and related compounds, *Helv. Chim. Acta*, 1977, **60**, 2595–2607. However, formation of the *aci*-transient within 1 ps suggests that the reaction proceeds from the excited singlet state of **1** to yield the ground state *aci*-intermediate **2** through a conical intersection.
24 P. Zuman, Additions of water, hydroxyde ion, alcohols and alkoxide ions to carbonyl and azomethine bonds, *ARKIVOC*, 2002, 85–140, http://www.arkat-usa.org/ark/journal/2002/General/2-540R/540R.asp.
25 G. M. Loudon, Mechanistic interpretation of pH–rate profiles, *J. Chem. Educ.*, 1991, **68**, 973–984.
26 W. Grünbein and A. Henglein, Pulsradiolytische Untersuchung zweibasischer Radikale der Reduktion von Nitrophenolen in wässriger Lösung, *Ber. Bunsen-Ges.*, 1969, **73**, 376–382.
27 W. Grünbein, A. Fojtik and A. Henglein, Pulsradiolytische Untersuchung kurzlebiger Hydrate von aromatischen Nitrosoverbindungen, *Monatsh. Chem.*, 1970, **101**, 1243–1252.
28 P. Wan and K. Yates, Photoredox chemistry of nitrobenzyl alcohols in aqueous solution. Acid and base catalysis reaction, *Can. J. Chem.*, 1986, **64**, 2076–2086.
29 M. V. George and J. C. Scaiano, Photochemistry of *o*-nitrobenzaldehyde and related studies, *J. Phys. Chem.*, 1980, **84**, 492–495.

PPS
Paper
www.rsc.org/pps

Primary photoreactions of phylloquinone (vitamin K_1) and plastoquinone-1 in solution †

Martin-A. Hangarter, Aldo Hörmann, Yavor Kamdzhilov and Jakob Wirz*

Departement Chemie, Universität Basel, Klingelbergstrasse 80, CH-4056 Basel, Switzerland. E-mail: J.Wirz@unibas.ch

Received 14th February 2003, Accepted 18th March 2003
First published as an Advance Article on the web 4th April 2003

The photoreactions of electron transport quinones vitamin K_1 (**1**) and plastoquinone-1 (**2**) were studied by picosecond pump–probe spectroscopy, nanosecond flash photolysis, step-scan FTIR spectroscopy, and by irradiation in glassy solvents at 77 K with optical and EPR detection. In polar solvents, charge transfer from the β,γ-double bond to the quinone moiety initiates intramolecular proton transfer from the side chain, $k = 2.7 \times 10^{11}$ s^{-1}, yielding 1,3-quinone methide diradicals, which establish a metastable equilibrium between the singlet and the triplet state. Subsequent proton transfer through the solvent forms 1,2-quinone methides. In apolar solvents the predominant primary photoreaction is formation of cyclic 'preoxetane' diradicals ($k_{form} > 3 \times 10^{11}$ s^{-1}, $k_{decay} \approx 1 \times 10^9$ s^{-1}), which revert to a photostationary *E*/*Z* mixture of the starting materials, unless they are trapped by oxygen. The β,γ-double bond in the isoprenoid side chain thus provides two efficient deactivation processes, which prevent the intermolecular photoreactions commonly observed with the parent quinones. A combined mechanistic scheme rationalises the known photoreactions of **1**, **2** and related compounds in solution.

Introduction

Electron transfer processes involving quinone acceptor molecules are ubiquitous in living organisms.[1] Quinones amount to 0.1–1% of the dry weight of leaves,[1a] and they exhibit strong absorption in the near UV extending to the visible range. Hence, the photochemistry of quinones in bioenvironments is undoubtedly relevant, notwithstanding their function to transport electrons and protons. UV irradiation of mitochondria and of preparations of photosystems I and II induces photooxidation of the quinones and thereby interrupts electron transport, which is restored upon replacement of the quinones.[1a,2] The two phylloquinone cofactors in cyanobacterial photosystem I have recently been localised.[3]

Electronically excited quinones are highly reactive towards most organic substrates,[4] forming 2 + 2 cycloaddition products[5a] and radicals by hydrogen abstraction[5b] or electron transfer.[6] Yet, there is no evidence that electron transport quinones attack their environment when they are electronically excited. How is their potentially deleterious reactivity prevented? Pioneering flash photolysis studies by Porter and co-workers[7,8] showed that intramolecular processes involving the isoprenoid side chain dominate the photoreactions of vitamin K_1 (**1**) and of plastoquinone-1 (**2**): '*Since Vit. K_1, ubiquinone, and plastoquinone all contain the β,γ-unsaturated phytyl chain it is difficult to avoid the conclusion that its presence in photosynthetic quinones is significant*'.[7]

Many products formed by irradiation of K-vitamins[9–13] and of plastoquinones[14] in solution have been isolated and identified. Product distributions strongly depend on the reaction conditions (solvent, presence of water and oxygen, *etc.*) and product analysis is complicated by the instability of several products to irradiation[11a] or to work-up.

Flash photolysis studies of electron transport quinones, initiated by Porter and co-workers[7,8] and continued by Creed *et al.*,[13] led to the identification of 1,2-quinone methide (1,2-QM) tautomers, which form chromenols and hydroperoxides (QM–O_2). A 1,3-quinone methide (1,3-QM) tautomer was tentatively identified as a precursor of the 1,2-QM formed from plastoquinone.[8] On the other hand, Wilson *et al.*[11a,15] proposed that the isolated hydroperoxides (QM–O_2) and trioxanes (PO–O_2) are both formed by trapping of a 'preoxetane' diradical (PO), the logical precursor for PO–O_2. A summary of these reactions, as proposed for menaquinone-1 (**3**) by Creed[13] and by Wilson[11,15] and their co-workers, is shown in Scheme 1.

Current progress in the elucidation of photosynthetic reaction centres and electron transport chains prompted us to complete and report a study of vitamin K_1 (**1**), plastoquinone-1 (**2**) and menaquinone-1 (**3**) that we initiated twenty years ago.[16] Using time-resolved spectroscopy and low-temperature irradiation we have observed and characterised both primary diradicals, PO and 1,3-QM. Interpretation of the results was aided by comparative experiments with compounds **4**–**9**.

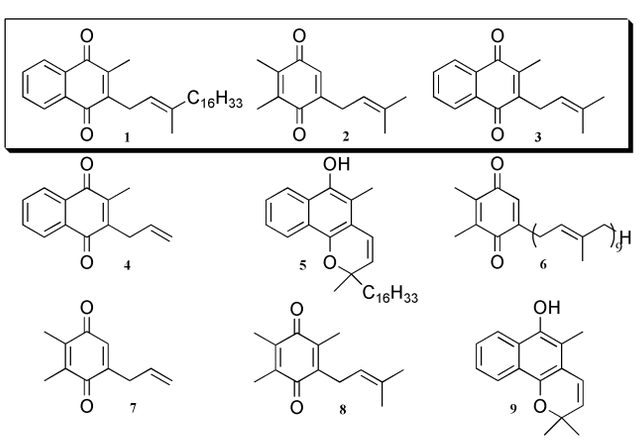

Experimental

Methods

A conventional flash photolysis setup[17] with 1000-J discharge flash lamps was used for transients with lifetimes exceeding ~20 μs. The nanosecond laser flash photolysis (LFP) setup

† Dedicated to the memory of Nobel Laureate, Lord George Porter FRSC FRS OM.

 DOI: 10.1039/b301808n

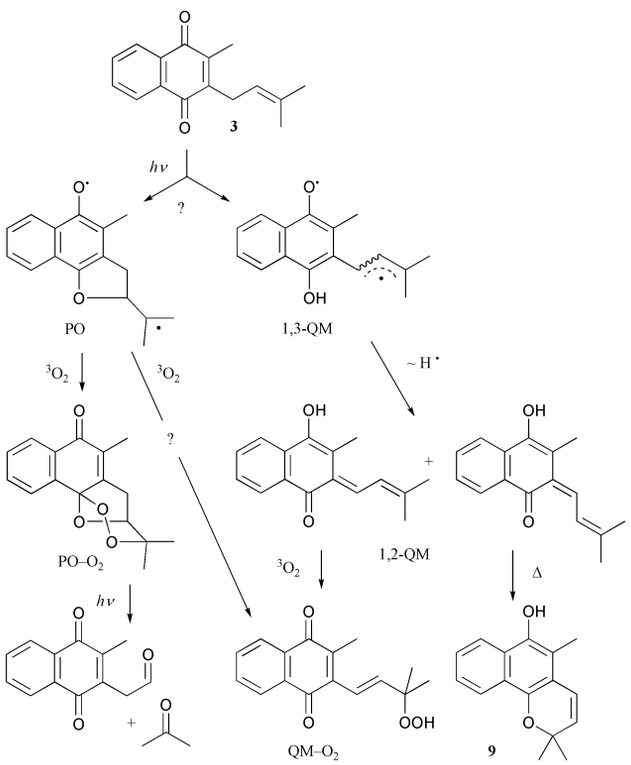

Scheme 1 Reaction paths proposed[11,13] for the photooxidation of menaquinone-1 (**3**).

could be operated in kinetic or spectrographic mode. An excimer laser (100–200 mJ pulse^{-1}, 25 ns) operated on KrF (248 nm), XeCl (308 nm) or XeF (351 nm) was used as an excitation source. Consistent results were obtained with a Nd glass laser in the early experiments.[16] Frequency tripling or quadrupling gave 355- or 266-nm pulses, respectively, of *ca.* 50 mJ per pulse and a half-width of *ca.* 20 ns. Kinetic traces were analysed by non-linear least-squares fitting of the appropriate rate laws. The instrument used for picosecond pump–probe spectroscopy (excitation at 248 nm, pulse energy 4 mJ, pulse duration 0.8 ps) and the methods used for data analysis have been described previously.[18]

Optical spectra at low temperatures were recorded with a quartz Dewar that was equipped with optical windows. The sample cells (fused quartz, 1-cm path length) were kept in a hollow copper sample holder that was cooled with a stream of nitrogen gas evaporated from a large liquid-nitrogen vessel. The temperature of the sample holder inside the quartz Dewar was measured with a calibrated thermocouple, and its readings were used to control a valve in front of a mechanical vacuum pump. Thus, the temperature could be controlled to within ± 2 K and reduced to slightly below 77 K by evaporating nitrogen from the vessel through the sample holder at reduced pressure.

The step-scan instrument was built by the design of Rödig and Siebert[19] using a Bruker IFS 66v/s Fourier transform infrared spectrophotometer equipped with a globar IR source, a KBr beam splitter, a nitrogen-cooled MCT detector KV100-1-B-7/190 and an external DC-coupled preamplifier from Kolmar, Inc., KA020-E6/MU/B. A Quantel Brilliant W Nd:YAG laser (266 or 355 nm, pulse width 6 ns, pulse energy ≤5 mJ, pulse frequency 10 Hz) was used for excitation. The spectral IR region was restricted to 2257–1130 cm^{-1} by using a cut-on/cut-off filter combination from LOT Oriel. Deuterated acetonitrile solutions of vitamin K_1 were used with an optical density of 0.4 at the excitation wavelength. The solution was flowed through the sample cell (CaF_2 windows, 200-μm path length) to avoid re-irradiation of transient intermediates and photoproducts. The experiment was carried out with a resolution of 8 cm^{-1}. The Fourier-transformed data were baseline corrected and factor analyzed in the region 1200–2000 cm^{-1}. Two significant factors were generally sufficient to reproduce the time evolution of the spectra within experimental accuracy. This procedure resulted in a substantial elimination of noise and massive data reduction. A first-order rate law was fitted to the reduced set of spectra so obtained.

Quantum yields for the formation of the 1,2-quinone methides (1,2-QM) from vitamin K_1 (**1**) and plastoquinone-1 (**2**) in degassed methanol solution were estimated as follows. The initial transient absorbances A_0 (at 485 nm for **1**, at 500 nm for **2**) formed by LFP (excimer laser, 351 nm) were converted to concentrations of the 1,2-QM transients by assuming a molar absorbance coefficient of 8000 M^{-1} cm^{-1} based on the irradiations at 77 K (*vide infra*). Actinometry of the laser flash was done with azobenzene in methanol assuming $\phi_{trans \longrightarrow cis} = 0.11$.[20]

Materials

Spectrograde solvents were used where available. Tetrahydrofuran (THF) and 2-methyltetrahydrofuran (MTHF) were refluxed over lithium aluminium hydride and subsequently over potassium, distilled under nitrogen, degassed, and kept over an equimolar alloy of sodium and potassium. Vitamin K_1 (**1**) was purchased from Fluka. Menaquinone-1 (**3**) and plastoquinone-1 (**2**),[21] 2-allyl-3-methylnaphthoquinone (**4**),[22] 2,3-dimethyl-5-allyl-1,4-benzoquinone (**7**),[22] and the chromenol derivatives (**5**) and (**9**)[23] were synthesised by the published procedures. Samples of the *Z*-isomer of vitamin K_1 (*Z*-**1**) and of plastoquinone-9 (**6**) were supplied by Roche. 2,3,6-Trimethyl-5-(3-methyl-2-butenyl)-1,4-benzoquinone (**8**) was synthesised as described by Scott[21b] for **2**. ^{1}H NMR (60 MHz, $CDCl_3$): δ 1.67 (s, 3H), 1.78 (s, 3H), 1.95 (s, 9H), 3.15 (d, 2H), 4.95 (t, 1H). UV (MeOH): λ_{max} = 266 nm ($\varepsilon = 1.7 \times 10^4$ M^{-1} cm^{-1}), 310 (5.5×10^2).

Quantitative analysis of the *E* and *Z* geometrical isomers of **1** by HPLC was done with an MS-SI 60.5 μ column using 3% diisopropyl ether in *n*-hexane as an eluent.[24]

Calculations

Density functional calculations were done using the B3LYP functional with the 6-31G* basis set, as provided in revision A.7 of the Gaussian 98[25] program package. The PCM continuum model[26] was used to simulate solvation in acetonitrile ($\varepsilon = 36.64$). All structures were fully optimised. Quoted energies include zero-point vibrational corrections. Frequencies were scaled with a factor of 0.9806.[27]

Results

The wavelength of excitation had no noticeable influence on the primary processes.[28] Also, the nature of the alkyl side chain beyond the first isoprene unit was found to be unimportant for the photochemistry in solution. Vitamin K_1 (**1**), its synthetic *Z*-isomer (*Z*-**1**), and menaquinone-1 (**3**) exhibited practically the same behaviour in all aspects of this study. The same was true for plastoquinone-9 (**6**) and plastoquinone-1 (**2**). Most of the experimental work was done with commercial vitamin K_1 (**1**) and with plastoquinone-1 (**2**), which is easily synthesised and purified. Therefore, we report quantitative data for these two compounds only.

Product studies

Commercial vitamin K_1 (**1**) is prepared from synthetic isophytol and consists of a mixture of two racemic geometrical isomers in an *Z*/*E* ratio of approximately 0.1–0.2.[24,29] The irradiation of a degassed solution of 10^{-4} M **1** in pentane with monochromatic light of 365 nm led to a photostationary equilibrium containing the *Z* and *E* geometrical isomers in a ratio of 0.4. The same equilibrium mixture was obtained starting from a

Table 1 Photoisomerisation of the exocyclic β,γ-double bond of **1** in degassed pentane (HPLC separation)[24]

Irr. time, *t*/min	*Z*/*E* Ratio	
	Sample (*Z*)-**1**	Sample (*E*)-**1**
0	9.6	0.18
5	6.0	0.19
140	0.60	0.35
195	0.43	0.37

sample that initially contained predominantly the *Z*-isomer (Table 1).

New photoproducts were formed in the presence of air and in more polar solvents. The dependence of the product distributions on the reaction conditions was determined qualitatively by thin layer chromatography (TLC) on silica gel using a 5 : 1 mixture of light petroleum, bp 40–60 °C, and ethyl acetate. Monochromatic light of 436 nm was used and irradiation was stopped at low conversions (<5%) in order to avoid secondary photolysis of the photoproducts. Menaquinone-1 (**3**) rather than vitamin K_1 (**1**), and plastoquinone-1 (**2**) and its methyl derivative (**8**) rather than plastoquinone-9 (**6**), were used for improved separation of the photoproducts by TLC. Relying on the product identifications available from previous studies,[9–14] it was possible to draw the following conclusions using only chromatographic retention times (comparison with authentic samples, where available) and UV spectra for compound identification.

The 2-methyl substituted derivatives **3** and **8** were depleted more rapidly than plastoquinone-1 (**2**). The main product from **3** in anaerobic solutions is the chromenol **9**. This product was practically absent when irradiations were carried out in aerated aprotic solutions. The main product from **3** in air-saturated acetonitrile was the hydroperoxide QM–O_2 (Scheme 1). In apolar solvents (CCl_4, isooctane) the cyclic peroxide PO–O_2 and the hydroperoxide QM–O_2 were formed in comparable yield. The effect of oxygen on the product distribution was much more pronounced for **3** than for the plastoquinones. Admission of air to acetonitrile solutions of the plastoquinones **2** or **8** resulted only in the formation of some minor, additional spots on the TLC. The main products were the same as in degassed solutions. The allyl analogues **4** and **7** reacted slowly in all solvents used, and products were not identified.

Pump–Probe experiments with 1 and 4

Sub-picosecond excitation of 2-allyl-3-methyl-1,4-naphthoquinone (**4**) in hexane produced a strong absorption band, $\lambda_{max} \approx 380$ nm extending to 600 nm with a broad maximum at 500 nm, within two picoseconds (not resolved, Fig. 1). The initial diffuse absorption decayed with a rate constant of 5×10^9 s^{-1}, leaving a structured band in the near UV, $\lambda_{max} = 357$, 381 and 398 nm, with weak absorption extending to 520 nm. The decay rate constant, $k \approx 1 \times 10^9$ s^{-1}, of that species was not accurately defined within the accessible 1.8-ns range of the delay line. The longer-lived transient is assigned to the preoxetane diradical PO of **4** (*cf*. Discussion).

Similar results were obtained with the allylnaphthoquinone **4** in methanol (not shown). The initial transient absorption, λ_{max} = 350 and 500 nm, was formed within a few picoseconds. The diffuse absorption decayed with a rate constant of about 5×10^9 s^{-1}, and the strong UV band, λ_{max} = 365 and 385 nm, remained nearly constant up to the maximum delay of 1.8 ns.

Pump–probe spectroscopy of vitamin K_1 (**1**) in isooctane (not shown) also gave similar results. The diffuse absorbance with a maximum at 500 nm decayed more rapidly, $k \approx 1 \times 10^{10}$ s^{-1}, and the remaining UV band, λ_{max} = 358 and 382 nm, decayed to about half of its initial intensity in the accessible time window of 1.8 ns. In contrast, excitation of **1** in methanol

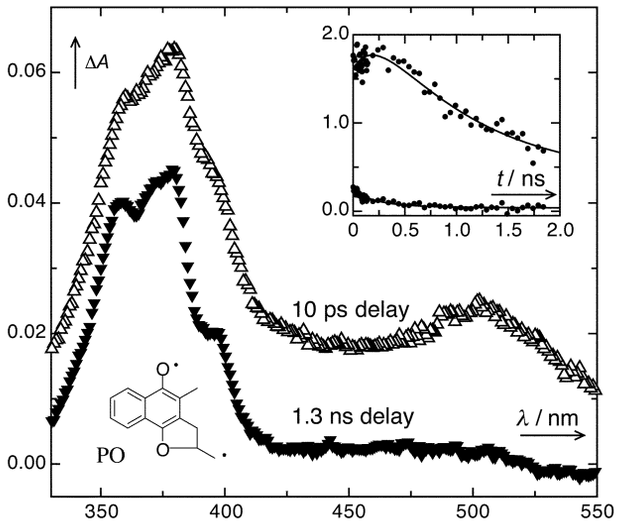

Fig. 1 Pump–probe spectra of 2-allyl-3-methyl-1,4-naphthoquinone (**4**) in hexane. The upper spectrum was recorded 10 ps after excitation, the lower one with a delay of 1.3 ns. The inset shows the coefficients of the first eigenvalue (upper trace) determined by factor analysis of 100 pump–probe spectra taken in the time range up to 1.8 ns and a biexponential kinetic trace obtained by global fitting ($k_1 \approx 5 \times 10^9$ s^{-1}, $k_2 \approx 1 \times 10^9$ s^{-1}). The lower trace of the inset is a kinetic analysis of the spectra in the range of 450 to 550 nm, where the fast decay dominates and is more accurately defined.

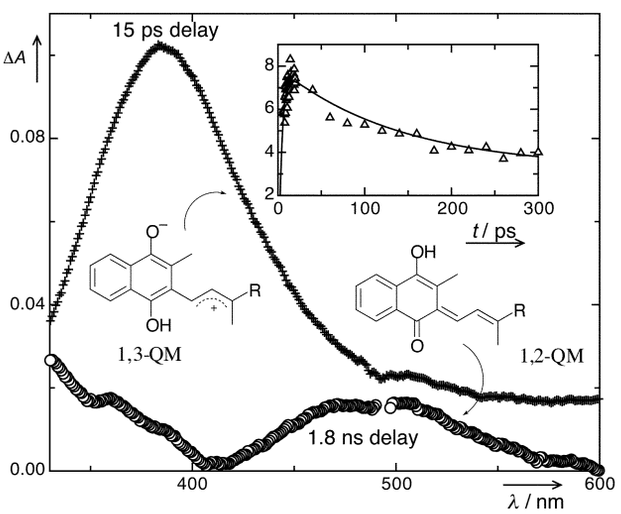

Fig. 2 Pump–probe spectroscopy of **1** in methanol. The displayed spectra were recorded with delays of 15 ps (top) and 1.8 ns (bottom) relative to the excitation pulse. The inset shows the coefficients of the first eigenvalue determined by factor analysis of 120 spectra recorded within 1.8 ns and a biexponential fit function, $k_1 = (2.7 \pm 0.5) \times 10^{11}$ s^{-1}, $k_2 = (7.2 \pm 0.6) \times 10^9$ s^{-1}.

(Fig. 2) gave entirely different results. Rapid, but resolved growth of a strong, Gaussian-shaped transient, λ_{max} = 385 nm, $k_{growth} = (2.7 \pm 0.5) \times 10^{11}$ s^{-1}, was followed by a slower decay, $k = (7.2 \pm 0.6) \times 10^9$ s^{-1}, leaving a broad, long-lived absorption in the visible, λ_{max} = 485 nm. The spectrum of the second, long-lived transient is in excellent agreement with that observed by nanosecond LFP (*vide infra*), which has been assigned to the 1,2-QM(**1**).[7,13] The first transient, λ_{max} = 385 nm, is attributed to the diradical 1,3-QM(**1**) (*cf*. Discussion).

Nanosecond flash photolysis

(a) Vitamin K_1 (1). LFP of **1** or **3** in methanol produced 1,2-QM, $\lambda_{max} \cong 485$ nm, within 20 ns (*cf*. the end spectrum in Fig. 2). The quantum yield for the formation of 1,2-QM was estimated as $\phi = 0.24 \pm 0.01$, where the error limit indicates

Table 2 Kinetic data of the 1,3-QM tautomers of **1** and **2** in various solvents

	Vitamin K_1 (**1**)		Plastoquinone-1 (**2**)				
Solvent	τ^0/μs	k_{O_2} [a]/M^{-1} s^{-1}	A_{330}/A_{400}	τ^0/μs	k_{O_2} [a]/M^{-1} s^{-1}	k_{HAc} [c]/M^{-1} s^{-1}	k_{Py} [c]/M^{-1} s^{-1}
CH_3OH	1.4×10^{-4}		0.35 ± 0.15	0.05 ± 0.01 [b]	–		
CH_3CN	10	$(5 \pm 1) \times 10^8$	0.4 ± 0.2	22 ± 5	$(2.0 \pm 0.3) \times 10^6$	2.5×10^8	1.2×10^{10}
THF	3–7	$(6 \pm 1) \times 10^8$	1.0 ± 0.5	15 ± 4	$(9 \pm 2) \times 10^6$	2.6×10^8	1.1×10^{10}
EtOEt		$(5 \pm 2) \times 10^8$	2.0 ± 1.0	9 ± 2	$(3.0 \pm 0.4) \times 10^7$	6.6×10^8	
CCl_4			–	6 ± 2	$(1.0 \pm 0.1) \times 10^8$		5.0×10^9
Isooctane	1.3	$(1.2 \pm 0.2) \times 10^9$	3.0 ± 1.0	8 ± 3	$(2.8 \pm 0.4) \times 10^8$	2.0×10^9	

[a] Oxygen concentrations from refs. 30. [b] CH_3OD: 0.24 ± 0.02; CD_3OD: 0.21 ± 0.02. [c] Rate constants for reaction with acetic acid and pyridine.

reproducibility. The estimate relies on an assumed absorbance coefficient ε_{485} = 8000 M^{-1} cm^{-1} (*vide infra*) of 1,2-QM(**1**). In aprotic solvents a different transient species was formed within the duration of the pulse (20 ns). This intermediate absorbed strongly in the near UV ($\lambda_{max} \approx$ 330 and 390 nm), and weakly throughout the visible region. The ratio of the absorbances at 330 and 390 nm depended strongly on the polarity of the solvents (Fig. 3, Table 2). The 390-nm band in acetonitrile agrees well with the absorbance observed by pump–probe spectroscopy in methanol (Fig. 2, 15 ps delay), and is attributed to 1,3-QM(**1**).

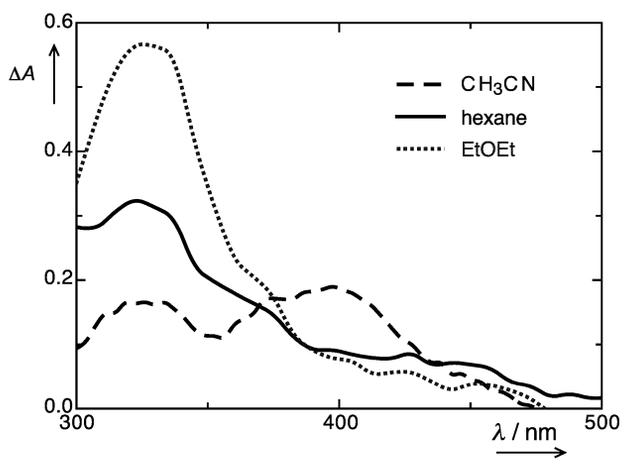

Fig. 3 Initial transient absorption spectra taken with a delay of 50 ns after excitation of vitamin K_1 (**1**) at 248 or 351 nm in hexane (solid line), acetonitrile (dashed line) and diethyl ether (dotted line).

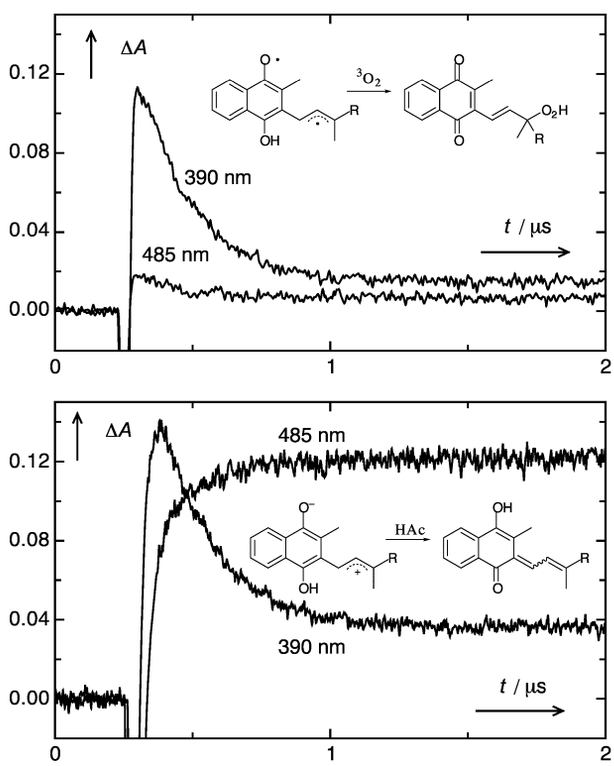

Fig. 4 Kinetic traces observed by LFP (248 nm) of **1** in acetonitrile monitored at 390 and 485 nm. Upper: 1 atm of oxygen, no 1,2–QM is formed; the slight decay is due to the small absorbance of 1,3-QM at 485 nm. Lower: Degassed with 10 mM acetic acid.

The decay of 1,3-QM(**1**), monitored below 400 nm or above 550 nm, always matched the rate of formation of 1,2-QM(**1**) observed at 485 nm (Fig. 4). The rate varied by orders of magnitude depending on the solvent and the added reagents, but was independent of the monitoring wavelength (Table 2). Acceleration of this reaction by addition of protic solvents, acetic acid or pyridine did not influence the amplitude of the growth in absorbance at 485 nm, *i.e.*, the amount of 1,2-QM(**1**) formed. In contrast, admission of oxygen reduced the formation of 1,2-QM in proportion to the amount quenched by oxygen. Hence, the observed oxygen quenching is a trapping reaction, which intercepts the formation of 1,2-QM. 2-Allyl-3-methyl-1,4-naphthoquinone (**4**) gave virtually no transient absorption by LFP in all solvents investigated, because the PO transient (Fig. 1) decays within a few nanoseconds.

(b) Plastoquinone-1 (2). Creed *et al.*[8] described the primary intermediate formed by LFP of **2** with absorption maxima at 330 and 420 nm ('P_{420}') and tentatively attributed this transient to 1,3-QM(**2**). The decay of 1,3-QM usually obeyed first-order kinetics accurately, except in degassed aprotic solvents, and the rate constants for the decay rate at the two maxima always matched those for the resolved growth of 1,2-QM(**2**) observed at 500 nm ('P_{500}').[8] As with 1,3-QM(**1**), both the rate constants (Table 2) and the spectra (Fig. 5) depended strongly on the solvent. The total yield of 1,3-QM strongly increased, and the ratio of the amplitudes at 330 and 420 nm decreased with increasing solvent polarity.

The quantum yield for the formation of 1,2-QM from **2** in methanol was estimated as ϕ = 0.05 ± 0.01, where the error refers to reproducibility. Admission of oxygen did not influence the yield of 1,3-QM(**2**), but its decay rate was accelerated in aprotic solvents and the yield of 1,2-QM was decreased accordingly. Thus, oxygen quenching of 1,3-QM intercepts the formation of 1,2-QM. Quenching rate constants were determined from the lifetimes in degassed, air- and oxygen-saturated solutions (Table 2); they were clearly below the limit of diffusion and decreased with increasing solvent polarity.

Addition of piperylene in up to 1 M concentration had no effect on either the intensity or the lifetime of 1,3-QM in any of the solvents used, suggesting that 1,3-QM is formed from the singlet state. Predominant formation of 1,3-QM via a short-lived triplet state was ruled out by a triplet energy transfer experiment. The addition of 2.1×10^{-4} M **2** (A_{355} = 0.4) to a solution of benzophenone (A_{355} = 0.6) in degassed acetonitrile strongly reduced the lifetime of triplet benzophenone, indi-

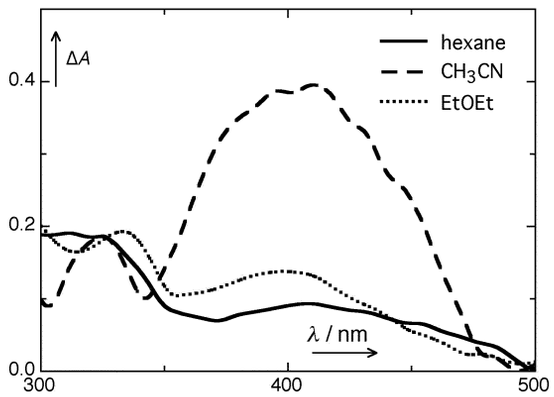

Fig. 5 Initial transient absorption spectra taken within 50 ns after LFP of plastoquinone-1 (**2**) in hexane (solid line), acetonitrile (dashed line) and diethyl ether (dotted line).

cating efficient energy transfer to **2**. The amplitude of 1,3-QM was substantially lower than in the absence of benzophenone, so that sensitisation of **2** appears to be inefficient in producing 1,3-QM.

The transformation of 1,3-QM(**2**) to 1,2-QM(**2**) is fast in methanol, $k = (2.0 \pm 0.4) \times 10^7\ s^{-1}$, but resolved by nanosecond LFP. Thus, the absence of oxygen quenching of 1,3-QM in methanol, noted by Creed *et al.*, may be attributed to its intrinsically short lifetime in that solvent. The kinetic isotope effect determined from the decay rate constants in CH_3OH and CD_3OD, $k_H/k_D = 4.2 \pm 0.8$ (Table 2, footnote b), is in reasonable agreement with the value of 2.8 reported by Creed *et al.*[8] About the same isotope effect is found for CH_3OH and CH_3OD, $k_H/k_D = 4.8 \pm 0.8$, which indicates that the reaction 1,3-QM(**2**) ⟶ 1,2-QM(**2**) proceeds by proton transfer through the solvent.

Addition of acetic acid (0.01 M) to aprotic solvents strongly reduced the lifetime of 1,3-QM(**2**) and increased the growth rates of 1,2-QM(**2**) correspondingly. Similar results were obtained by addition of pyridine. The bimolecular rate constants k_{HAc} and k_{Py} are given in Table 2. Addition of 1×10^{-4} M NaOD to acetonitrile (1% D_2O) accelerated the decay of 1,3-QM from $4.5 \times 10^4\ s^{-1}$ to $6.7 \times 10^5\ s^{-1}$. The decay at 330 and 400 nm was now accompanied by simultaneous growth in absorbance at $\lambda_{max} = 590$ nm. Creed *et al.* had shown that the anion 1,2-QM(**2**)$^-$ absorbs at this wavelength and had estimated the acidity constant of 1,2-QM(**2**) as $pK_a \approx 9$.

(c) LFP of plastoquinones 2 and 7 at reduced temperature. 2,3-Dimethyl-5-allyl-1,4-benzoquinone (**7**) differs from **2** only by lacking two methyl substituents on the β,γ-double bond. In sharp contrast to **2**, LFP of solutions of **7** in methanol, acetonitrile or isooctane gave practically no transient absorption. By analogy to the behaviour of allylnaphthoquinone **4** (*vide supra*), we assumed that **7** decays by reversible cyclisation to a preoxetane diradical PO, which is too short-lived for detection by nanosecond LFP. Indeed, a short-lived transient, $\lambda_{max} \approx 390$ nm, was detected by nanosecond LFP of **2** and of **7** at temperatures below −160 °C in light petroleum and in MTHF. The lifetime of these transients was not affected by the addition of piperylene but, in the case of **2**, we observed a significant reduction of the lifetime when the solvents were air-saturated (Table 3).

The Arrhenius factors determined from the lifetime data for PO(**2**) given in Table 3 are $\log(A/s^{-1}) = 9.4 \pm 0.3$ and $E_a = 5.8 \pm 0.5$ kJ mol^{-1}. The low value of the *A*-factor suggests that the diradical is in a triplet state and that ISC determines its rate of decay. Extrapolation to room temperature gives a lifetime of 1–10 ns, and indeed this transient was not detected by LFP with a time resolution of 20 ns. Extrapolation to 77 K predicts a lifetime of microseconds. Therefore, the transient is not expected to persist for detection by optical or EPR spectroscopy upon steady-state irradiation at 77 K.

Table 3 Temperature dependence of the lifetime τ/ns of the preoxetane diradicals PO of **2** and **7** (averages of three measurements)

	Plastoquinone-1 (**2**)		Allylbenzoquinone (**7**)	
T/K	Light pet.	MTHF	Light pet.	MTHF
88	1500 ± 200	1200 ± 400	900 ± 200	1000 ± 400
88[a]	520 ± 60[a]	430 ± 20[a]		
93	800 ± 50	700 ± 90		
103	450 ± 40	320 ± 35	500 ± 180	500 ± 180
113	120 ± 15	150 ± 5	170 ± 80	200 ± 70

[a] Air saturated.

Conventional (μs) flash photolysis

Detailed investigations of the 1,2-QM transients of **1** and **3** were published by Creed *et al.*,[8,13] who showed that these transients exhibit biphasic decays. We add just one additional observation. Flash photolysis of an aerated ethanol solution containing 2×10^{-4} M of vitamin K_1 (**1**) produced a strong orange coloration due to 1,2-QM(**1**),[7,13] two thirds of which decayed with a rate constant of $0.020 \pm 0.002\ s^{-1}$. After 5 min, the remaining, longer-lived isomer was exposed to a second flash that was filtered to $\lambda > 450$ nm in order to avoid further excitation of residual **1**. The second flash hardly changed the absorbance at 480 nm, but initiated another period exhibiting the 'fast' decay, $k = 0.024 \pm 0.006\ s^{-1}$, Fig. 6.

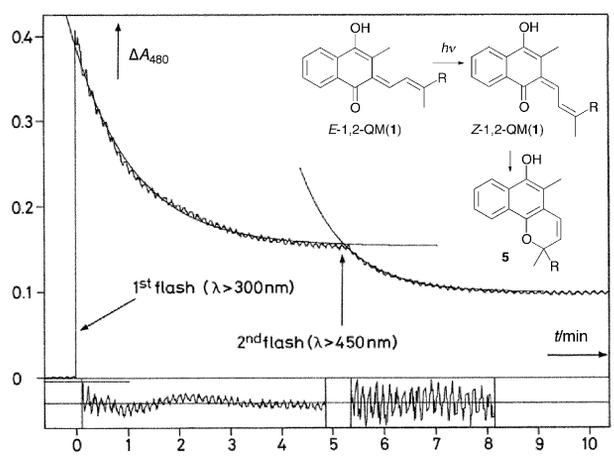

Fig. 6 Dual flash photolysis of **1** in ethanol showing photoisomerisation of the long-lived *E*-isomer of 1,2-QM to the short-lived *Z*-isomer.

Low-temperature irradiations.

(a) Vitamin K_1. A clean conversion of **1** to the *Z*-isomer of 1,2-QM(**1**) was observed upon 365-nm irradiation of **1** in an EPA glass (5 parts diethyl ether, 5 parts isopentane, 2 parts ethanol) at a temperature of 77 K (Fig. 7). Under these conditions, the 1,2-QM tautomer was stable indefinitely. The assignment of the low-temperature photoproduct to the *Z*-isomer of 1,2-QM is based on its decay rate observed after rapid thawing of the irradiated glass. The same spectrum was formed by irradiation of chromenol **5** in EPA at 77 K.

Photochemical conversion of **1** to the primary intermediate 1,3-QM was observed in an aprotic glass of MTHF (Fig. 8). The spectrum obtained by exhaustive 365-nm irradiation of **1** in MTHF at 77 K is shown in the upper part of Fig. 8 (solid line). Here the ratio of the absorbance at 330 nm to that at 390 nm is considerably larger than was found in the same solvent by

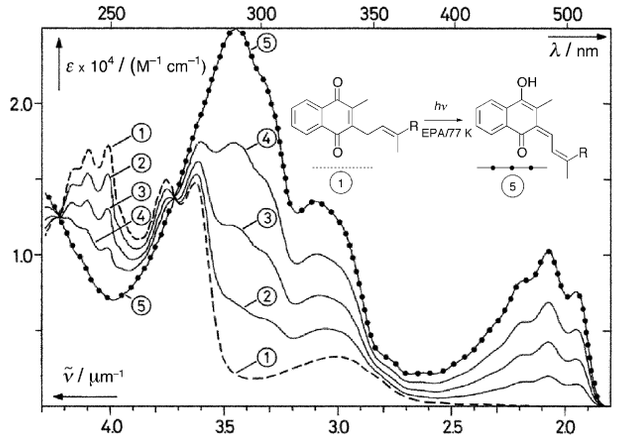

Fig. 7 Irradiation (365 nm) of vitamin K_1 (**1**) in EPA glass at 77 K.

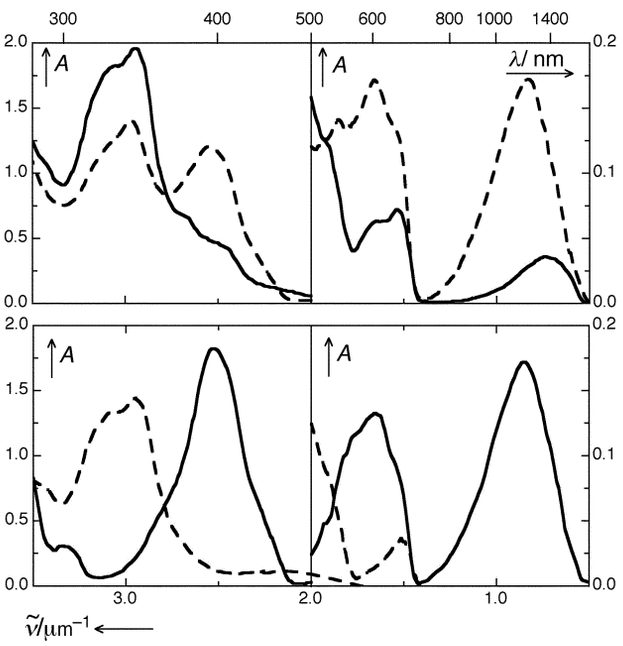

Fig. 8 Irradiation of vitamin K_1 (**1**, 1×10^{-4} M) in MTHF glass at 77 K. Upper part: Photoproduct absorbance by 1,3-QM(**1**) after irradiation (solid line) and after tempering for 30 min at 88 K (dotted line). Lower part: Estimated spectral contributions of the singlet state (solid line) and of the triplet state (dotted line) of 1,3-QM(**1**). Solvent overtones in the near IR were subtracted using the spectrum recorded before irradiation as a baseline.

spectrographic flash photolysis at ambient temperature. The MTHF glass appears to be sufficiently hard at 77 K so that very little solvent reorganisation occurs after the photochemical transformation of the solute. The solvation process was then directly observed by allowing the glass to warm up by only a few degrees towards the glass transition temperature ($T_g \cong 88$ K).[31] The spectrum of 1,3-QM(**1**) then shifted irreversibly to that shown as a dashed line in the upper part of Fig. 8, which was recorded after re-cooling to 77 K. The most obvious changes induced by the brief tempering process are the strong absorbance increases at 390 nm and in the near infrared region, and the absorbance decrease at 330 nm. The IR band is substantially blue-shifted, whereas the other bands essentially change only their intensity, but not their position. The changes in band intensities are attributed to a shift in the equilibrium from the triplet to the singlet state of 1,3-QM(**1**) that is induced by solvation and possibly some conformational relaxation of the diradical.

The lower part of Fig. 8 shows an attempt to separate the spectral contributions of the singlet (solid line) and the triplet state (dashed line) of 1,3-QM(**1**). In order to achieve this separation, it was assumed that the first absorption band $\lambda > 800$ nm is due entirely, that at 390 nm largely, to the singlet state. The coefficients of linear combinations of the two upper spectra ($\lambda < 800$) were thus varied to best remove the shape at 390 nm from the triplet spectrum. While the achieved separation clearly depends on a rather arbitrary choice of coefficients, we may mention that such procedures generally produce reliable results in the separation of the two components of linear dichroism in spectra obtained from partly oriented samples.[32]

(b) Plastoquinones. Irradiation of 2,3-dimethyl-5-allyl-1,4-benzoquinone (**7**) at 365 nm in MTHF or alkane glasses at 77 K did not give rise to any changes in the absorption spectra, as expected. In contrast, irradiation of 2-methylplastoquinone (**8**) in MTHF at 77 K rapidly produced persistent absorption in the near UV and visible (λ_{max} = 330 and 400 nm), as well as a weak band in the near IR (λ_{max} = 1250 nm, dashed line in Fig. 9). The sample was then tempered in the dark towards the glass transition temperature ($T_g \cong 88$ K). This produced changes in the shapes of the bands at 400 nm and in the near IR, and the sharp band at 330 nm disappeared almost entirely (dotted line). Further tempering to 99 K led to the disappearance of these bands, leaving the absorption spectrum of 1,2-QM(**8**) (λ_{max} = 500 and 360 nm, solid line).

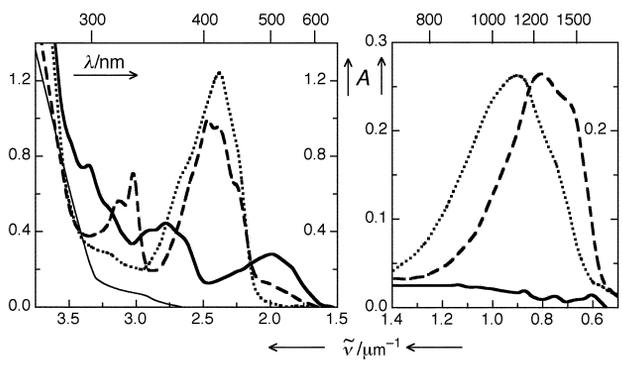

Fig. 9 Irradiation of 2-methylplastoquinone (**8**, 1×10^{-4} M) in MTHF glass at 77 K. Black line: Absorbance before irradiation. Dashed line: After at 365-nm irradiation (20 min) at 77 K. Dotted line: After tempering for 30 min at 88 K. Thick solid line: After tempering for 30 min at 98 K. The spectra in the near IR region (right-hand graph) were obtained in a separate experiment with 5×10^{-4} M **8**, and solvent overtones were subtracted using the spectrum recorded before irradiation as a baseline.

EPR Spectroscopy

Direct evidence for the triplet nature of 1,3-QM(**1**) was obtained by EPR spectroscopy (Fig. 10). Brief irradiation of **1** in a glassy MTHF solution at 77 K gave rise to a strong, persistent EPR spectrum centred at 323 mT, which was characteristic for a randomly oriented triplet species with zero-field parameters $|D/hc| = 0.011$ and $|E/hc| \leq 0.001$ cm^{-1}. A weak signal at half field, 161.5 mT, was also observed. The temperature dependence of the signal intensity obeyed Curie's law, $I \cdot T$ = const, in a temperature range from 5 to 80 K (five data points), but signal saturation was substantial with microwave powers exceeding 0.1 μW at lower temperatures. The signal decayed to about 1/10th of its original intensity when the sample was kept at 92 K for 10 min. After re-cooling, the remaining signal still obeyed Curie's law within the limits of error. A similar spectrum with slightly smaller zero-field splitting, $|D/hc| = 0.010$, was obtained by irradiation of **1** in a hydrocarbon glass at 77 K, which also obeyed Curie's law in the range of 5–77 K (nine data points). Samples of plastoquinone-9 (**6**) and of methylplastoquinone (**8**) in either 2-methylbutane or MTHF gave only radical signals centred at 320 mT after irradiation at 77 K.

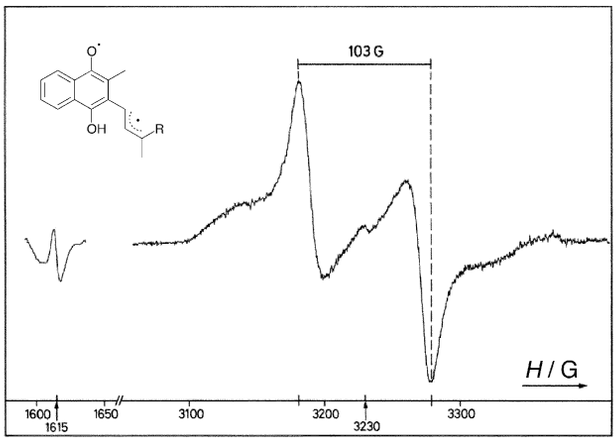

Fig. 10 EPR spectrum generated by brief irradiation (365 nm) of vitamin K_1 (**1**) in MTHF at 77 K.

Step-scan FTIR experiments

Time-dependent IR-difference spectra obtained by 266-nm excitation of **1** in CD_3CN are shown in Fig. 11. The strong negative peaks at 1661 and 1296 cm^{-1} are due to depletion of the starting material **1**, which does not appreciably recover within the time window of 75 μs. The initial photoproduct shows several positive bands in the range of 1300–1600 cm^{-1} (Table 4). Global analysis of these spectra and fitting with a first-order rate law gave a rate constant of $k = (2.3 \pm 0.3) \times 10^5$ s^{-1}, consistent with the measurements by optical LFP. Two of these spectra, taken at delays of 500 ns and 75 μs, are shown in Fig. 12, together with predicted IR frequencies and relative intensities obtained by DFT calculations (Table 4) for singlet and triplet 1,3-QM(**1**) and for 1,2-QM(**1**).

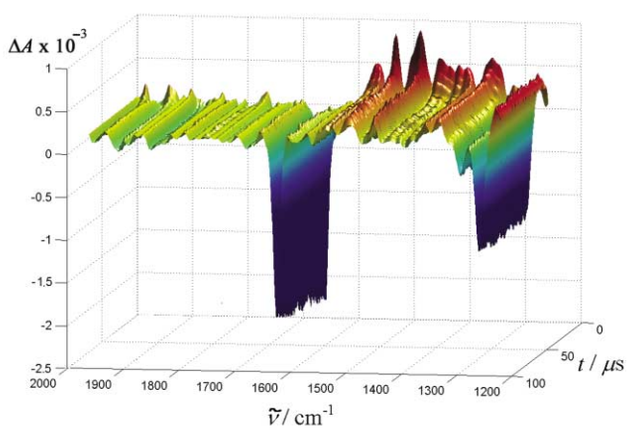

Fig. 11 Reconstructed difference spectra determined by eigenvalue analysis of 150 step-scan FTIR spectra collected within 75 μs after 266-nm excitation of **1** in CD_3CN, which was degassed by bubbling with argon gas.

Discussion

Our analysis of the data obtained in this work draws on the insight gained earlier by Porter and co-workers using flash photolysis,[7,8] as well as on the results of preparative work (isolation and identification of photoproducts). In particular, the oxygen trapping experiments by Snyder and Rapoport,[9] and by Creed[13,14a] and Wilson[15] and their co-workers are important. In addition to the photooxidation products PO–O_2 and QM–O_2, the chromenols **5** and **9** as well as the chromenol formed from **2** have been isolated and fully characterised.

Irradiation of **1**–**3** in solution produces a strong colour change from yellow to orange. The long-lived, orange products do not survive normal work-up procedures, but their identification as 1,2-quinone methide tautomers of the parent compounds is well established.[7,12,13] Creed and coworkers[13] showed that the decay of 1,2-QM formed from **3** in ethanol is biphasic (τ = 15 s and 156 min). The faster, first-order component was attributed to cyclisation of *Z*-1,2-QM(**3**) to the chromenol **9**. The slower, oxygen- and solvent-sensitive decay was attributed to *E*-1,2-QM, which afforded the hydroperoxide QM–O_2 upon admission of oxygen after irradiation. The occurrence of $E \longrightarrow Z$ photoisomerisation of the 1,2-QM was demonstrated as shown in Fig. 6.

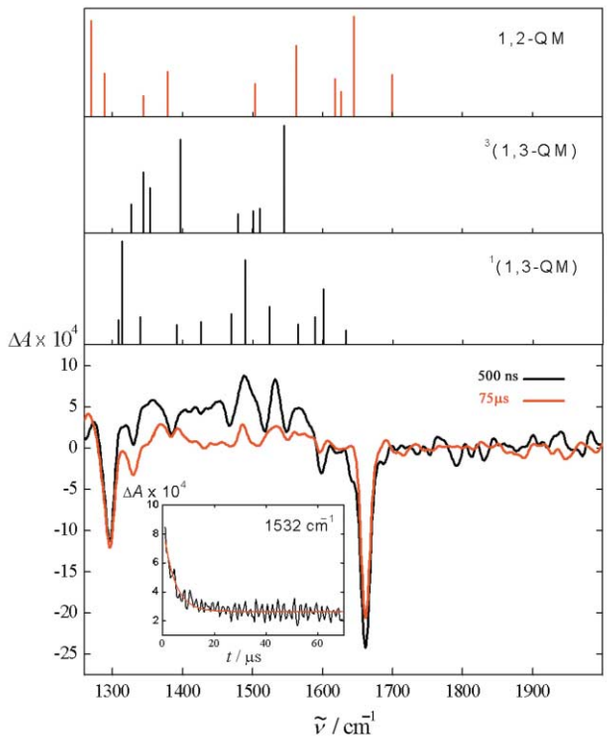

Fig. 12 Reconstructed IR difference spectra of **1** at delays of 500 ns and 75 μs (red) relative to the excitation flash (266 nm). Top: predicted IR frequencies and relative intensities obtained by DFT calculations for singlet and triplet 1,3-QM(**3**) and for 1,2-QM(**3**). The inset shows a single exponential fit to the decay of the transient peak at 1532 cm^{-1}.

In their nanosecond LFP study of plastoquinone-1 (**2**) and plastoquinone-9 (**6**) Creed, Hales and Porter[8] identified a transient precursor ('P_{420}') to the corresponding 1,2-quinone methide ('P_{500}'). Previous time-resolved work on vitamin K_1 (**1**) is limited to the microsecond time scale and has not provided any information on the phototautomerisation mechanism of **1**.

The reaction sequence shown in Scheme 2 is a revised version of Scheme 1, based on the additional findings of this work, which are discussed below. The two primary reactions considered by previous authors (Scheme 1), cyclisation to a preoxetane diradical PO, and intramolecular 1,4-H transfer forming 1,3-QM diradicals, both occur simultaneously and lead to different photoproducts. Scheme 2 allows for a consistent rationalisation of the main photoreactions of the K-vitamins and, by analogy, of the plastoquinones.

Apolar solvents

The predominant reaction path in apolar solvents is formation of the preoxetane diradicals PO, $\lambda_{max} \approx 380$ nm (**1**, **4**, Fig. 1) and 390 nm (**2**, **7**) within a few picoseconds. The assignment of the PO transients rests mainly on the structure of the isolated trioxane trapping products PO–O_2. Consistently with the proposed structure, their absorption spectra are similar to those of the corresponding semiquinone radicals.[33] The transient absorption spectrum of **1** recorded with 10 ps delay after the laser pulse resembles the triplet–triplet absorption of 1,4-

Table 4 IR band positions/cm^{-1} (rel. int.) for vitamin K_1 (**1**) and its quinone methide tautomers. For the QM transients entries in a given row do not imply an assignment

Vitamin K_1 (**1**)			1,3-QM(**1**)			1,2-QM(**1**)	
				Calculated (**3**)			
Assignment	Measured	Calculated (**3**)	Measured	Singlet	Triplet	Measured	Calculated (**3**)
$\nu_{C=O}$	1661 (1.0)	1705 (0.7)	1661[a]	1633 (0.1)	1544 (1.0)	1690 (0.5)	1699 (0.4)
$\nu_{C=C}$	1620 (0.3)	1642 (0.1)	1597[a]	1600 (0.5)	1509 (0.2)	1661[a]	1644 (1.0)
$\nu_{C(ar)=C(ar)}$	1596 (0.3)	1616 (0.2)	1571 (0.5)	1589 (0.3)	1500 (0.2)	1642 (0.4)	1626 (0.2)
δ_{CH}	1464 (0.2)	1466 (0.1)	1560 (0.5)	1564 (0.2)	1479 (0.2)	1559 (0.6)	1617 (0.4)
δ_{CH}	1380 (0.2)	1383 (0.1)	1532 (0.9)	1524 (0.4)	1396 (0.9)	1537 (0.8)	1562 (0.7)
$\nu_{C(ar)=C(ar)}$	1330 (0.3)	1330 (0.1)	1489 (1.0)	1489 (0.8)	1353 (0.4)	1526 (0.8)	1503 (0.3)
ν_{C-CO}	1296 (0.7)	1293 (1.0)	1453 (0.7)	1469 (0.3)	1345 (0.6)	1486 (0.9)	1378 (0.5)
			1403 (0.5)	1426 (0.2)	1327 (0.3)	1392 (0.9)	1344 (0.2)
			1356 (0.6)	1391 (0.2)	1252 (0.1)	1369 (1.0)	1288 (0.4)
			1343 (0.7)	1340 (0.3)	1236 (0.3)	1330[a]	1269 (1.0)
			1296[a]	1314 (1.0)		1296[a]	1245 (0.2)
				1309 (0.3)			

[a] Depletion bands in the difference spectra.

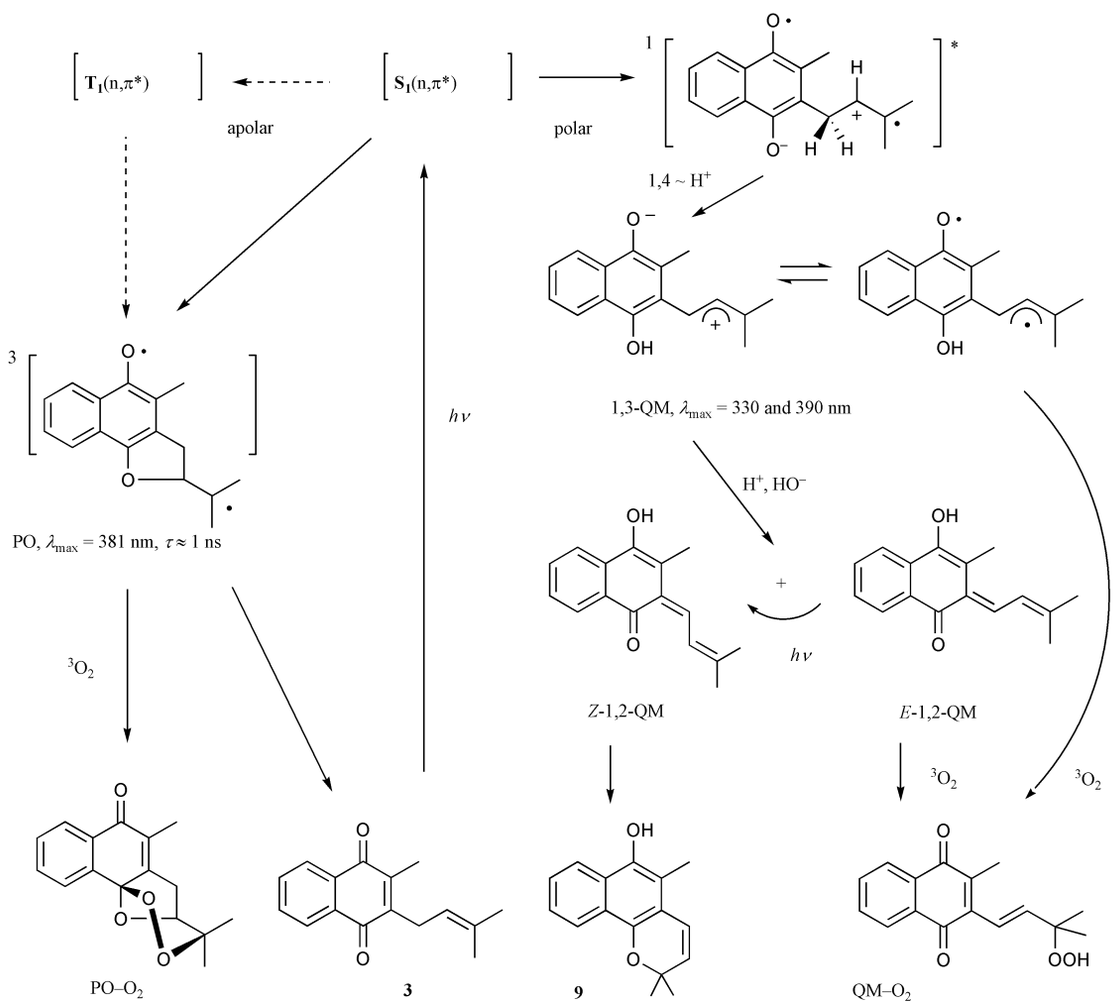

Scheme 2 Photoreactions of menaquinone-1 (**3**) in solution.

naphthoquinone, λ_{max} = 365 nm,[34] but exhibits fine structure indicating that the PO diradical is also formed within 2 ps, presumably from the singlet excited state of **1**. If the diffuse absorbance decaying with a rate constant of about 1×10^{10} s^{-1} is indeed due to the triplet state of **1**, its rapid decay suggests that it also cyclises to the PO diradical.

The PO diradicals are too short-lived for detection by nanosecond LFP at room temperature, but they were observed at reduced temperatures (Table 3). By extrapolation, their lifetimes at 77 K are predicted be in the microsecond region. Therefore, it is not surprising that they escape detection by EPR and optical spectroscopy at 77 K.

In anaerobic solutions the diradicals PO revert to the starting quinones. This energy wasting process leaves its trace in an *E* to *Z* isomerisation of the exocyclic β,γ-double bond. Irradiation of either the *E* or the *Z*-isomer of vitamin K_1 in degassed pentane leads to rapid approach of a photostationary mixture with a *Z*/*E* - ratio of 0.4 (Table 1). Presumably the γ-substituents reach conformational equilibrium during the lifetime of the PO diradical. At room temperature, the lifetime of the PO

Table 5 DFT energies (kJ mol^{-1}) including zero-point corrections of the 1,3-QM (singlet and triplet) and 1,2-QM tautomers relative to the parent quinones **2** and **3**

	Plastoquinone-1 (**2**)		Menaquinone-1 (**3**)	
	Gas phase	PCM[a]	Gas phase	PCM[a]
^{1}(1,3-QM)	122	89.9	166	140[b]
^{3}(1,3-QM)	88	90.1	114	149
1,2-QM	10	−2.2	37	33

[a] PCM solvation model (acetonitrile).[26] [b] The optimized structure had one imaginary frequency.

diradicals of **1** and **4** is only a few nanoseconds and the presence of oxygen does not noticeably affect their lifetime. Quantitative chemical trapping to form the trioxanes PO–O_2 at room temperature is nevertheless possible, because compounds **1**–**3** are largely photostable in apolar solvents, so that even inefficient trapping can eventually give high chemical yields of the oxidation product upon prolonged irradiation (λ > 430 nm). Oxygen quenching of the PO diradicals of **2** and **7** was, however, substantial at −185 °C (Table 3). We expect that formation of PO–O_2 would be much more efficient in oxygen-saturated solutions at reduced temperature.

Polar solvents

The transient absorptions dominating the initial spectra obtained by flash photolysis of **1** and **2** are the 1,3-quinone methide (1,3-QM) diradicals. Although these transients kinetically behave as a single species, several observations indicated that they are in fact a mixture of two species that are in rapid thermal equilibrium, the lowest singlet and triplet state of 1,3-QM. The first indication came from the observation of a pronounced solvent effect on the relative intensity of the absorption maxima at 330 and 390 nm for **1** (Fig. 3), 330 and 420 nm for **2** (Fig. 5). The ratio of the initial transient absorbances A_{330}/A_{390} observed by LFP of **1** progressively decreased from a value exceeding 10 in isooctane to nearly 1 in highly polar aprotic solvents such as acetonitrile. We take this to indicate that the polar singlet state of the 1,3-QM diradicals is stabilised relative to the triplet in polar solvents. The absorption bands attributed to the singlet diradical are stronger in 1,3-QM(**2**) (Fig. 5) than in 1,3-QM(**1**) (Fig. 3). Consistently, only **1** gave an EPR spectrum characteristic for a triplet species (Fig. 10) upon irradiation at 77 K.

Comparison of the absorption changes induced by low-temperature irradiation of vitamin K_1 (**1**) and methylplastoquinone (**8**), Figs. 8 and 9, again indicates that 1,3-QM(**1**) favours the triplet, and 1,3-QM(**8**) favours the singlet. The intensity of the features attributed to the singlet 1,3-QM tautomers (the near-IR bands and the bands at 390 and 420 nm for **1** and **8**, respectively) increase strongly upon thawing of the sample from **1**, much less with **8**. The 330-nm bands attributed to the triplet states, on the other hand, are reduced slightly with **1**, but disappear completely from the spectrum obtained from **8**. This indicates that irradiation of **1** at 77 K produces predominantly the triplet state of 1,3-QM(**1**), irradiation of **8** predominantly the singlet state 1,3-QM(**8**). As the polar singlet will be solvated preferentially, the singlet spectrum of 1,3-QM(**1**) increases strongly upon thawing. The triplet spectrum of 1,3-QM(**8**) disappears completely, yielding just a small additional amount of singlet.

The energies obtained by the DFT calculations for the parent compounds **2** and **3** and their 1,3-QM (singlet and triplet) and 1,2-QM tautomers are given in Table 5. While the triplet state is predicted to be the ground state of both 1,3-QM diradicals in the gas phase, the equilibrium is predicted to be inverted in a polar solvent. These predictions agree remarkably well with our findings.

The two multiplicities of the 1,3-QM intermediates are emphasised in the valence structures of Scheme 2 by showing a zwitterion for the singlet and a diradical for the triplet state. The chemical behaviour implied by these structures is in accord with the observations. The lifetime of the 1,3-QM diradicals is reduced in the presence of oxygen, and oxygen quenching intercepts the formation of 1,2-QM (Fig. 4). We would expect that triplet oxygen adds preferentially to the triplet state of 1,3-QM, and this is borne out by the rate constants for oxygen quenching (Table 2), which decrease markedly with increasing solvent polarity, particularly for 1,3-QM(**2**).

On the other hand, the zwitterionic singlet state of the 1,3-QM diradicals appears well disposed to react to the 1,2-QM by proton transfer through the solvent or with added acid or base. Singlet 1,3-QM is an unusual molecule: it carries a strongly acidic site (OH) as well as a strongly basic site (O^-). The DFT calculations for **2** and **3** predict that 112 and 129 kJ mol^{-1}, respectively, are released by the proton transfer reaction ^{1}(1,3-QM) ⟶ 1,2-QM in the gas phase. These values are reduced to 92 and 107 kJ mol^{-1}, respectively, using a continuum model for solvation (Table 5), which translates to a difference of about 17 pK_a units between the acids ^{1}(1,3-QM) and 1,2-QM. The pK_a of 1,2-QM(**2**) was estimated as 9,[8] so that ^{1}(1,3-QM) is predicted to be a very strong acid, p$K_a \approx -8$.

Not surprisingly, the reaction ^{1}(1,3-QM) ⟶ 1,2-QM is fast in methanol ($k = 7 \times 10^9$ s^{-1} for **1**, 2×10^7 s^{-1} for **2**), much slower in aprotic polar solvents and slowest in hydrocarbon solvents. In light petroleum the decay kinetics deviate from first-order, because the tautomerisation 1,3-QM ⟶ 1,2-QM may require the encounter of two molecules of 1,3-QM in the absence of other proton transfer reagents.

The quantum yields for the formation of the 1,2-QM transients in methanol were estimated as $\phi = 0.24$ (**1**) and 0.05 (**2**). This, together with the product analyses, suggests that the reaction *via* the preoxetane diradicals predominates even in polar solvents. However, nanosecond LFP detects only the absorptions by the QM transients.

Previous work on 1,3-quinone methides

Leary and Porter[7] noted that 1,2-QM(**1**) was formed within ≤20 μs in both degassed and aerated ethanol, whereas in the aprotic solvents dioxane or heptane it appeared on a time scale of hundreds of microseconds, and only when the solvent was degassed. These findings are now readily understood: The short lifetime of 1,3-QM in alcohol solvents precludes trapping by oxygen. The lifetime of the 1,3-QM diradical is orders of magnitude higher in dry aprotic solvents, so that oxygen trapping, presumably yielding the hydroperoxides QM–O_2, becomes competitive. The effect of oxygen on the distribution of isolated products can also be understood. Admission of oxygen essentially suppresses the formation of chromenol **9** from menaquinone-1 (**3**), but has little effect on the yield of the chromenol from plastoquinone-1 (**2**), because oxygen trapping of the (largely singlet) 1,3-QM formed from **2** is less efficient.

The nanosecond LFP study of plastoquinones **2** and **6** by Creed, Hales and Porter[8] identified a transient precursor ('P_{420}') to the corresponding 1,2-quinone methide ('P_{500}'). The present work confirms their assignments of the transient intermediates, but two modifications should be noted. Firstly, we assign the 1,2-quinone methides ('P_{500}') to geometrical isomers *E* and *Z* rather than to the *syn*- and *anti*-conformers of *Z*-1,2-QM. Conformers of 1,2-QM would not be expected to exhibit kinetically distinct behaviour on a time scale of hours.[35] Secondly, the formation of 1,2-QM from the 1,3-QM diradicals proceeds by proton transfer through the solvent, not by hydrogen atom transfer. The argument for hydrogen abstraction from the solvent (methanol) was based on the observation of a kinetic isotope effect of $k_H/k_D \approx 3$ using CH_3OH and CD_3OD as solvents.[8]

However, the rate constants $k_{MeOH} \approx 4k_{MeOD} \approx 4k_{CD_3OD}$ given in Table 2 show that the isotope effect is due isotopic substitution at the oxygen, not at the carbon atom. Moreover, the sharp acceleration of the reactions 1,3-QM ⟶ 1,2-QM by acids and bases, as well as the slow, nonexponential decays of 1,3-QM observed in dry, aprotic solvents, argue for a proton transfer mechanism. The reaction of hydroxyl ions with 1,3-QM(**2**) is essentially diffusion-controlled, $k_{OD^-} = 6.7 \times 10^9$ M^{-1} s^{-1}, and produces the anion 1,2-QM^-. The reaction rate constants obtained with pyridine are of similar magnitude (Table 2), but the reaction does not yield free ions in aprotic solvents. Presumably a pyridinium–$(1,2\text{-QM})^-$ ion pair is formed, which decays by back transfer of the proton to yield 1,2-QM and pyridine.

The seminal investigation of plastoquinone by Creed, Hales and Porter[8] has spurred a number of further studies by other investigators. IR, Raman and EPR spectra of 'radicals' generated by low-temperature irradiation of several electron transport quinones including vitamin K_1 (**1**) and plastoquinone-9 (**6**) were reported by Burie *et al.*[36] These authors supported the hypothesis of intramolecular hydrogen transfer from the first isoprene unit of the side chain to the proximal carbonyl group of the quinone ring. The main features in the reported EPR spectra were broad radical peaks centred at 336 mT. Weak shoulders with about the same separation of 10.3 mT as the main peaks of the triplet spectrum observed by us (Fig. 10) were noted on the wings of the radical peaks. However, these features were attributed to hyperfine structure arising from the side chain protons. Such hyperfine couplings would be expected to be one order of magnitude lower. In a note added in proof, the authors mention observation of a very weak signal at half-field, characteristic for a triplet state. The characteristic triplet EPR spectrum formed from **1** (Fig. 10) is dominant only after very brief irradiation and when the spectrum is recorded with very low microwave powers. Broad signals arising from carbon-centered monoradicals, as in the spectra shown by Burie *et al.*, are formed upon further irradiation.

Prior to the above work, Serbodov and co-workers had reported that irradiation of **1** at low temperatures generates EPR absorptions characteristic for triplet diradicals.[37] The spectra were attributed to 1,3-QM(**1**). Zero-field parameters $D = 200 \pm 3$ Oe[37a] (EPA glass) and 185–194 Oe[37b] (various solvents) were given, which corresponds to about twice the value of $D = 10.3$ mT (103 Oe) determined in this work (Fig. 10). We surmise that the values of ≈190 Oe refer to the distance of the outer peaks in the diradical spectra, as in some other papers of the same group, so that the reported values actually amount to $2|D|$. In agreement with Serbodov,[37b] we observed a slow decay of the EPR triplet spectrum formed from **1** at 77 K.

The low-temperature IR spectra reported by Burie *et al.*[36] have better resolution and signal-to-noise ratios than our time-resolved IR spectra. The main features reported for the diradical formed by irradiation of **1** in CH_2Cl_2 at 10 K are at 1532, 1488, 1405, 1389 and 1361 cm^{-1}, and they agree remarkably well in shape, position and relative intensity with our time-resolved spectra of the 1,3-quinone methide (Fig. 12, Table 4). Three possible structures, including the 1,3-QM, were considered for this species. Its reactivity in solution observed here clearly indicates assignment to the 1,3-QM.

Parent 1,3-benzoquinone methide (**10**) and 1,3-naphthoquinone methide (**11**) have been prepared from unambiguous precursors by Berson and co-workers.[38] Both diradicals gave rise to persistent EPR signals, which were characteristic for randomly oriented molecules in a triplet spin state: $|D/hc| = 0.0266$, $|E/hc| = 0.0074$ cm^{-1} for **10** (decay above 40 K), and $|D/hc| = 0.0204$, $|E/hc| = 0.0052$ cm^{-1} for **11** (linear Curie plot 15–84 K, curvature below 15 K was attributed to saturation). The temperature dependence of the EPR signal intensities indicated that the triplet state is the ground state of both **10** and **11**, but stereochemical studies suggested that a thermally accessible singlet state is the reactive entity in cycloaddition reactions of **10**. The zero-field parameter $|D| = 10.3$ mT of diradical 1,3-QM(**1**) corresponds to an average distance of $r \approx 650$ pm between the two unpaired electrons (point dipole model: $|D|/G = 2.78 \times 10^{10}$ pm^3/r^3).[39] This is about 140 pm larger than that estimated from $|D(\mathbf{11})/hc| = 0.0204$ cm^{-1}, a reasonable value considering the extended conjugation in 1,3-QM(**1**) relative to **11**.

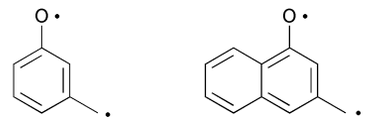

10 **11**

General remarks

The allyl quinones **4** and **7** were chosen as model compounds to test the hypothesis of Wilson and coworkers[11,15] that the photoreactions of excited K-vitamins are initiated by intramolecular exciplex formation with charge transfer from the first exocyclic double bond to the quinone (top right-hand structure in Scheme 2). Charge transfer from the terminal double bond of **4** and **7** requires much more energy than in the corresponding dimethyl derivatives **2** and **3**, so that exciplex formation should be disfavoured. We found that **4** and **7** do not form any of the quinone methide transients observed with **1**–**3**. On the other hand, **4** and **7** do form the short-lived preoxetane diradicals PO. We conclude that the formation of the 1,3-QM diradicals in polar solvents (right-hand part of Scheme 2) proceeds from an intramolecular exciplex. On the other hand, cyclisation to the PO diradicals (left-hand part of Scheme 2), which dominates in apolar solvents, apparently does not require exciplex interaction with the side chain.

The process of 1,4-H transfer from the side chain forming the 1,3-quinone methides observed by LFP of **1**–**3**, originally proposed for **2** by Creed, Hales and Porter,[8] is without precedent. Nevertheless, we feel that the spectroscopic and kinetic results described in this work provide a secure identification of the 1,3-QM transients. Intramolecular 1,5-hydrogen transfer reactions of excited ketones are well known (Norrish Type-II reaction). In the case of **1** and **2**, 1,5-hydrogen transfer would require abstraction of strongly bound vinylic hydrogen. The intramolecular exciplex hypothesis proposed by Wilson, and substantiated here, may explain the unusual occurrence of 1,4-H transfer: charge transfer from the double bond to the quinone moiety will render the α-protons quite acidic, and increase the basicity of the quinone oxygen atoms. Thus, the primary reaction, $k = 2.7 \times 10^{11}$ s^{-1}, yielding the 1,3-QM diradicals from an intramolecular exciplex may be better described as an intramolecular *proton* transfer.

The direct observation of equilibrating singlet and triplet diradicals is also quite unusual. Note that the singlet states of the 1,3-QM diradicals of **1** and **2** absorb at much longer wavelengths than the corresponding triplet states, as expected.[16b] The first absorption bands of the singlet 1,3-QM diradicals of **1** and **8** (Figs. 8 and 9) lie far in the infrared region (~1400 nm). The optical spectra of the 1,3-QM diradicals oberved by LFP (Figs. 3 and 5) and in the low-temperature irradiations consistently show that polar environments favour the polar (more polarisable) singlet states.

Conclusion

The β,γ-double bond in the isoprenoid side chain of electron transport quinones acts as an effective shield, which protects the environment from attack by the highly reactive quinones after adventitious electronic excitation. The present work

provides comprehensive evidence for the primary photoproducts generated by irradiation of K-vitamins and plastoquinones in solution. In polar solvents, intramolecular exciplex formation initiates 1,4-proton transfer yielding 1,3-quinone methide diradicals that coexist in a thermal equilibrium of the singlet and triplet states. The singlet diradicals undergo further proton transfer through the solvent or adventitious acids and bases yielding the well-known 1,2-quinone methides. The triplet diradicals are trapped by oxygen. Very fast formation of preoxetane diradicals competes with the formation of the 1,3-QM diradicals, and predominates in apolar solvents. The preoxetane diradicals were directly observed for the first time. Exciplex formation is not prerequisite for cyclisation to the preoxetane diradicals, but it is for formation of the 1,3-QM diradicals.

Acknowledgements

This work was performed under project 20-68087.02 of the Swiss National Science Foundation.

References

1 (*a*) *Biochemistry of Quinones*, ed. R. A. Morton, Academic Press, New York, 1965; (*b*) *Vitamin K Metabolism and Vitamin K-dependent Proteins*, ed. J. W. Suttie, University Park Press, Baltimore, 1980; (*c*) H. Inouye and E. Leistner, Biochemistry of Quinones, in *Chem. Quinonoid Compd.*, ed. S. Pataiand Z. Rappoport, Wiley, Chichester, 1988, vol. 2, pp. 1293–1349.

2 J. Biggins, N. A. Tanguay and H. A. Frank, Electron transfer reactions in photosystem I following Vitamin K_1 depletion by ultraviolet irradiation, *FEBS Lett.*, 1989, **250**, 271–274; I. Vass, E. Turcsányi, E. Touloupakis, D. Ghanotakis and V. Petrouleas, The Mechanism of UV-A Radiation-Induced Inhibition of Photosystem II Electron Transport Studied by EPR and Chlorophyll Fluorescence, *Biochemistry*, 2002, **41**, 10200–20208.

3 R. Bittl, S. G. Zech, P. Fromme, H. T. Witt and W. Lubitz, Pulsed EPR Structure Analysis of Photosystem I Single Crystals: Localization of the Phylloquinone Acceptor, *Biochemistry*, 1997, **36**, 12001–12004; P. Jordan, P. Fromme, H. T. Witt, O. Klukas, W. Saenger and N. Kauss, Three-dimensional structure of cyanobacterial photosystem I at 2.5 Å resolution, *Nature*, 2001, **411**, 909–917.

4 J. M. Bruce, Light-induced Reactions of Quinones, *Quart. Rev.*, 1967, **21**, 405–428; H. Ulrich and R. Richter, in *Houben-Weyl, Methoden der organischen Chemie*, ed. E. Müller, Thieme-Verlag, Stuttgart, 1977, vol. VII/3a/Part I, pp. 706–713,.

5 *CRC Handbook of Organic Photochemistry and Photobiology*, ed. W. M. Horspool and P.-S. Song, CRC Press, Boca Raton, FL, 1995; (*a*) D. Creed, *1,4-Quinone Cycloaddition Reactions with Alkenes, Alkynes, and Related Compounds*, pp. 737–747; (*b*) K. Maruyama and Y. Kubo, *Photochemical Hydrogen Abstraction Reactions of Quinones*, pp. 748–756.

6 M. Mac and J. Wirz, Salt effects on the reactions of radical ion pairs formed by electron transfer quenching of triplet 2-methyl-1,4-naphthoquinone by amines. Optical flash photolysis and step-scan FTIR investigations, *Photochem. Photobiol. Sci.*, 2002, **1**, 24–29.

7 G. Leary and G. Porter, The Photochemistry of Two Phytyl Quinones: α-Tocopherylquinone and Vitamin K_1, *J. Chem. Soc. A*, 1970, 2273–2278.

8 D. Creed, B. J. Hales and G. Porter, Photochemistry of plastoquinones, *Proc. R. Soc., London A*, 1973, **334**, 505–521.

9 C. D. Snyder and H. Rapoport, The role of the quinone in oxidative phosphorylation. Evidence against carbon-oxygen bond cleavage, *Biochemistry*, 1968, **7**, 2318–2326; C. D. Snyder and H. Rapoport, Photooxygenation of phylloquinone and menaquinones, *J. Am. Chem. Soc.*, 1969, **91**, 731–737.

10 (*a*) S. Fujisawa, S. Kawabata and R. Yamamoto, Photodegradation and stabilization of Vitamin K_1, *Yak. Zass*, 1967, **87**, 1451–1456; (*b*) M. Ohmae and G. Katsui, Photolysis of Vitamin K_1 (V), *Vitamins (Japan)*, 1970, **41**, 178–184 and references therein.

11 (*a*) R. M. Wilson, T. F. Walsh and S. K. Gee, Laser Photochemistry: The Wavelength Dependent Oxidative Photodegradation of Vitamin K Analogs, *Tetrahedron Lett.*, 1980, **21**, 3459–3462; (*b*) R. M. Wilson, S. W. Wunderly, T. F. Walsh, A. K. Musser, R. Outcalt, F. Geiser, S. K. Gee, W. Brabender, L. Yerino, Jr., T. T. Conrad and G. A. Tharp, Laser Photochemistry: Trapping of Quinone–Olefin Preoxetane Intermediates with Molecular Oxygen and Chemistry of the Resulting Trioxanes, *J. Am. Chem. Soc.*, 1982, **104**, 4429–4445.

12 R. P. Gandhi, M. P. S. Ishar, R. Srivastava and R. Sarin, Nuclear magnetic resonance and UV spectral probe of photochemical steady states of Vitamin K_1, *J. Photochem. Photobiol. A: Chem.*, 1994, **78**, 153–160.

13 D. Creed, H. Werbin and T. Daniel, The Mechanism of Photooxidation of the Menaquinones, *Tetrahedron Lett.*, 1981, **22**, 2039–2042.

14 (*a*) D. Creed, H. Werbin and E. T. Strom, A Novel Tricyclic Peroxide from the Photochemical Oxidation of Plastoquinone-1, *Chem. Commun.*, 1970, 47–48; (*b*) D. Creed, H. Werbin and E. T. Strom, Photochemistry of electron-transport quinones-II, *J. Am. Chem. Soc.*, 1971, **93**, 502–511; (*c*) W. H. Watson, J. E. Whinnery, D. Creed, H. Werbin and E. T. Strom, Photochemistry of electron-transport quinones-III, *Tetrahedron*, 1974, **30**, 2037–2042.

15 R. M. Wilson, The Trapping of Biradicals and Related Photochemical Intermediates, in *Organic Photochemistry*, ed. A. Padwa, Marcel Dekker, New York, 1985, vol. 7, ch. 5, pp. 339–466.

16 (*a*) M. A. Hangarter, Ph. D. Thesis, *Photochemische Primärprozesse von Plastochinon, einem Glied der Elektronentransportkette der Photosynthese*, University of Basel, 1983; (*b*) J. Wirz, Spectroscopic and kinetic investigations of conjugated biradical intermediates, *Pure Appl. Chem.*, 1984, **56**, 1289–1300.

17 G. Porter and M. A. West, in *Techniques of Chemistry* Vol. VI, Part II, 3rd edn., ed. G. G. Hammes, Wiley-Interscience, New York, 1974.

18 E. Hasler, A. Hörmann, G. Persy, H. Platsch and J. Wirz, Singlet and Triplet Biradical Intermediates in the Valence Isomerization of 2,7-Dihydro-2,2,7,7-tetramethylpyrene, *J. Am. Chem. Soc.*, 1993, **115**, 5400–5409.

19 C. Rödig and F. Siebert, Errors and Artifacts in Time-Resolved Step-Scan FT-IR Spectroscopy, *Appl. Spectrosc.*, 1999, **55**, 893–901; C. Rödig, H. Georg, F. Siebert, I. Rousso and M. Sheves, Temperature effects of excitation laser pulses during step-scan FT-IR measurements, *Laser Chem.*, 1999, **19**, 169–172.

20 G. Zimmerman, L.-Y. Chow and U.-J. Paik, The Photochemical Isomerization of Azobenzene, *J. Am. Chem. Soc.*, 1958, **80**, 3528–3531.

21 (*a*) O. Isler, R. Rüegg, A. Studer and R. Jürgens, Specificity of the Vitamin K_1 constitution and its analogs toward coumarin linkages, *Z. Physiol. Chem.*, 1953, **295**, 290–309; (*b*) P. M. Scott, Chemical Studies Concerning the Possible Role of Chromanyl Phosphates and Quinones in Oxidative Phosphorylation, *J. Biol. Chem.*, 1965, **240**, 1374–1380; (*c*) F. Bohlmann and K.-M. Kleine, Über ein neues Chinon aus höheren Pflanzen, *Chem. Ber.*, 1966, **99**, 885–888.

22 K. Maruyama and Y. Naruta, Synthesis of naturally occurring quinones. Part 3. Allylation of quinones with allyltin reagents. New synthesis of coenzyme Q1 and plastoquinone-1, *J. Org. Chem.*, 1978, **43**, 3796–3798; I. Tabushi, K. Yamamura, K. Fujita and H. Kawakubo, Specific inclusion catalysis by β-cyclodextrin in the one-step preparation of Vitamin K_1 or K_2 analogs, *J. Am. Chem. Soc.*, 1979, **101**, 1019–1026, in our hands the latter procedure gave poor yields of **4**.

23 D. McHale and J. Green, The preparation of ubichromenols and related chromenols, *Chem. Ind. (London)*, 1962, 1867.

24 M. Vecchi, M. Schmid, W. Walther and F. Gerber, Determination of the diastereomers of Vitamin K_1, *J. High Resolut. Chromatogr. Chromatogr. Commun.*, 1981, **4**, 257–259.

25 M. J. Frisch, G. W. Trucks, H. B. Schlegel, G. E. Scuseria, M. A. Robb, J. R. Cheeseman, V. G. Zakrzewski, J. A. Montgomery, Jr., R. E. Stratmann, J. C. Burant, S. Dapprich, J. M. Millam, A. D. Daniels, K. N. Kudin, M. C. Strain, O. Farkas, J. Tomasi, V. Barone, M. Cossi, R. Cammi, B. Mennucci, C. Pomelli, C. Adamo, S. Clifford, J. Ochterski, G. A. Petersson, P. Y. Ayala, Q. Cui, K. Morokuma, D. K. Malick, A. D. Rabuck, K. Raghavachari, J. B. Foresman, J. Cioslowski, J. V. Ortiz, A. G. Baboul, B. B. Stefanov, G. Liu, A. Liashenko, P. Piskorz, I. Komaromi, R. Gomperts, R. L. Martin, D. J. Fox, T. Keith, M. A. Al-Laham, C. Y. Peng, A. Nanayakkara, C. Gonzalez, M. Challacombe, P. M. W. Gill, B. Johnson, W. Chen, M. W. Wong, J. L. Andres, M. Head-Gordon, E. S. Replogle and J. A. Pople, Gaussian, Inc., Pittsburgh, PA, 1998.

26 M. Cossi, V. Barone, R. Cammi and J. Tomasi, Ab initio study of solvated molecules: a new implementation of the polarizable continuum model, *Chem. Phys. Lett.*, 1996, **255**, 327–335.

27 A. P. Scott and L. Radom, Harmonic Vibrational Frequencies: An Evaluation of Hartree–Fock, Møller-Plesset, Quadratic Configuration Interaction, Density Functional Theory, and Semiempirical Scale Factors, *J. Phys. Chem*, 1996, **100**, 16502–16513.

28 The choice of irradiation wavelengths is essential in preparative work due to secondary photolysis of the photoproducts (ref. 11*b*).
29 A. Rüttimann, Recent Advances in the Synthesis of K-Vitamins, *Chimia*, 1986, **40**, 290–306.
30 E. Wilhelm and R. Battino, Thermodynamic Functions of the Solubilities of Gases in Liquids at 25 °C, *Chem. Rev.*, 1973, 1–9; R. Battino, T. R. Rettich and T. Tominaga, The Solubility of Oxygen and Ozone in Liquids, *J. Phys. Chem., Ref. Data*, 1983, **12**, 163–178; J. F. Coetzee and I. M. Kolthoff, Polarography in Acetonitrile. III. Brønsted Acids. Amperometric Titration of Amines with Perchloric Acid, *J. Am. Chem. Soc.*, 1957, **79**, 6110–6115.
31 A. Campbell and J. E. Willard, Viscosities of Some Organic Glasses Used as Trapping Matrices, *J. Phys. Chem.*, 1984, **88**, 1445–1449.
32 J. Michl and E. W. Thulstrup, *Spectroscopy with Polarized Light*, VCH, New York 1986.
33 K. B. Patel and R. L. Willson, Semiquinone Free Radicals and Oxygen, *J. Chem. Soc., Faraday Trans.*, 1973, **69**, 814–825.
34 Y. Chiang, A. J. Kresge, B. Hellrung and P. Schünemann and J. Wirz, Flash Photolysis of 5-Methyl-1,4-naphthoquinone in Aqueous Solution: Kinetics and Mechanism of Photoenolization and of Enol Trapping, *Helv. Chim. Acta*, 1997, **80**, 1106–1121.
35 This was independently realised by D. Creed (personal communication, November 24, 1980), who assigned the biphasic decay of the 1,2-QM tautomers of menaquinone-1 (**3**) to the *E*- and *Z*-isomers in a later paper (ref. 13).
36 J.-R. Burie, A. Boussac, C. Boullais, G. Berger, T. Mattioli, C. Mioskowski, E. Nabedryk and J. Breton, FTIR Spectroscopy of UV-generated Quinone Radicals: Evidence for an Intramolecular Hydrogen Atom Transfer in Ubiquinone, Naphthoquinone, and Plastoquinone, *J. Phys. Chem.*, 1995, **99**, 4059–4070.
37 (*a*) G. G. Lazarev, M. V. Serbodov and N. G. Khrapova, EPR study of intramolecular photoreduction of Vitamin K_1, *Izv. Akad. Nauk. SSSR, Ser. Khim.*, 1979, 1409–1411; (*b*) M. V. Serbodov, Photolysis of Vitamin K_1 at low temperatures, *Izv. Akad. Nauk. SSSR, Ser. Khim.*, 1982, 2004–2009.
38 M. Rule, A. R. Matlin, D. E. Seeger, E. F. Hilinski, D. A. Dougherty and J. A. Berson, Non-Kekulé molecules derived conceptually by heteroatom-for-carbon substitution in alternant hydrocarbons, *Tetrahedron*, 1982, **38**, 787–798.
39 P. Michon and A. Rassat, Nitroxides. LXIX. 1,4-Bis(4′,4′-dimethyloxazolidine-3′-oxyl)cyclohexane Structure Determination by Electron Spin Resonance and Nuclear Magnetic Resonance, *J. Am. Chem. Soc.*, 1975, **97**, 696–700.